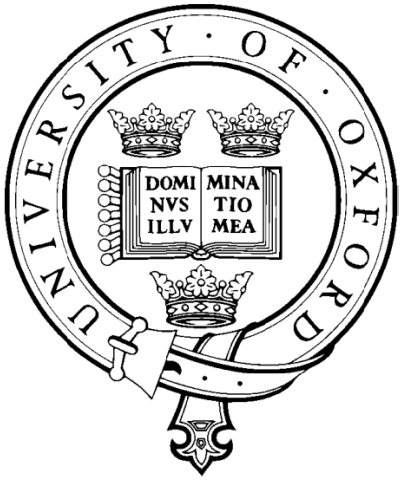
Preparation and Evaluation of Modular Probes of Reductive Stress



Alexandra Lovelock

Worcester College

University of Oxford

A thesis submitted for the degree of

Doctor of Philosophy

Michaelmas Term 2022

Abstract

"Preparation and evaluation of modular probes of reductive stress"

Alexandra Lovelock, Worcester College, University of Oxford

DPhil Thesis, Michaelmas Term 2022

This thesis explores the synthesis of and subsequent use of monometallic lanthanide complexes and their reductive potential for selected biomarkers. Attempts on a bimetallic complex are also reported.

Chapter 1 outlines the properties of lanthanides with a focus on their photophysical and chemical behaviour, and the kinetic requirements for complexes containing lanthanides. Medical applications and discussions on the key reductive biomarkers to this thesis are also discussed.

Chapter 2 explores the use of anthracene as a functional chromophore in a DO3A-based lanthanide complex, and the synthetic protocol and characterisation of these complexes by NMR, luminescence, and UV. Interaction of these complexes with singlet oxygen and irradiative stimuli is focused on in detail.

Chapter 3 discusses attempts on synthesis of a bimetallic lanthanide complex based on the anthryl-functionalised DO3A complexes discussed in Chapter 2.

Chapter 4 investigates synthesis and characterisation of benzoazide-functionalised DO3A lanthanide complexes. Studies on their reduction potential are undertaken using two biomarkers, and the difference in reactivity is briefly discussed.

Chapter 5 reports synthesis and characterisation of DO3A lanthanide-containing complexes functionalised with nitrobenzene. Investigations into the reduction potential of these complexes to a previously chosen reductant are undertaken and discussed.

Chapter 6 discusses the conclusions reached during the course of this work, and suggests possible avenues for future research.

Chapter 7 contains experimental techniques for processing data, and procedures for synthesis and characterisation of these complexes.

Contents

Abstract ..... **i**
Contents ..... **iii**
Acknowledgements ..... **v**
Impact of COVID-19 ..... **vii**
Abbreviations ..... **viii**
1 Introduction **1**
1.1 General Aspects of the Lanthanide Series **1**
1.2 Lanthanide Luminescence **1**
1.3 Sensitised Luminescence **5**
1.4 Mechanisms of Energy Transfer **7**
1.5 Quenching **8**
1.6 Magnetic Features **11**
1.7 Isomerism **13**
1.8 Stability of Lanthanide Complexes **15**
1.9 Use of Lanthanides **19**
1.9.1 Imaging and Magnetic Resonance Imaging 19
1.10 Key Biomarkers **23**
1.10.1 Oxygen 23
1.10.1.1 Singlet Oxygen ($^1O_2$) and Reactive Oxygen Species (ROS) 24
1.10.1.2 Oxygen and Cancer 28
1.10.2 Hydrogen Sulfide (H_2S) and Reactive Sulfur Species (RSS) 29
1.10.2.1 Probing H_2S in Biology 33
1.10.2.2 H_2S Therapeutics 41
1.10.3 Nitrobenzene (NO_2) and Reactive Nitrogen Species (RNS) 43
1.10.3.1 Nitro Compounds and Hypoxia 47
1.10.3.2 Nitrobenzene Derivatives 49
1.11 Aims of the Project **52**
1.12 References **53**
2 A Redox Active Luminescent Lanthanide Complex **60**
2.1 Introduction **60**
2.2 Synthesis and Characterisation **62**
2.3 The Impact of Deuterated Solvent on Photophysical Properties **67**

2.4 The Impact of Oxygenation 71
2.5 Oxygenation and Irradiation 74
2.6 Conclusions 77
2.7 References 78
3 Attempts on a Hetero-Metallic Luminescent Lanthanide Complex 79
3.1 Introduction 79
3.2 Synthesis and Attempted Isomer Separation 84
3.3 Conclusion 88
3.4 References 89
4 Reducible Luminescent Lanthanide Complexes 90
4.1 Introduction 90
4.2 Synthesis and Characterisation 92
4.3 Reactivity with NaHS 95
4.4 Zinc Reduction of Azides 102
4.5 Degassed Solutions and Luminescence 107
4.6 Conclusion 109
4.7 References 110
5 An Alternative Reducible Luminescent Lanthanide Complex 111
5.1 Introduction 111
5.2 Synthesis and Characterisation 113
5.3 Zinc Reduction of Nitrobenzene 116
5.4 Conclusion 120
5.5 References 121
6 Conclusions 122
6.1 Conclusions and Future Work 122
6.2 References 126
7 Experimental 127
7.1 General 127
7.2 Experimental – A Redox Active Luminescent Lanthanide Complex 129
7.3 Experimental – Attempts on a Hetero-Metallic Luminescent Lanthanide Complex 134
7.4 Experimental – Reducible Luminescent Lanthanide Complexes 135
7.5 Experimental – An Alternative Reducible Luminescent Lanthanide Complex 140
7.6 References 143

Acknowledgements

First of all, I would like to thank Professor Stephen Faulkner for offering me a place in his research group. He has been a wonderful supervisor, constantly supportive and encouraging, and always willing to answer emails even when it's gone midnight and work should have been finished hours ago. For allowing me to go home when things got tough in life and continuing to work with me every week virtually across continents. Your constant faith in me even when things have gone wrong, and your reassurance every step of the way has been so important to me getting to this stage, and I will always be grateful for it.

To the staff of the Chemistry Research Laboratory, I would also like to say thank you. Particular thanks to Dr Nick Rees for teaching me how to use the machines effectively, and for every phased NMR spectra you provided for me. Thank you as well to all of the technical and support staff as well, for all the laughs and conversations that were anything but chemistry.

To my research group, thank you for letting me work alongside you these last four years. Special thanks go to Dr Katherine/Katie Fisher and Dr Carlos Andres Guzman Gil. You have helped me so much over the years when I've had questions about chemistry, presentations, needed advice in life, or even just a laugh. Even across the world, your help has been appreciated.

Katie in particular, thank you for always being there for me and for taking the time to work through this degree with me. You've been an amazing, true, and trustworthy friend, and I am glad that I have had the chance to get to know you (and Matthew) over the last few years. To Matthew, thank you as well for your support and all the laughs. I hope to see you both soon.

To Carlos, you've been an amazing friend to me since the day we met. Even though you finished early into my start at Oxford, the effort you put into helping me in those first few

months really helped my confidence in a new environment and gave me encouragement when I needed it most. It's been wonderful having you in my life these last few years; I have enjoyed every moment and look forward to seeing you again one day now we've finally made it out of Wonderland.

Thanks as well to the Mechell family. We may not be in contact anymore, but that doesn't mean that I don't appreciate for everything you have done for me. For giving me a home when the world shut down, for always making sure I was looked after, and for encouraging me with my degree even when you had no idea what I was talking about.

To my friends in Australia, I know we haven't always had the best contact because life gets in the way, but I'm thankful for those who stuck around. To Courtney in particular, always there to cheer me up when I was down, I've probably thrown way too much trauma your way but I'm glad you still love me anyways. To Georgia and Amber, thank you for sticking it out with me these last few years and always giving me a reason to be proud of what I've done.

To my Aunty Lynn and Uncle Kieran, thank you for always giving me a place to stay when I came to visit, and encouragement when I was feeling down. I have enjoyed the time spent with you over the years, all the restaurants and pubs tried, and places visited. Thanks as well for all the knitting supplies, I shall continue to put them to good use.

Most importantly I need to thank my family: Mum Ria, Dad Neil, and Brother Hayden. If it weren't for you, I couldn't have afforded this opportunity to live overseas and study at such a prestigious institution. For the emotional support, even when I was cut off from you because of COVID, and for always helping me when I needed it most. It's been a tough few years doing this doctorate on my own, but it's all been worth it, and now I get to add the first 'real' doctor to the list of doctors in our household. Sorry guys, it definitely counts more.

Impact of COVID-19

Before the COVID-19 pandemic began, work was planned to prepare *in vitro* cell and enzyme studies on the probes generated in this thesis. Unfortunately, with the university-wide shut down, the department was shut for several months, and when time came for me to return to the lab it was found that most of my probes had deteriorated in storage. As such, synthesis had to be restarted, and these plans were put aside. Social distancing limited laboratory working hours following reopening, meaning that synthesis was slow upon restarting, and was slowed further upon introduction of the part II research students in January 2021. This cut further into available working time.

Due to the time constraints experienced as a result, *in vitro* enzyme reduction studies and cell line testing was postponed, and eventually cancelled in order to meet the time constraints imposed by the DPhil. These *in vitro* studies would have eventually led to collaboration with the department of Oncology in cell line testing, and examination of spheroid mimics of hypoxia, and eventually to ischaemic heart models. Unfortunately, the initial stages took longer than anticipated, and COVID-19 shutdowns and laboratory restrictions led to lack of time. The thesis presented here focuses on synthetic chemistry and spectroscopy as a consequence of these limitations.

COVID also had a direct impact on my own well-being, and my situation was further complicated by housing and financial issues that I ran into during the COVID-19 pandemic, which among other factors culminated in me moving back to Australia midway through 2022 to move back with family, so laboratory work had to be finished faster than planned.

Abbreviations

$\langle S_z \rangle$	reduced value of average spin polarisation
μ_B	bohr magneton
y_I	gyromagnetic ratio of nucleus
°C	degrees in Celsius
µL	microliters
µM	micromolar
$^1O_2$	singlet oxygen
3MST	3-mercaptopyruvate sulfurtransferase
$^3O_2$	triplet oxygen
Å	angstroms
A	lanthanide-specific correction factor
$A/\hbar$	hyperfine coupling constant
ACE	angiotensin converting enzyme
ACN	acetonitrile
ALS	amyotrophic lateral sclerosis
ATP	adenosine triphosphate
B	quenching effect of water molecules, pertaining to the Horrocks eqn.
BET	back energy transfer
BNZ	benznidazole
br.	broad
$C_6H_{11}BrO_2$	tert-butyl bromoacetate
CBS	cystathionine β-synthase
$CDCl_3$	deuterated chloroform
CEA	carcinoembryonic antigen
CO	carbon monoxide
CSE	cystathionine-γ-lase
CT	computerised tomography

Cyclen	1,4,7,10-tetraazacyclododecane
d	doublet
D_1	constant accounting for ligand field coefficient
D_2	constant accounting for geometry-independent constants
D_2O	deuterated water
DCM	dichloromethane
DMPD	N,N-dimethyl-P-phenylenediamine
DNA	deoxyribonucleic acid
DO3A	2,2',2''-(1,4,7,10-tetraazacyclododecane-1,4,7-triyl)triacetic acid
DOTA	1,4,7,10-tetraazacyclododecane-1,4,7,10-tetraaceticacid
DTPA	diethylenetriamine pentaacetate
Dy	dysprosium
EDTA	ethylenediaminetetraacetic acid
Er	erbium
Et_2O	diethyl ether
Eu	europium
g	grams
Gd	gadolinium
GI	gastrointestinal
H_2O_2	hydrogen peroxide
H_2S	hydrogen sulfide
HCl	hydrochloric acid
HNO	nitroxyl
HNO_3	peroxynitrous acid; also written as ONOOH
HO	hydroxyl radical
HOMO	highest occupied molecular orbital
hr	hours
HS^-	hydrosulfide anion

HSO_3^-	hydrogen sulfite
IR	infra-red
ISC	intersystem crossing
k	Boltzmann constant in the calculation of contact shift
k_b	energy constant for back energy transfer
k_{D2O}	rate of quenching in D_2O
K_{et}	rate of energy transfer
k_f	energy constant for forward energy transfer
k_{H2O}	rate of quenching in water
LIS	lanthanide-induced shift
LLB	lanthanide luminescent bioprobe/s
LMCT	ligand to metal charge transfer
$Ln(CF_3SO_3)_3$	lanthanide (generic) trifluoromethanesulfonate
LTP	long term potentiation
LUMO	lowest unoccupied molecular orbital
M	molar
m	multiplet
m/z	mass to charge ratio
MeCN	acetonitrile
MeOD	deuterated methanol
MeOH	methanol
mg	milligrams
$MgSO_4$	magnesium sulfate
MHz	megahertz
min	minutes
M_J	ground crystal field state
mL	millilitres
MLCT	metal to ligand charge transfer

mM	millimolar
MNZ	metronidazole/s
MRI	magnetic resonance imaging
MS	mass spectrometry
ms	milliseconds
Na_2S	sodium sulfide
NaCl	sodium chloride
$NaHCO_3$	sodium bicarbonate, or sodium hydrogen carbonate
NaHS	sodium hydrosulfide
NaN_3	sodium azide
$NaNO_2$	sodium nitrite
NaOH	Sodium hydroxide
NH_4Cl	ammonium chloride
NIR	near Infra-red
nm	nanometres
NMDA	N-methyl-D-aspartate
NMR	nuclear magnetic resonance
NO	nitric oxide
NO_2	nitrobenzene
NSF	nephrogenic systemic fibrosis
O_2^-	superoxide
$ONOO^-$	peroxynitrite
ONOOH	peroxynitrous acid; also written as HNO_3
ONZ	ornidazole/s
P5P	pyridoxal-5'-phosphate
PAG	propargylglycine
paraCEST	paramagnetic chemical exchange saturation transfer
PBS	phosphate-buffered saline

PDT	photodynamic therapy
PET	positron emission tomography
pKa	acid dissociation constant
ppm	parts per million
q	quenching
r	radius
r	spherical coordinate in calculation of pseudocontact shift
r_1	longitudinal contrast agent's ability to affect relaxation time
r_1	transverse contrast agent's ability to affect relaxation time
RNS	reactive nitrogen species
ROS	reactive oxygen species
RSS	reactive sulfur species
$Ru(bpy)_3^{2+}$	ruthenium 2,2'-bipyridine
s	singlet
S_0	chromophore ground state
S_1	chromophore excited singlet state
S^{2-}	sulfide anion
$S_2O_4^-$	dithionite
$S_2O_5^{2-}$	disulfite
SAP	square antiprism
$SnCl_2$	stannous chloride
SO_2	sulfur dioxide
SPECT	single-photon emission computerized tomography
SPRC	5-propargyl-L-cysteine
SQR	Sulfide quinone reductase
T	absolute temperature
T_1	chromophore triplet excited state in energy transfer
T_1	relaxation time of longitudinal relaxation contrast agents

T_2	relaxation time of transverse relaxation contrast agents
Tb	terbium
TFA	trifluoroacetic acid
TLC	THIN LAYER CHROMATOGRAPHY
TSAP	twisted square antiprism
UV	ultraviolet
UV-Vis	UV-Visible (spectroscopy)
Yb	ytterbium
Zn	zinc
Δ_c	contact shift
Δ_d	diamagnetic shift
ΔE	change in energy
Δ_p	pseudocontact shift
ε	extinction coefficient
λ_{max}	wavelength of maximum intensity
σ	sigma
ϕ	spherical coordinate in calculation of pseudocontact shift
θ	spherical coordinate in calculation of pseudocontact shift

1 Introduction

1.1 General Aspects of the Lanthanide Series

The 4*f* elements known as the lanthanides bear similar chemical properties across the periodic table which is derived from their electronic properties. Their 4*f* shell is responsible for the optical and magnetic properties inherent to this class of element,[1] and is able to penetrate the xenon core configuration that is shielded by the 5s and 5p subshell electrons. Despite their key properties, in most cases they play a negligible role in bonding – this is instead dominated by electrostatic interactions between the ligand and the metal ion. This metal ion most commonly bears a +3-oxidation state (though +2 and +4 states are also possible for some), rendering them classed as hard acids that bind preferentially to high charge density donor atoms such as N and O. As they bind together, the resulting geometry is predominantly controlled by the selected donor ligand/s.

1.2 Lanthanide Luminescence

The luminescent emission of the lanthanide group extends from UV (gadolinium, Gd), to visible (europium, Eu and terbium, Tb) to near infra-red known as NIR (ytterbium, Yb and neodymium, Nd). Their emissive properties are influenced by the extent of the excite state's ability to be populated and the ease in which the non-radiative pathways can be minimised. These are called luminescent properties, seen as emission of light uninfluenced by a rise in temperature and caused by their electronic configurations and bonding.[2] The poor ligand-4*f* orbital overlap means the emission spectra observed in lanthanide complexes can be considered quasi-atomic, where energy transfer occurs between defined spin-orbit energy levels. These are categorised according to Russel-Saunders coupling as $^{2S+1}L_J$ where S, L, and J

are the spin, total orbital angular momentum, and total angular momentum respectively. Because of the parity forbidden and spin forbidden nature of the *f-f* transitions, all lanthanide ions exhibit long-lived emission.

The absorption and emission spectra of lanthanides tend to possess a larger number of peaks than their *d*-metal counterparts due to the large number of terms caused by the multiple microstates available for each electronic configuration. The energy spacing between these microstates is unique to each lanthanide and is related to the wavelength of transitions. Spectra generated from lanthanides are also sharp as vibronic coupling experienced by the lanthanides is negligible and there is minimal overlap between the ligand-centred orbitals and the lanthanide contracted valence orbitals. As an example, transitions for the Eu^{3+} ion are from the excited $^5D_0$ state to the ground ^7F_J levels, resulting in emission spectra peaks where $\Delta J = 0 – 6$ by whole integers. Transitions from higher excited states of ^5D_X where $x = 1 – 3$ are less common, as at ambient temperatures quenching of these excited states occurs through non-radiative processes.

Lanthanides are known to generate two main types of luminescence: fluorescence and phosphorescence. **Figure 1 - 1** depicts the two mechanistic pathways through which these are generated through the presence of an organic chromophore. Fluorescence is observed as an inter-state transition, usually from excited (S_1) to ground state (S_0) with no changes in spin, whilst phosphorescence involves a spin change from the triplet excited state (T_1) to S_0. Both types are long lived with the individual lifetime dependent on the energy gap between the emissive state and the state below in the complex of interest. In this analysis, terbium and europium have proven the ideal lanthanides of choice, with the change in energy (ΔE) = 12,300 ($^5D_0 \rightarrow {}^7F_6$) and 14,800 ($^5D_4 \rightarrow {}^7F_0$) respectively.[2]

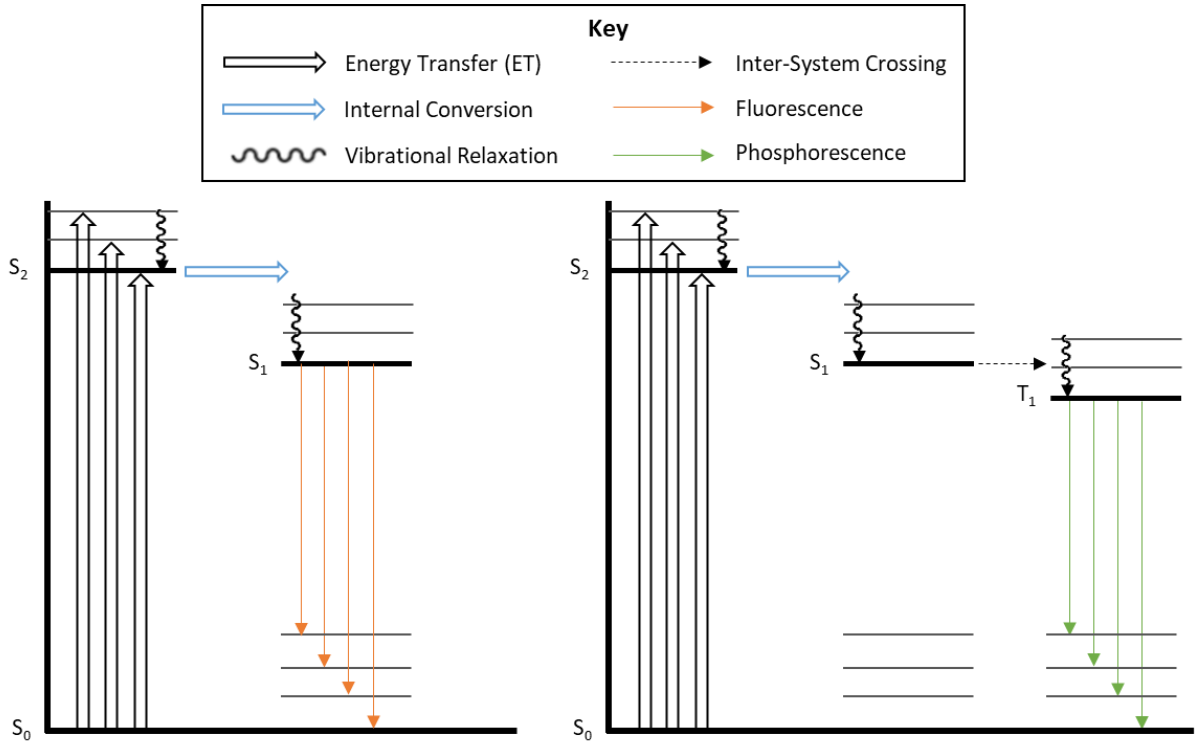


Figure 1 - 1 Simplified Jablonski diagrams showing the process of fluorescence and phosphorescence generation through an organic chromophore

Absorption by trivalent ions results in characteristic line luminescence seen as sharp, narrow emission bands which are caused by the core-like nature of these *f* orbitals. A visual representation of these can be found in **Figure 1 - 2**.[3] These bands feature several types of spectra, as since the electrons play a negligible role in bonding, atomic, ionic, and complex spectra are present. As a result, the lifetime length of these emission bands is long due to the Laporte selection rules and the forbidden nature of the *f-f* transitions. This causes energy transfer the excited state to ground state to occur at a much slower rate than is typically absorbed.[3]

Lanthanide complexes usually display strong ionic bonding and small crystal fields effects as a result of the contracted nature of these valence orbitals. These are shielded by the $5p^6 6s^2$ subshell causing parity-forbidden 4*f-f* absorptions, narrow line emissions,[4, 5] and low molar absorption coefficients. This crystal field splitting is considered small in comparison to spin-orbit coupling. Due to the ionic bonds in these complexes, coordination geometry is dictated

by the structure and electrostatics of the chosen ligand. Multidentate ligands are necessary to form complexes with low lability, since lanthanide ions do not covalently bond.[6] Complexes with simple ligands are therefore classified as highly labile,[7] even if thermodynamically favoured.

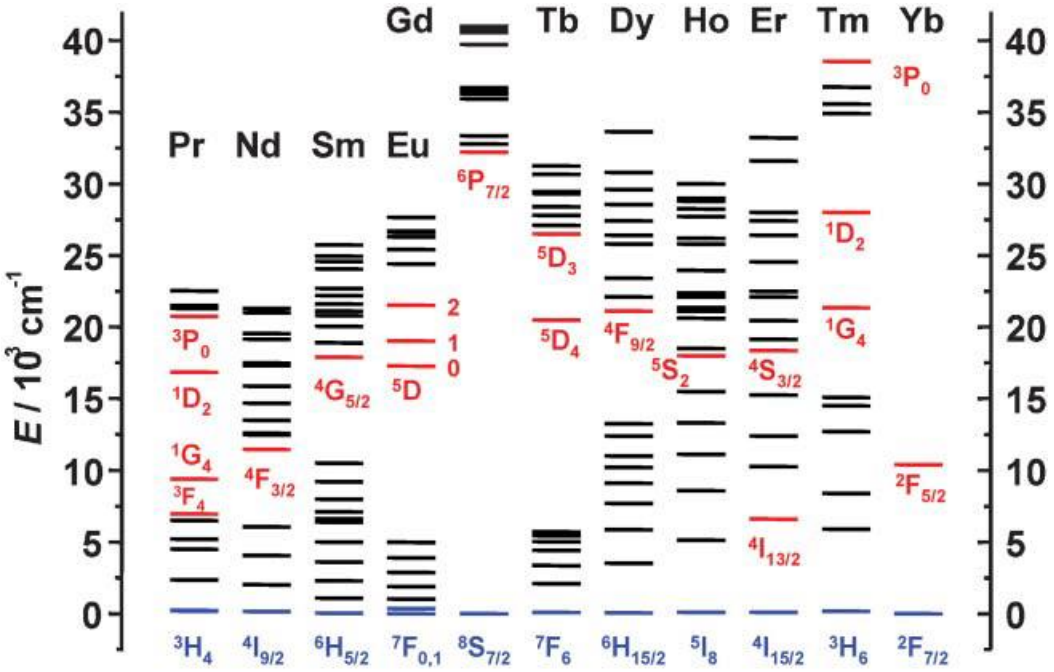


Figure 1 - 2 Partial energy diagram for the lanthanide ions, showing main luminescent levels (red) and fundamental levels (blue), taken from reference[2]

Decay times range between the lanthanides with ytterbium, neodymium and erbium possessing nanosecond timelines, microseconds for dysprosium, and up to milliseconds for europium and terbium.[8] In a trivalent lanthanide ion, most electronic transitions involve 4*f* subshell electron redistribution. The Laporte-forbidden transitions limits the effectiveness of direct excitation of the lanthanide excited state manifold, however it is possible to enable relaxation of the electric dipole selection rules through two possible mechanisms: triplet sensitisation, or through sequential charge transfer.[9] In most lanthanides, the ligand triplet state is observed to participate in the energy process.

1.3 Sensitised Luminescence

Lanthanide complexes can utilise the presence of an antenna to allow direct sensitisation of the lanthanide ion. To create this effect, an organic chromophore and a chelating ligand are bound to each other. This can then be excited and used to transfer energy to the chelated metal.[10] **Figure 1 - 3** demonstrates the various pathways through which this excitation can occur and the subsequent types of luminescence that might result. Sharp emission bands are observed after rapid internal conversion, originating from the metal ion.[4] Choice of this chromophore is dictated by the choice of lanthanide and its emissive state energy, or in the reverse where the choice of lanthanide is dependent on the excited state energy of the chromophore.

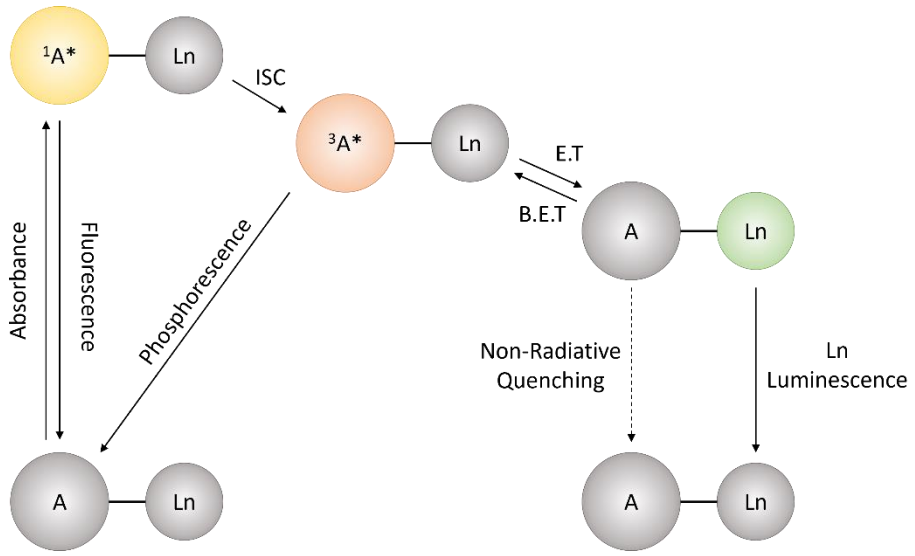


Figure 1 - 3 Pathways for excitation through the antenna effect to generate lanthanide luminescence. ^{1}A* = antenna singlet excited state, ^{3}A* = antenna triplet excited state, Ln = Lanthanide, ISC = intersystem crossing, ET = energy transfer, BET = back energy transfer

It is possible to overcome the low extinction coefficients associated with lanthanides through use of an indirect pathway.[11] This enables the emissive state of the lanthanide to be populated from the excited state of the antenna chromophore – usually aromatic – that possesses a large extinction coefficient in comparison to the lanthanide.[12] Efficiency is maximised when

both the chromophore and the antenna are bound in proximity within a stable coordination complex. With cyclen-based chromophores such as 2,2',2''-(1,4,7,10-tetraazacyclododecane-1,4,7-triyl)triacetic acid (DO3A) seen in **Figure 1 - 4**, an additional chromophore can be added, enabling further exclusion of any solvent molecules from around the complex. This enables minimisation of oscillators such as O-H which quench lanthanide luminescence.[10] In europium and terbium complexes, it is assumed that the energy transfer from ligand triplet levels accounts for the sensitised emission that is observed from these complexes.[13]

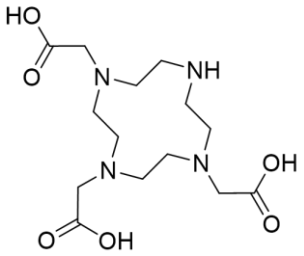


Figure 1 - 4 DO3A

Chromophores are employed to overcome the typically low extinction coefficients observed in lanthanide(iii) ions which are usually calculated/observed at $\varepsilon < 1\ M^{-1}cm^{-1}$),[12] making them an attractive alternative for previously used organic fluorophores. This is also due to their more photochemically stable nature and other properties including absorbance of visible light.[14] Organic chromophores in particular are used for sensitisation of visible emitting ions (Eu^{3+}, Tb^{3+}) whilst visible and NIR emitting lanthanides can be sensitised using a wider range of chromophores, including *d*-block metals. This is achieved using energy transfer from metal to ligand charge transfer (MLCT) states, with the most efficient energy transfer occurring when the donor triplet state exceeds the acceptor state by at least 2000 cm^{-1}. This minimises back energy transfer (BET) whilst simultaneously maintaining good energy overlap.[15]

1.4 Mechanisms of Energy Transfer

In the antenna effect, energy transfer is known to occur between the lanthanide and the chosen chromophore. In a classic situation, the chromophore singlet excited state (S_1) is populated through a single or multiphoton excitation process. Inter-system crossing (ISC) then occurs to populate the chromophore triplet state (T_1) to the lanthanide excited state through either Dexter exchange when direct orbital overlap is observed, or through Förster energy transfer in a through-space mechanism involving indirect contact.[11, 14] Direct energy transfer from the lanthanide to the S_1 state is also possible, as is sequential charge transfer to the lanthanide where the lanthanide possesses a +2 oxidation state (i.e. Yb, Eu).

Figure 1 - 5 provides a visual guide as to the specific mechanisms of Dexter and Förster energy transfer. Use of bridging ligands enables Dexter exchange to also occur over longer distances; this is known as a Dexter-type mechanism and helps meditate the super exchange process. Complexes that contain NIR emitting lanthanides can be used with a wider range of sensitising chromophores than those that emit in the UV or visible ranges, including metal complexes and organic dye molecules.[16]

As Dexter exchange is distance dependent, the rate of exchange decays exponentially as the distance between atoms increases. This means that Dexter energy transfer is usually possible only up to distances less than 10 Å, though as mentioned this can be extended in highly conjugated systems and using bridging ligands. Förster energy transfer, however, transfers energy through a dipole mechanism, resulting in a dependence on distance described as r^{-6}, though in lanthanide systems this can also be observed as r^{-8}. This transfer depends on spectral overlap. In lanthanides, this is often insufficient, but can end up the only possible mechanism distances beyond the range of Dexter transfer.

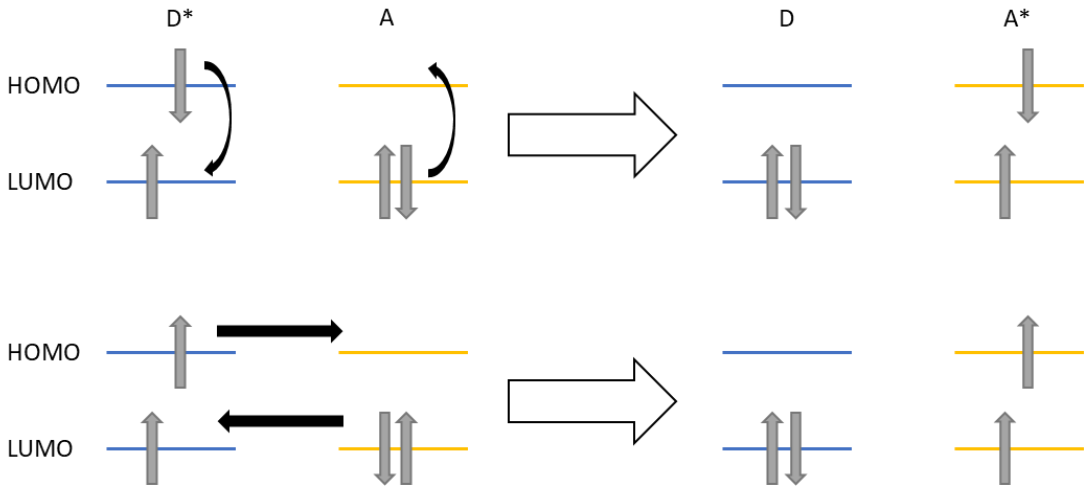


Figure 1 - 5 A visual guide to Förster Transfer (top) and Dexter Exchange (bottom). D and A represent the donor and acceptor respectively, whilst * dictates the excited state. The black arrows represent simultaneous rearrangement in the electronic configuration. Adapted from Mikhnenko & Blom[17]

Theoretically it is possible for europium to undergo excitation via sequential charge transfer, however the ligand to metal charge transfer (LMCT) state is generally lower in energy than the emissive $^5D_0$ state. As a result, LMCT precludes formation of the lanthanide excited state. Europium fluorescence has previously been observed to be influenced by temperature and choice of solvent, and similar observations have been found for samarium and terbium.[3] When the solvent molecule and lanthanide ion are directly bound to each other, the lifetime is greatly reduced, as deactivation is controlled by Förster energy transfer, meaning a greater influence for closely bound oscillators depending on the choice of solvent.

1.5 Quenching

Overlap of *f-f* transitions and vibrational harmonics (X-H e.g. O-H, C-H, usually present in solvent molecules) is a common mechanism for non-radiative deactivation of lanthanide excited states. This rate is inversely proportional to the energy gap between the lanthanide emissive and ground states, and the smaller the energy gap, the shorter the lifetime. The efficiency of quenching can also be reduced by incorporating the selected ion into an encapsulating ligand.

There are two types of quenching possible – static and dynamic/collisional. Static quenching is defined as inhibition by an external quencher of excited state formation, whilst in dynamic quenching, an already formed excited state is deactivated by a quencher.[18] This has been observed to occur via transfer of energy to vibrational excited states of small oscillators found within the coordination sphere. This includes bonds such as O-H or N-H bonds found in solvents.

It is also possible for quenching to occur via ligand oscillators. Unless in exceptional circumstances, the quantum yield observed in a substance is always between 0 and 1. This quantum yield is defined as the ratio of photons emitted:absorbed, and is affected by bound oscillators to various lanthanides at different strengths. When quenching occurs, the luminescence output of a lanthanide is reduced, therefore lowering the quantum yield.[19-21]

Luminescence deactivation from the excited state in solution occurs using high-energy vibrations of either the solvent molecules or the bound ligand itself. This energy transfer is known as quenching and has been observed in both solid-state and solution. O-H oscillators have proven the most effective quenchers and evidence for other oscillators such as N-H, C-H and C=O have also been observed to a lesser extent.[19] Water has also exhibited quenching effects, though the intensity of this effect is inversely proportional to the energy gap between the emitting state and the ground state.

Many applications that use lanthanides require water-soluble complexes, which can prove challenging as they have a high affinity for these molecules and are easily quenched. Given that O-H oscillators are the most efficient quenchers, particularly in aqueous solvents, it is possible to determine the number water molecules present within the coordination sphere

in comparison to the rate of quenching between protonated water (H_2O) and deuterated (D_2O). By ignoring other contributing factors, Equation 1.1 arises:[19]

$$q = A(k_{H_2O} - k_{D_2O}) \qquad \textbf{Equation 1.1}$$

This equation determines the sensitivity of the specific lanthanide ion to vibronic quenching because of O-H oscillators. Beeby *et al.* (1999) previously reported the proportionality constants for europium and terbium, which were measured at 0.525 ms^{-1} and 2.1 ms^{-1} per O-H oscillator respectively with q ± 0.5.[19] This is only pertinent to complexes where this information is relevant in the determination of luminescence intensity and all factors can be easily identified.

The reduction of lanthanide lifetimes can be observed when comparing in solvents like water and D_2O, as the solvent O-D oscillators are less effective at quenching the luminescence than O-H oscillators from water. This means that luminescence lifetimes are observed as shorter in water than D_2O and the quenching effect of luminescence observed in water and D_2O can be determined through the Horrocks equation seen in Equation 1.2. This includes a correction factor to allow for the quenching effect closely diffusing water molecules has on the lifetime:

$$q = A(k_{H_2O} - k_{D_2O}) - B \qquad \textbf{Equation 1.2}$$

In this equation, A represents a lanthanide-specific correction factor and B represents the quenching effect of closely diffusing water molecules where $0.1 < B < 0.3$.[22] Factors A and B are again dependent on the lanthanide chosen for this corrected equation, as for europium A = 1.2 ms and B = 0.25 + 0.075x, whilst for terbium A = 5 ms and B = 0.06. In the former, x represents the number of amide N-H oscillators. The quenching capability of O-H and N-H

oscillators differs between lanthanides as well as N-H quenches Eu 1.5 times greater than O-H. In terbium complexes N-H are only half as effective.[19]

1.6 Magnetic Features

Most lanthanides possess partially filled 4*f*-orbitals, generating strong single-ion anisotropy that leads to electronic structures of high complexity that are unique to each lanthanide accompanied by a large unquenched orbital moment caused by the near degeneracy of these orbitals.[23] There is no one way to define the shape of these orbitals, as each lanthanide possesses its own unique orientation and anisotropy, however one of the most common geometries found is the cubic geometry, often seen in molecules in which the x, y, and z axis are symmetrically related.[24] **Figure 1 - 6a** visualises the shape of the *f*-electron cloud of each lanthanide, which has been found to be dependent on the angular dependence of the *f* orbitals and the magnitude of the ground crystal field (M_J) state. Cubic geometries are depicted here under M_J = 0 and ±2. The shape of the orbital densities is also dependent on the number of electrons, as seen in **Figure 1 - 6b**.[23]

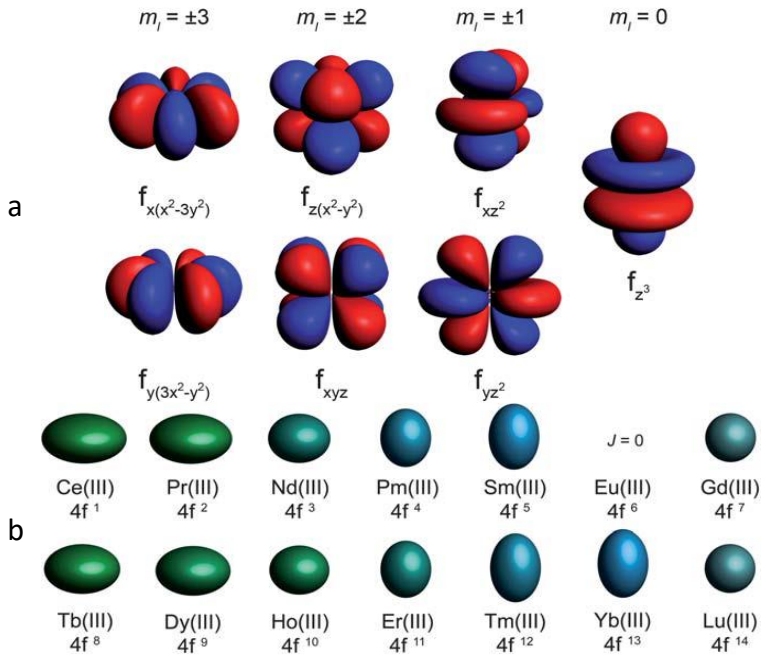


Figure 1 - 6 a) Visual representation of the 4*f* orbitals in order from the highest magnitude to lowest magnitude M_J state (oblate – prolate); b) Approximations of the 4*f* electron distribution. Europium is not depicted due to its *J* = 0 ground state. Taken from[23]

Lanthanide induced shift (LIS), or hyperfine shift, is a shift induced in a nuclei's chemical shift when in the presence of a paramagnetic lanthanide. This occurs through interaction with unpaired electrons and is defined as the difference in chemical shift of the nucleus between a diamagnetic system, and its corresponding paramagnetic system. Two factors contribute to this shift: contact shift (Δ_c) which originates directly at the nucleus and involves a through-bond transmission of unpaired electron-spin density to the nucleus from the lanthanide; and pseudocontact (Δ_p), which is a through-space mechanism involving dipole-dipole interaction between the unpaired electrons on both the lanthanide ion and the nucleus.[25] By combining these contributions with the diamagnetic shift (Δ_d), the resulting paramagnetic induced shift can be calculated as seen in Equation 1.3:

$$\boldsymbol{\Delta_c = \Delta_c + \Delta_p + \Delta_d} \qquad \textbf{Equation 1.3}$$

Contact shift is calculable according to Equation 1.4 as seen below:

$$\boldsymbol{\Delta_c = \langle S_z \rangle * \frac{\mu_B A}{3kT y_I \hbar} * 10^6} \qquad \textbf{Equation 1.4}$$

Where $\boldsymbol{\Delta_c}$ is the contact shift (ppm), $\langle \boldsymbol{S_z} \rangle$ is the reduced value of the average spin polarisation in the general case of S > ½ and that spin orbit coupling is present, μ_B is the Bohr magneton, k is the Boltzmann constant, T is the absolute temperature, $\boldsymbol{y_I}$ is the nucleus' gyromagnetic ratio, and A/$\hbar$ is the hyperfine coupling constant (rad/s).

Pseudocontact shift can also be calculated, assuming the ligand field splitting of the lowest J state is small compared to kT. This was first derived by Bleaney and is expressed as seen in Equation 1.5 Equation 1.5.[26, 27] In this equation, geometric information is dependent on the distance between the lanthanide (treated as the coordinate origin), and the angle between the z axis and nucleus.

$$\Delta_p = \boldsymbol{D_1}\frac{(3cos^2\theta-1)}{r^3} + \boldsymbol{D_2}\frac{(sin^2\theta cos^2\phi)}{r^3} \qquad \textbf{Equation 1.5}$$

Where Δ_p is the pseudocontact shift, D_1 and D_2 are constants accounting for ligand field coefficients and geometry-independent constants, and r, θ, and ϕ are spherical coordinates (with a lanthanide ion as the origin point) of the observed nucleus. The D coefficient is specific to the lanthanide ion in question and is responsible for the change of sign observed when comparing NMR chemical shifts in spectra of analogous lanthanide complexes. This Bleaney equation becomes simplified when calculating pseudocontact shifts for axially symmetric systems, as seen in Equation 1.6 which eliminates the geometrical component.

$$\Delta_p = \boldsymbol{D_1}\frac{(3cos^2\theta-1)}{r^3} \qquad \textbf{Equation 1.6}$$

The effect of these shifts is seen in ^{1}H NMR spectra, where spectra of lanthanide complexes have large shift ranges that are often accompanied by broad resonances. For europium complexes, shifts are found in the -50 to + 50 ppm range, ytterbium in -150 to +150 ppm, and terbium between -500 and + 500 ppm.

Previous research has found that, in the case of paramagnetic lanthanide ions, the effects observed in proton spectra related to those in this thesis are founded entirely in pseudocontact contributions.[28]

1.7 ISOMERISM

Ligands based off a cyclen tri- or tetra- N substituted backbone such as 2,2',2''-(1,4,7,10-tetraazacyclododecane-1,4,7-triyl)triacetic acid and 1,4,7,10-tetraazacyclododecane-1,4,7,10-tetraaceticacid are referred to as DO3A and DOTA respectively and are well known for their ability to bind with lanthanides. The resulting complexes exhibit two main different geometries: square antiprism (SAP) and twisted square antiprism (TSAP). These are

differentiated by their twist angle as SAP twists at 40°, where TSAP only twists 30°. **Figure 1 - 7** demonstrates the differences in these orientations. In DOTA, the four nitrogen atoms from the cyclen body are found to form one square face of a prism below the lanthanide ion, whilst the four carboxylate oxygens form the other face above to create a pocket within which the lanthanide resides. The ninth coordination site contains a water molecule, which when bonded to the TSAP isomer undergoes exchange at a rate 50 times the speed of the SAP species.

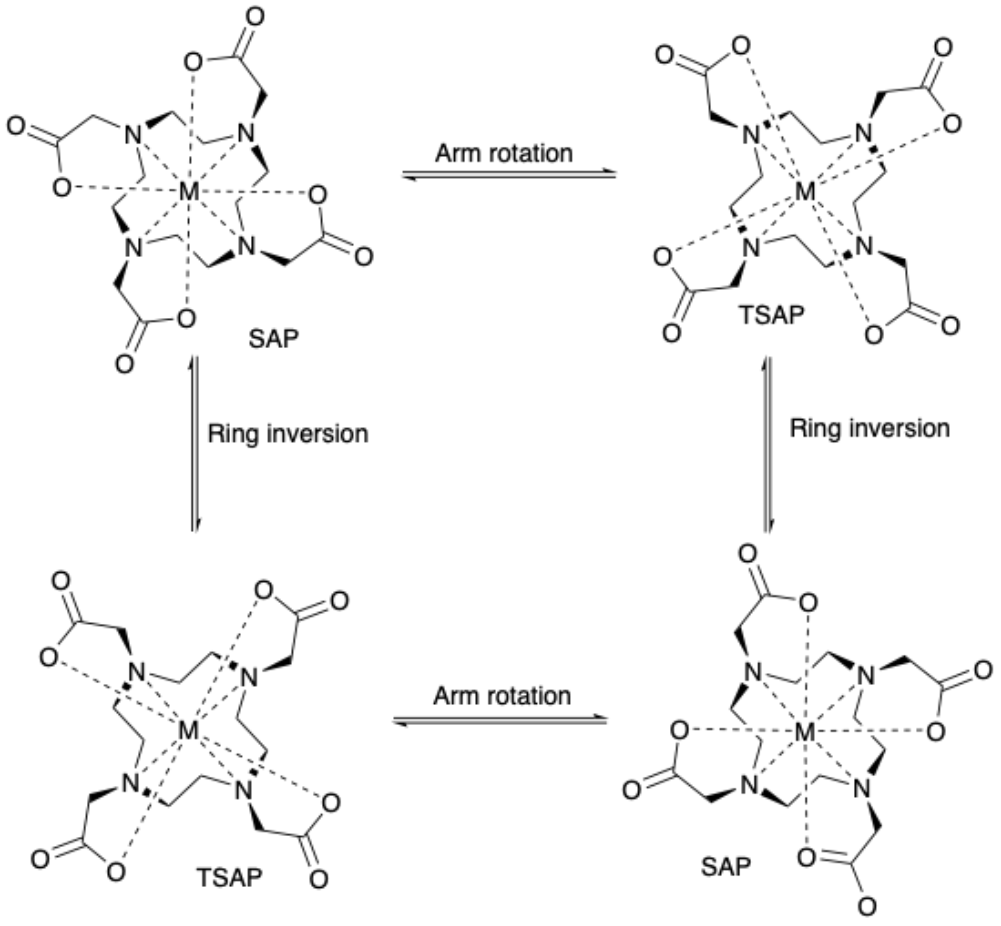


Figure 1 - 7 Isomerism of DOTA-based lanthanide complexes and their interconversion pathways. Taken from[29]

Interconversion between the SAP and TSAP isomers is possible, with the energy barrier for arm rotation in DO3A found to be much lower than for DOTA. This results in fast interconversion for DO3A, generating broad resonances in ^{1}H NMR and slower interconversion for DOTA, giving sharp NMR peaks.[30] The geometry of these structure is also dependent on the lanthanide of choice, with larger lanthanide ions (between Ln^{3+} and Pm^{3+}) adopting the TSAP geometry and complexes of Sm^{3+} and Lu^{3+} adopting a SAP geometry.

The dominant isomer can be determined through NMR analysis of the ratio between the equatorial and axial proton nuclei. For europium complexes specifically, proton resonances in the ^{1}H NMR spectra that shift to higher chemical values correspond to protons lying closer to the magnetic axis, whereas those that move to lower chemical shifts are closer to an equatorial position.[26] In a typical analysis, TSAP conformers are seen to undergo a chemical shift between 15-20 ppm whilst the SAP conformer shifts 30-40 ppm. Whilst systems with broken symmetry have more complex NMR spectra than their axially symmetrical counterparts, distinguishment between SAP and TSAP conformers proves possible through comparison to these axially symmetric complexes.

1.8 Stability of Lanthanide Complexes

For effective sensitisation, proximity or an exchange pathway, and a pocket that enables irreversible lanthanide binding is required. This is dependent on the structure of the chosen ligand. This structure also heavily influences the metal ion inner coordination spheres, emission properties, kinetic and thermodynamic stability, and photophysical properties of their corresponding lanthanide.[31] As lanthanides have a low degree of covalency, the coordination of their complexes is also dependent on the structure, steric influences, and

electrostatic considerations of the ligand, with ligands with large denticity needed to form thermodynamically stable complexes.[6]

The usefulness of a ligand is determined by a few required characteristics: a small singlet-triplet energy separation, a high extinction coefficient for the sensitiser absorption band (between λ = 337 and 420 nm), a fast energy transfer step, and a 7-9 coordinating ligand. Within this coordinating ligand, it is preferable that at least one donor is included to minimise the distance between the lanthanide and the sensitiser.[32] Incorporation of appropriate chromophores enables efficient lanthanide sensitisation which helps overcome the problems associated with the low extinction coefficients that lanthanides possess.[11]

Applications and uses of lanthanide complexes rely heavily on the inherent stability of the complex during the course of its use. It is therefore of tantamount importance that kinetic and thermodynamic stability of these complexes are high. Thermodynamic stability is usually favourable if an appropriate number of hard donor atoms are used and arranged for coordination. The size and character of the lanthanide ions indicates that high coordination numbers are favoured in binding, commonly involving 8-10 donor atoms.[7]

Ligands such as ethylenediaminetetraacetic acid (EDTA) and diethylenetriamine pentaacetate (DTPA) seen in **Figure 1 - 8** have been previously established as suitable ligands, with their complexes proving more labile than complexes with *d*-block counterparts. In macrocyclic ligands with at least seven donor atoms the inherent lanthanide(iii) ion's rapid exchange

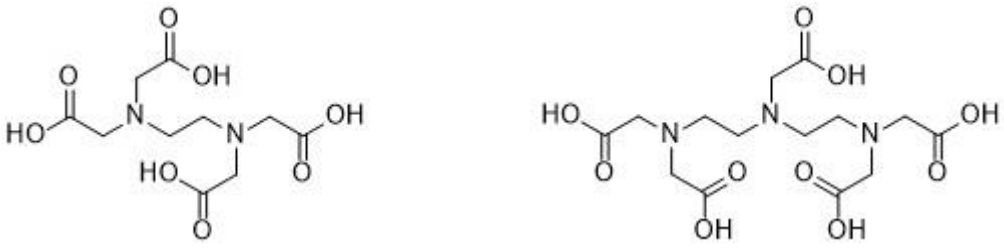


Figure 1 - 8 EDTA (left) and DTPA (right)

kinetic can be suppressed,[7] with complexes containing DOTA seen to be kinetically inert. **Figure 1 - 9** shows a collection of previously studied complexes using these ligand backbones. The high kinetic and thermodynamic stability of these complexes is rooted in their possession of hard Lewis donors (N and O), which are known to bind preferentially to hard Lewis acids such as the lanthanide ions and restrict their inherent lability.[12]

Macrocyclic compounds are commonly synthesised and used in combination with lanthanides to generate complexes of higher stability than those using open-chain chelating ligands due to the macrocyclic effect. In similar effect to polydentate complexes such as DO3A or DOTA, vacant coordination sites are often occupied by solvent molecules. DO3A in particular has high potential, as its vacant amine site enables greater chemical functionalisation though less kinetic stability than DOTA. This functionalisation can be enabled by N-alkylation to add a fourth arm and attach chromophores to the structure; however the choice of arm significantly influences the overall kinetic stability of the complex and N-alkylation can lead to complex destabilisation through increasing steric strain.[33] It is possible that this increase in strain results in a reduction of the macrocycle's ability to encapsulate lanthanide ions within the DO3A complex.

Thermodynamic considerations are made with regards to the number of interactions with hard donors, which increases the overall electrostatic interactions. This stability originates from enthalpically favoured complexation of lanthanide ions of an electropositive nature with electron rich ligands. Despite this, kinetic stability is considered more important because of the possibility that demetallation could occur in biological systems, leading to conditions such as Nephrogenic Systemic Fibrosis (NSF).[39, 40]

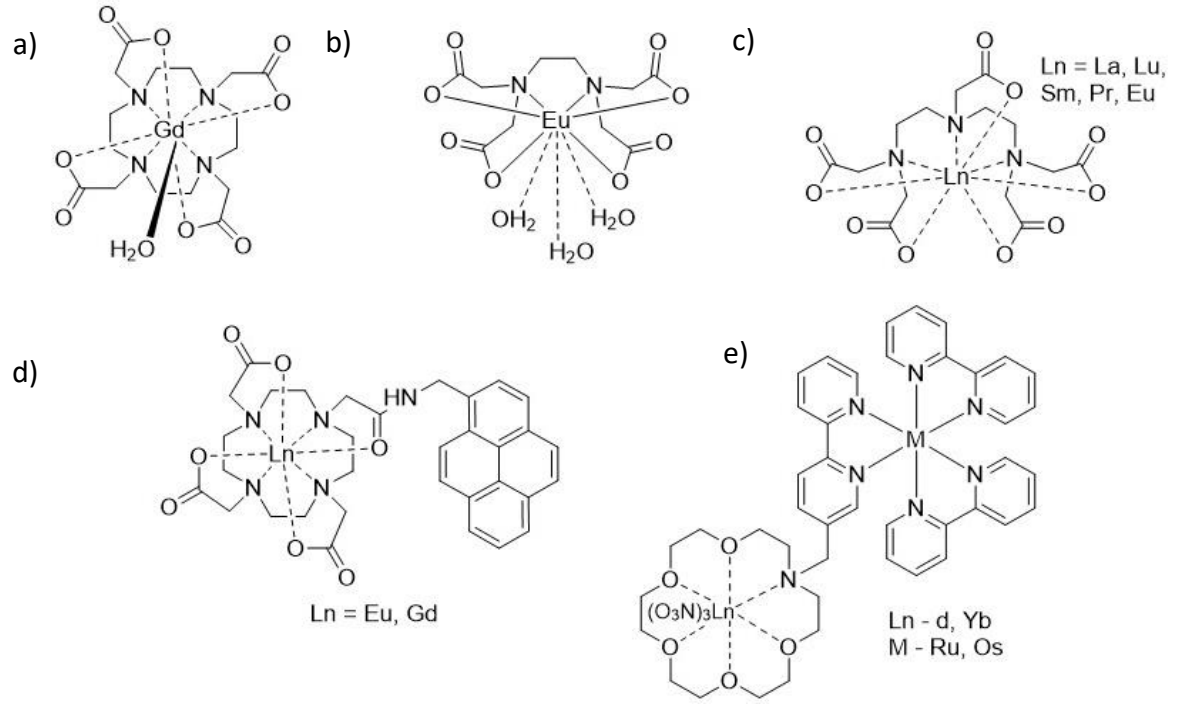


Figure 1 - 9 Examples of lanthanide complexes possessing strong ligand backbones. Based on a) DOTA,[34] b) EDTA,[35] c) DTPA,[36] d) functionalised DO3A,[37] and e) a macrocycle[38]

Complexes that possess high thermodynamic and kinetic stability are also sought after with respect to metal ion dissociation. Ideally, these complexes would saturate the coordination shell of the metal ion, and this would prevent saturation with water molecules.[11] In total, these factors combine to create complexes where demetallation is highly unfavourable, with an increase in stability as charge density on the metal ion increases. This causes stronger electrostatic metal-ligand interactions.

1.9 USE OF LANTHANIDES

1.9.1 IMAGING AND MAGNETIC RESONANCE IMAGING

Molecular imaging is a process that enables study of biological processes *in vivo* non-invasively through a range of modalities to view at the cellular and molecular level. Magnetic Resonance Imaging (MRI) is one of the most evolved methods and is a prominent technique in biomedical research and diagnostic imaging. It can provide physiological information in the early stages of clinical investigation,[41] and offers fast scanning capabilities with quality resolution images and a lack of ionising radiation.[42]

For a lanthanide complex to be successfully cast as an imaging agent it is important that the complex can be absorbed by the cell, which can enable exploitation of the inherent luminescent properties to generate an image. The mechanism of this cell uptake is usually dependent on the aromatic chromophore bound to the complex.[43] Due to the aforementioned parity and spin forbidden nature of the *f-f* transitions in these elements, emission is long lived and this characteristic is exploited in optical probes, bioassays, and other medical applications including imaging.[44] This also, however, results in very low molar absorption coefficients. As a result, lanthanide luminescence is often sensitised through employment of the antenna effect.

Toxicity of the chosen contrast agent is also of vital importance, as lanthanides are generally of moderate to high toxicity by nature, though the extent of this is dependent on whether the lanthanide is a free ion or bound, the route of administration, and the dosage applied.[45] Whilst predominantly chemical in nature, their toxicity is based on competition with calcium in biological processes, and their interactions with cells and tissues have potential to induce both radiation and chemical toxicity.[45] Toxicity also arises from effects of colloidal precipitate

formation and accretion in membranes,[46] and they possess the ability to inhibit lymphocyte activation, neutrophilic chemotaxis and aggregation among others. Through displacing and competing against calcium for their binding sites, lanthanides inhibit the electron transport process in mitochondria, leading to neurotoxic effects, interrupted axonal activity, and inhibited contractions in cardiac muscle.[45]

Previously studied animal models suggest that absorption of lanthanides in the gastrointestinal (GI) tract is poor[47], and after administration form colloidal hydroxides or phosphates within blood. This eventually accumulates up to 78% of the original dosage in organs including but not limited to the liver, spleen, kidney, pancreas, and in the bones.[45] Chelated lanthanides are removed from the body much more rapidly compared to their free ion counterparts, with whole-body half-times of only several hours compared to days. This removal can also be sped up through administration of a calcium or zinc DTPA ligand to minimise the risk of acute toxicity, a phenomenon thankfully rarely reported in humans.[47]

Several characteristics of the lanthanides enable their exploitation in fields such as biomedical imaging. Time-gated luminescence can utilise these complexes due to the longer lifetime of their luminescence. In this method, the detector is delayed so that upon activation of the detector the majority of biomaterial has returned to the non-emissive ground state, resulting in signals primarily consisting of the targeted complex.[48] Determination of the chemical shift and spin relaxation behaviour of proximal nuclei around the metal centre is influenced by the size and directional dependence of magnetic susceptibility when in a magnetic field.

In particular, the relative size of principal orthogonal components is important. The electric susceptibility tensor's magnitude and anisotropy proves a defining factor for observed optical transitions when under molecular symmetry constraints.[49] MRI demonstrates the greatest

spatial resolution and clinical potential in comparison to other methods such as X-Ray and computerised tomography (CT) Scanning, however it is limited by low sensitivity, and is less effective in comparison to radio-nuclear methods like positron emission tomography (PET) and single-photon emission computerized tomography (SPECT). It relies on relaxation enhancement of local tissue water protons in association with a contrast agent. **Figure 1 - 10** provides a comparison of the imaging capabilities of X-Ray, CT, and MRI scans.

A redox-responsive MRI response can be created using contrast agents where a redox reaction is induced either on the metal ion or the ligand. Gadolinium is not redox responsive, however other lanthanides such as europium which demonstrate activity can be utilised. Other methods of analysis through contrast mechanism can be adapted, including Paramagnetic Chemical Exchange Saturation Transfer (paraCEST) or ^{19}F MRI. It is also important to understand what happens to the luminescence complex within a cell-imaging probe once cellular uptake is accomplished.[5]

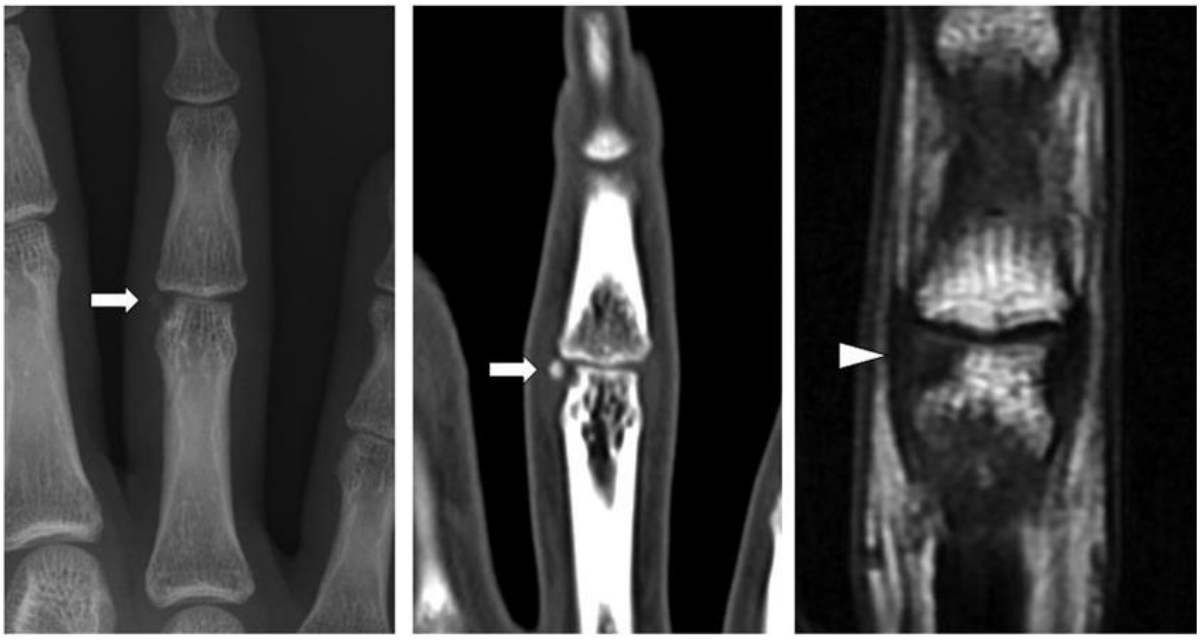


Figure 1 - 10 Comparison of images obtained through X-Ray (left), coronal CT (middle) and T1-weighted MRI (right). Taken from Takata *et al.*[50]

There are two types of contrast agent depending on whether they induce longitudinal relaxation or transverse relaxation. These describe the amount of time taken for protons to realign with the external magnetic field and exchange energy with other nuclei respectively, abbreviated as T_1 and T_2 and representing the relaxation times of the tissue water.[41, 51] The ability of a contrast agent to affect these relaxation times is denoted as r_1 and r_2 respectively.

Gadolinium (Gd)-based contrast agents are some of the most frequently used MRI contrast agents, particularly in areas of research pertaining to detection of cerebral and medullary tumours.[52] They have also been used in enhancement of T_1-weighted MRI for imaging of the central nervous system for detection of metastases in what has been referred to in past as an 'optimal method'. Gd compounds are most used due to their thermodynamic and kinetic stability, which utilises the unique magnetic properties of the ion to enhance the relaxation rate. Two commonly used contrast agents in commercial use are Magnevist® and Dotarem®, which are complexes that bind a Gd atom within linear DTPA and cyclic DOTA respectively.[41] A summary of these and other Gd-based contrast agents can be found in **Figure 1 - 11**.

Gd-based contrast agents generally have excellent safety profiles due to the well-encapsulated nature of the lanthanide ion within these chelated polydentate ligands and are heavily used within the medical field for imaging purposes. They have been proven to be well tolerated in patients excluding those suffering from renal failure,[39, 53] and demonstrate the high kinetic and thermodynamic stability required of lanthanide-based complexes for use. These complexes in particular are stable as due to the primarily ionic bonding nature of lanthanides such as Gd, they are able to form stable complexes through binding to these charged ligands as well as macrocyclic ligands with pendent donor groups.[46]

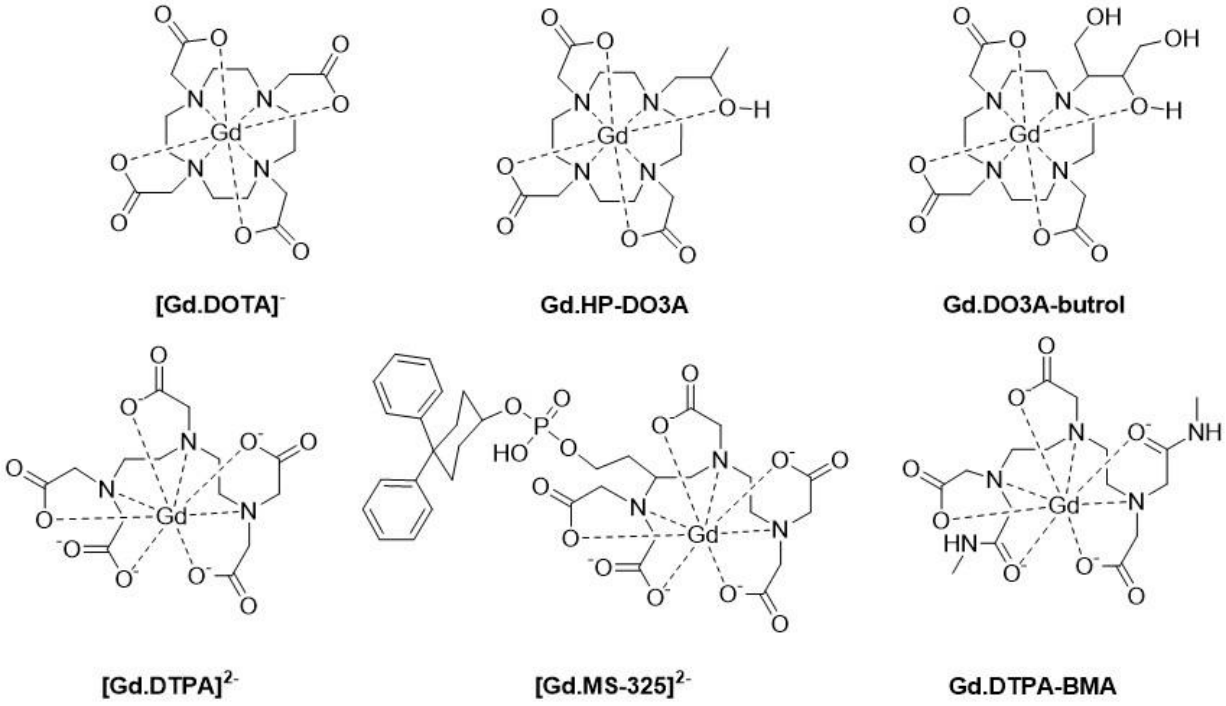


Figure 1 - 11 Some of the clinically used Gd-based complexes. In order from top left to bottom right: Dotarem®,[54] Prohance® functionalised with HP,[55] Prohance® functionalised with butrol (also known as gadobutrol),[56] Magnevist®, Angiomark®,[57] and Omniscan® [58]

1.10 Key Biomarkers

1.10.1 Oxygen

Organisms possess both extracellular and intracellular redox states, both of which are heavily regulated. Dysregulation of these is associated with several pathophysiological conditions such as chronic inflammation and ischaemia. Lack of oxygen in cellular tissues results in hypoxia, which affects the metabolism and physiology of cells,[59] and this is especially important with regards to tumours,[42] as tumours that grow rapidly require high oxygen levels which promotes angiogenesis in the cancer cells. In cancer treatment, hypoxia has a significant effect on its progression, and is associated with a poor diagnosis.

Tumours have also shown instances where in solid growths, hypoxic regions are observed.[59] Hypoxia and ischemia are still yet to be fully understood, however, and this is further limited by the difficulties in performing real-time measures of concentration. Though difficult, determination of oxygen concentration is essential for fields such as biological and

environmental science. The tissue redox state is essential in many physiological and pathological processes[42] and can be exploited through a variety of redox-responsive MRI probes.

This process, however, is dependent on complicated equipment or calibration and can generate unwanted by-products in the process. To facilitate an easier process of quantification, sensing devices that rely on more simplistic and affordable instrumentation is required.[60] Ratiometric luminescent sensors have proved a suitable answer for this problem. Europium and terbium are the most luminescent lanthanide ions, with terbium being the most luminescent, however europium has the distinct difference of being redox active where terbium is not. This has led to investigation into the viability of europium complexes as redox probes.[44] Other lanthanides such as cerium and praseodymium have also demonstrated redox behaviour.[61]

1.10.1.1 Singlet Oxygen ($^1O_2$) and Reactive Oxygen Species (ROS)

The term reactive oxygen species (ROS) particularly encompasses chemicals formed from incomplete reduction of oxygen,[62] and these are believed necessary for regulation of standard physiological functions. Similar terms are used for reactive sulfur (RSS) and reactive nitrogen (RNS) species. Biologically, these free radicals originate through oxidative metabolism within cells, producing specialised products. These include hydroxyl radicals (HO), the superoxide anion (O_2^-), singlet oxygen ($^1O_2$), as well as the oxidant hydrogen peroxide (H_2O_2).[63] One of the key functions of this subclass of molecule is the heavily regulated homeostasis of the reduction and oxidation (redox) pathways.

Early exposure to oxidative stresses has been linked to the potential risk of lifelong consequences, however this risk is heavily dependent on context such as the location, timing,

and local environment. In recent years, the causes of this oxidative stress (ROS or oxygen-containing radicals and their reaction products) have been recognised as signalling intermediates, responsible for adaptive or maladaptive molecular responses. A major source of ROS generation is mitochondria, where uncoupling of electron transport has been observed.[63] Other structures such as cytoplasmic enzyme systems, endoplasmic reticulum-bound enzymes, and plasma membrane surfaces have also been found to contribute.

Reactive oxygen is an extremely important component in the synthesis and use of some lanthanide complexes, as oxygen sensors work by collision due to the inability of probes to directly quantify oxygen. This collision involves the triplet states of both oxygen and the ligand, and when collision occurs, the ligand triplet state converts to the ground states. This then generates a ROS through a Diels-Alder mechanism, seen in in Equation 1.7:

$$S_1 + {}^3O_2 \leftrightarrow S_0 + {}^1O_2 \qquad \textbf{Equation 1.7}$$

For this to occur, overlap between the lowest unoccupied molecular orbital (LUMO) and highest occupied molecular orbital (HOMO) is required as seen in **Figure 1 - 12a**. Generally, probes designed for measure of oxygen also consequently generate ROS as by-products and are reliant on simple machinery, data processing and collection. This complicates matters. In an ideal situation, a probe would solely measure the oxygen concentration without the generation of by-products. An example is provided in **Figure 1 - 12b**.

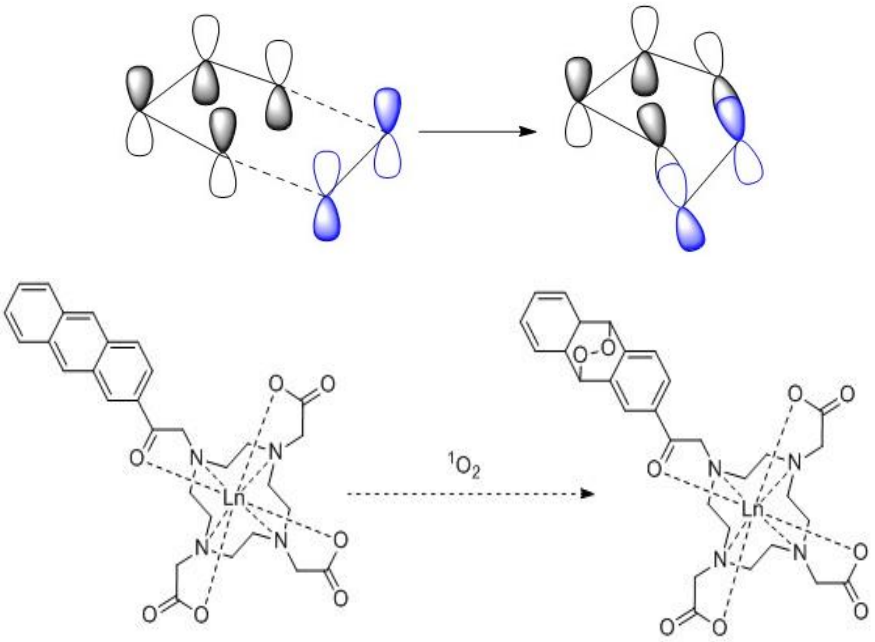


Figure 1 - 12 a) The required molecular overlap of the diene HOMO (black) and the dienophile LUMO (blue), showing the molecular symmetry of the orbital orientations, allowing for the symmetry-allowed Diels-Alder mechanism to occur b) an example of an ideal Diels-Alder mechanism in a lanthanide complex through reaction with singlet oxygen

Changes in luminescence intensity are also observed when energy transfer occurs between the lanthanide and chromophore. **Figure 1 - 13** demonstrates the pathway in more visual detail. Within this report, the complexes reported generally follow a Dexter-like exchange, as the antenna chromophore interacts over a longer distance with the centrally bound lanthanide. In this process, energy transfer occurs from the ligand triplet state to the lanthanide.[64]

Anthryl functionalised complexes have shown promise as potential systems capable of responding to oxygen biomarkers. With these complexes, the structure is not luminescent until reaction with oxygen, whereupon the oxygen triplet state converts to a single excited state upon collision with the chromophore excited triplet state. As a result, the complex reacts with the singlet ROS species as opposed to the triplet state sensitising emission, causing broken conjugation, and generating an endoperoxide system.

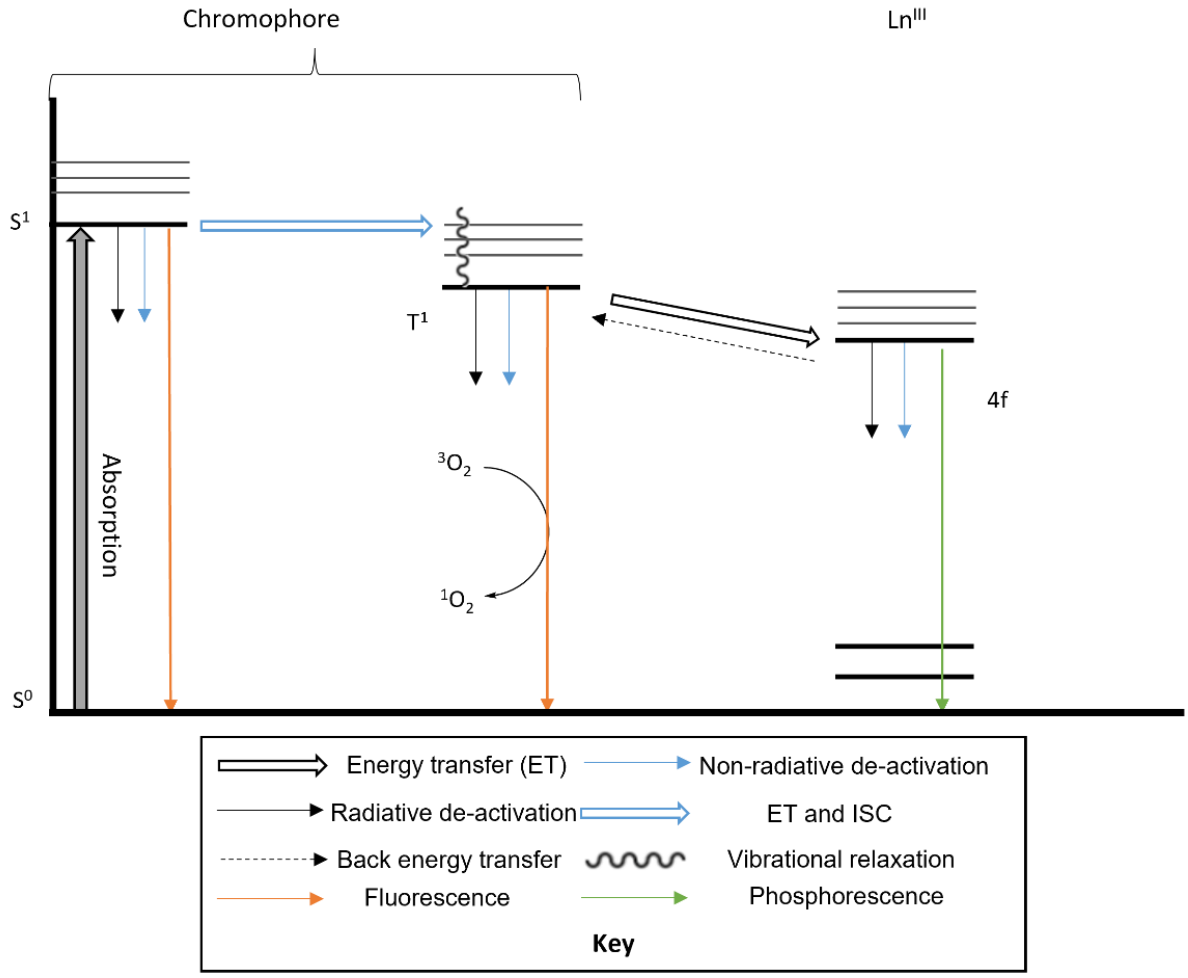


Figure 1 - 13 Possible pathways of action of a lanthanide complex

Singlet oxygen is the lowest excited electronic state of oxygen and is considered a toxic species *in vivo* due to its ability to oxidise several types of biological molecules such as proteins, lipids, and DNA. It is also suggested to play a role in pathways including but not limited to cell signalling,[62, 65] select antibacterial responses,[66] cell growth,[67] cell death,[62, 68] and changes in the pore transition capabilities of the mitochondrial membrane.[69] Photodynamic therapy (PDT) also utilises this oxidant to destroy malignant cells and tissues in cancer treatment.[70]

As $^1O_2$ has significance in both chemical and biological processes, detection of this molecule is of paramount importance. Direct monitoring of emission is possible at λ = 1270 nm; however, this results in a weak signal due to the decrease efficiency of emission.

Monometallic lanthanide luminescent probes are most commonly used in detection of dissolved oxygen concentration, however their primary weakness lies in their monometallic nature with only one emissive chromophore.[59] This means that determination of the source of weak emission is impossible, and it is indeterminate whether it is caused by high oxygen concentration or low complex concentration.

1.10.1.2 Oxygen and Cancer

Higher levels of ROS are often found in cancer cells due to the increased metabolism and dysfunction within the mitochondrial cells. This adaptive change is deemed necessary for progression, metastasis, tumourigenesis, and resistance to chemotherapeutic treatments. Subsequently, this increase also provides the opportunity to activate various apoptotic pathways and/or inhibit chemotherapeutic resistance. This is possible through generation of ROS and/or inhibition of antioxidant defences. Regulation of cell signal transduction and apoptosis pathways can also be undertaken by these ROS, indicating the large variety of biological processes influenced by the presence of these species.[62] When intracellular levels of ROS are found, damage to proteins, nucleic acids, membranes, lipids, and organelles can be found, inducing various cell death processes such as apoptosis.

Europium has been previously tested and proven as a redox-responsive MRI agent as Eu^{3+} chelate complexes, and has been used in diagnosis of blood flow and strokes.[71] Other lanthanides such as dysprosium have been investigated regarding their potential as a contrast agent with high magnetic field properties. Other uses of these lanthanide complexes extend potentially to X-Ray PDT cancer treatment and other more specific functions such as identification of specific proteins. As an example, both ytterbium and erbium are combined with $NaYF_4$ for detection of alpha-fetoprotein and carcinoembryonic antigen (CEA) respectively.[72, 73]

Previous fluorescent probes have been crafted using anthracene bound into a xanthene ring. These give sensitive fluorescent responses, however they are limited to higher pH values[70] and by steady-state investigations. Complexes such as $Ru(bpy)_3^{2+}$ are quenched by oxygen through exploitation of the interactions observed between the triplet ground state and the triplet excited state of molecular oxygen[59]. These complexes can quantify oxygen[74] which has

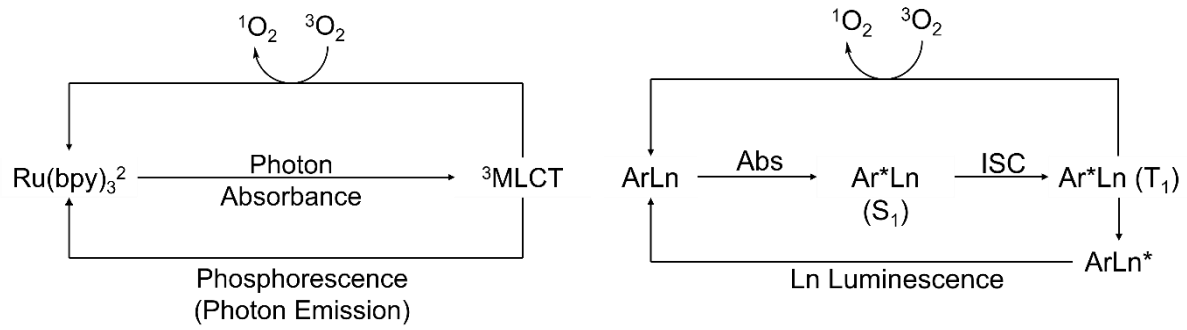


Figure 1 - 14 Possible pathways of action for Ru(bpy) (left) and a lanthanide complex (right)

two potential pathways that can lead to ground state regeneration: oxygen collision or phosphorescence as seen in **Figure 1 - 14**. Oxygenation is only possible if oxygen is present and as the concentration of oxygen increase, the probability of the phosphorescence pathway decreases. Similar exchange pathways are observed in lanthanide complexes, where fast k_{et} means a Dexter pathway and T_1 should quench before collision with oxygen can occur. This would result in no ROS generation.

1.10.2 Hydrogen Sulfide (H_2S) and Reactive Sulfur Species (RSS)

RSS is the term given to redox-active sulfur compounds. These are compounds that can oxidise or reduce molecules in physiological conditions and include other species such as disulfide-S-oxides, thiyl radicals, and sulfenic acids. The base structures of these RSS species can be seen in **Figure 1 - 15**. These reactive species can be free radicals,[75] which are defined as having at least one pair of unpaired electrons. Not all species demonstrate this

characteristic though, as $^1O_2$ and many RSS are non-radicals that remain classified as reactive. One example important to this thesis is the RSS H_2S.

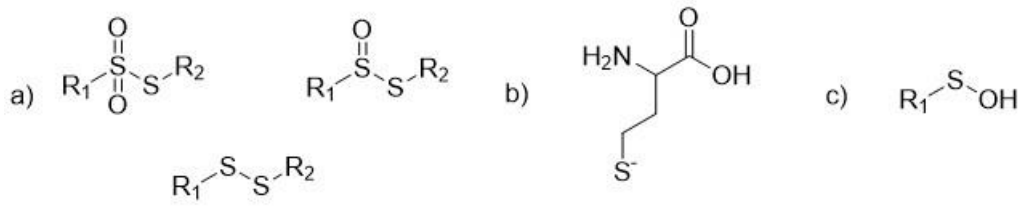


Figure 1 - 15 Base structures of the RSS species. a) disulfide-S-oxides, b) thiyl radicals, c) sulfenic acid

Studies of H_2S have previously identified it as a factor in the regulation of tumour cells and their biology.[76] Colon cancer cell lines and tissues in particular have been observed to overexpress cystathionine-β-synthase (CBS) in efforts to maintain cellular bioenergetics and grow, which in turn stimulates production of H_2S. This encourages tumour angiogenesis, extending the tumour's blood supply reach. When inhibition of CBS is induced, *in vivo* studies show inhibition of tumour growth. *In vitro* studies further demonstrated inhibited cell growth and spread, and suppressed cell responses.[77]

Within organisms, most signalling molecules act on receptors and/or enzymes through binding, but this is not observed with H_2S because of its chemical properties and their role in biological functions. It is important to consider these properties before using H_2S in any therapeutic models and studies, including but not limited to acidity, water solubility, and reductant ability. When in equilibrium with other species such as nitric oxide (NO) in aqueous solution, H_2S is observed to be weakly acidic (at 37 °C pKa is 6.76) and forms two dissociation states (pKa levels at each are 6.88 and 19 respectively)[78]: the sulfide anion $(S^2)^-$ and the hydrosulfide anion (HS^-) as seen in Equation 1.8: [79, 80]

$$\boldsymbol{H_2S \leftrightarrow HS^- + H^+ \leftrightarrow S^{2-} + 2H^+} \qquad \textbf{Equation 1.8}$$

This results in approximately 81.5% HS^- and 18.5% dissociated HS^- and undissociated acid respectively.[81, 82] Sulfide can also be generated, but this is very minor as the second dissociation step has such a high pKa.[78] Another property of H_2S that is potentially problematic is its ability to be oxidised, which can lead to SO_2 and persulfide for example, which possibly have their own biological activities that may interfere.

This has been previously reported in ovarian cancer cells, and separate studies of cells in both animals and cancer patients have suggested that H_2S derived from cancerous cells additionally acts for tumour growth as an autocrine stimulator.[76] One major difference between cancerous and non-cancerous cells in this context is the location of CBS[76] – in cancerous cells CBS is primarily found in the mitochondria, where in normal cells it is predominantly found in the cytosol of the cell. In the mitochondria, these levels are regulated via proteolytic processes such as the Lon protease.

Research on H_2S has led to two approaches for therapeutic treatment involving sulfide-based treatments – inhibitors of either CBS or cystathionine-γ-lase (CSE). Both of these methods lead to suppression of endogenous sulfide formation, and suppression of H_2S-releasing compounds and gas. Another possible treatment involves modulation of the endogenous H_2S pathways, which could be involved in pharmacological actions of some of both approved and experimental drugs. A previous study that explored the potency vs biological efficacy of several H_2S inhibitors (structurally unrelated) found differences *in vitro* and *in vivo*, with DL-propargylglycine (PAG) proving the least potent in the former, and the most effective neuro-protectant in the latter.[83] Conversely, the most potent inhibitor aminooxyacetic acid showed protective properties against stroke at low doses, and worsens the pathology at higher doses. **Figure 1 - 16** provides the chemical structures of these inhibitors.



Figure 1 - 16 PAG (left) and aminooxyacetic acid (right)

There are several methods that allow for detection of H_2S including gas chromatography with flame photometry, fluorescent probes, colorimetric methylene blue, monobromine assays, and ion-selective or polarographic electrodes. These methods, however, are not sensitive or rapid enough to meet near real-time detection of physiological H_2S concentrations.[78] Additionally, these techniques often involve tissue and cell lysate destruction, and can also require post-mortem processing. As a result, they are only capable of estimations of concentrations in the nano- to milli- molar ranges.[84]

The most common method used is the methylene blue method in which zinc or lead is used to trap the sulfur compound. Acidification is then performed and reacted with N,N-dimethyl-P-phenylenediamine (DMPD – see **Figure 1 - 17**), generating methylene blue which is detected using colorimetry. This process works best under acidic conditions but does not differentiate between bound and un-bound H_2S. This method has also been reported as lacking sensitivity and is limited in the level of H_2S it can detect, as it cannot detect nanomolar amounts.

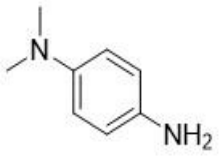


Figure 1 - 17 DMPD

Contrastingly, gas chromatography is a method that can detect such low levels and is also capable of distinguishing between acid-labile and free sulfide. Amperometry is another method of detection which allows for more direct measurement and monitoring of H_2S production in real time, but is limited by the calibration stability of the equipment which

requires frequent recalibration. Additionally, small quantities are difficult to detect. Another option for measurement is use of H_2S-specified probes to detect cell generation of H_2O_2 but this is not always adequate when measuring quantities in the sub-micromolar ranges.[85]

1.10.2.1 Probing H_2S in Biology

The common techniques used to detect H_2S previously discussed can detect H_2S in bulk measurements in tissue samples, cells, and serum, but are not adequate for detection of biological concentrations (high nano-molar to low milli-molar). Instead, fluorescence imaging probes using microscopy are used, which have higher sensitivity and compatibility with living cells and a greater spatiotemporal resolution.[86] These offer a better approach for H_2S detection as well as other small molecules because of their affinity for cell permeability and their high sensitivity.

Under mild conditions it is possible for azides to be selectively reduced by H_2S to generate amines, and this reduction can be used to create molecular H_2S probes.[87, 88] Previous studies have found that by attaching a functional azide group to rhodamine, sulfidefluor-1 (SF1) and sulfidefluor-2 (SF2) probes (see **Figure 1 - 18a**) with turn-on responses following H_2S-mediated reduction could be generated. This mechanism can be seen in **Figure 1 - 18b**.[84] These probes were also shown to be more selective for H_2S over a large range of other RSS compounds including glutathione and cysteine, and several ROS and RNS compounds. They have also proven capable of monitoring living cells for changes in H_2S.

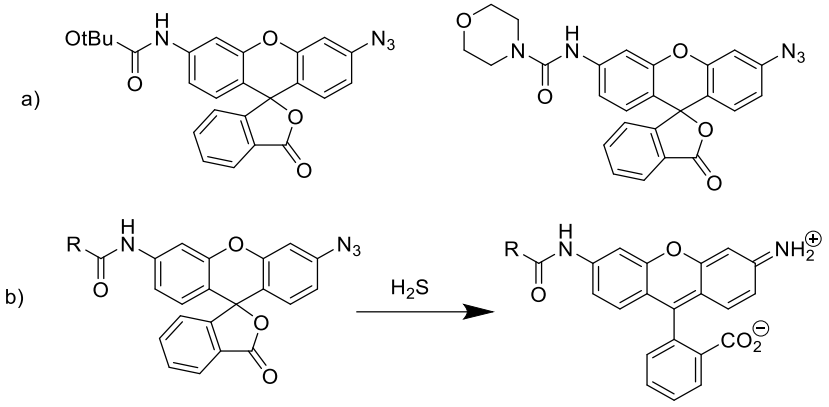


Figure 1 - 18 a) SF1 (left) and SF2 (right) and b) generalised interaction of SF1 and SF2 with H_2S[84]

SF2 was shown to possess more favourable fluorescence properties *in vitro*, with lower background reactivity to analytes, a greater fluorescence response specifically to H_2S, and a higher selectivity for other analytes including glutathione (by 5-fold), sulfite (4-fold), and superoxide (4-fold). SF1, however, demonstrated a higher affinity for turn-on response than SF2 in biological cell testing on HEK293T cells.[84] From these results, it can be determined that increased lipophilicity and cell retention can be attributed to the presence of the tert-butyl groups whilst higher selectivity is caused by the cyclic region in SF2.

Use of azides in this reductive manner activates the sensing group and induces a change in the efficiency of energy transfer between the lanthanide and the azide antenna chromophore. This was studied by Tropiano and can be seen in **Figure 1 - 19**.[89] Analysis of this reduced amino structure indicates that this is the only structure that forms. This structure demonstrated high selectivity for NaHS when compared to other reducing agents, Cl^-, and HCO_3^- among others, with only glutathione inducing an enhanced signal.

This signal, however, required four times as much sulfide and only produced a two-fold signal. These results indicated that selectivity for sulfide-containing species such as NaHS was much higher than other biologically relevant species. A linear response over a wide concentration range was observed, and it was also noted this structure had long luminescence lifetimes. This

was evidence for a stable metal centre and eliminated the possibility of sulfide coordination or displacement of solvent.[89]

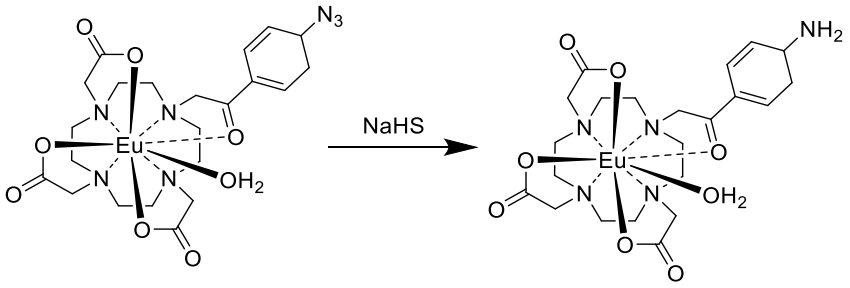


Figure 1 - 19 Reduction of an Eu^{3+} azide to an amine in the presence of NaHS. Adapted from [89]

These initial studies have since expanded to other fluorophore scaffolds, with one scientist developing a dansyl fluorophore with a sulfonyl azide[90] that has been shown to react rapidly with H_2S at extremely low concentrations (down to 1 µM) in phosphate buffer. A summation of this process can be seen **Figure 1 - 20a**. This releases a dansyl amide that possesses strong fluorescence and can detect between 5-100 µM H_2S in bovine serum upon UV detection (see **Figure 1 - 20b**).[90] Prior to reaction with H_2S, the dansyl fluorophore is itself non-fluorescent, and addition of hydrogen sulfide sourced from Na_2S shows 40-fold enhancement with a detection minimum of 1 µM which is attributed to dansyl amide formation.[90] Selectivity analysis studied reducing anions which showed no obvious response for the majority at 1 mM concentration, a substantially higher concentration than that selected for sulfide.

Other sulfur anions HSO_3^-, $S_2O_4^{2-}$, and $S_2O_5^{2-}$ were shown to be the only anions to induce an increase in fluorescence intensity, however this change was much smaller than the change induced by sulfide. This was seen to be the case even when anion concentration was up to 4 times higher than the sulfide. The only compound able to induce strong responses was benzyl mercaptan, and this poses a potential interference problem. Risk in this is minimal, however, as this is hardly ever present in biological systems.

Additional studies on this structure also suggested that biological substrates and anions generally found in blood do not negatively impact quantitative detection of hydrogen sulfide within a biological environment. Studies on mice also found the average sulfide concentration to be within previously reported concentrations.[90, 91] Overall, studies showed this probe has many advantages including its simple structure and synthetic route, affordability, general stability and stability in storage, fast response to sulfide, and high selectivity for sulfide over other anions. Other examples include azido-heptamethine cyanine dyes to function as a ratiometric fluorescent indicator[92]. These use an NIR heptamethine cyanine fluorophore combined with an azide structure to selectively detect for H_2S in both solution and bovine serum. They possess 'good cell permeability and negligible background fluorescence' and with this, confocal ratiometric imaging is also possible.[92]

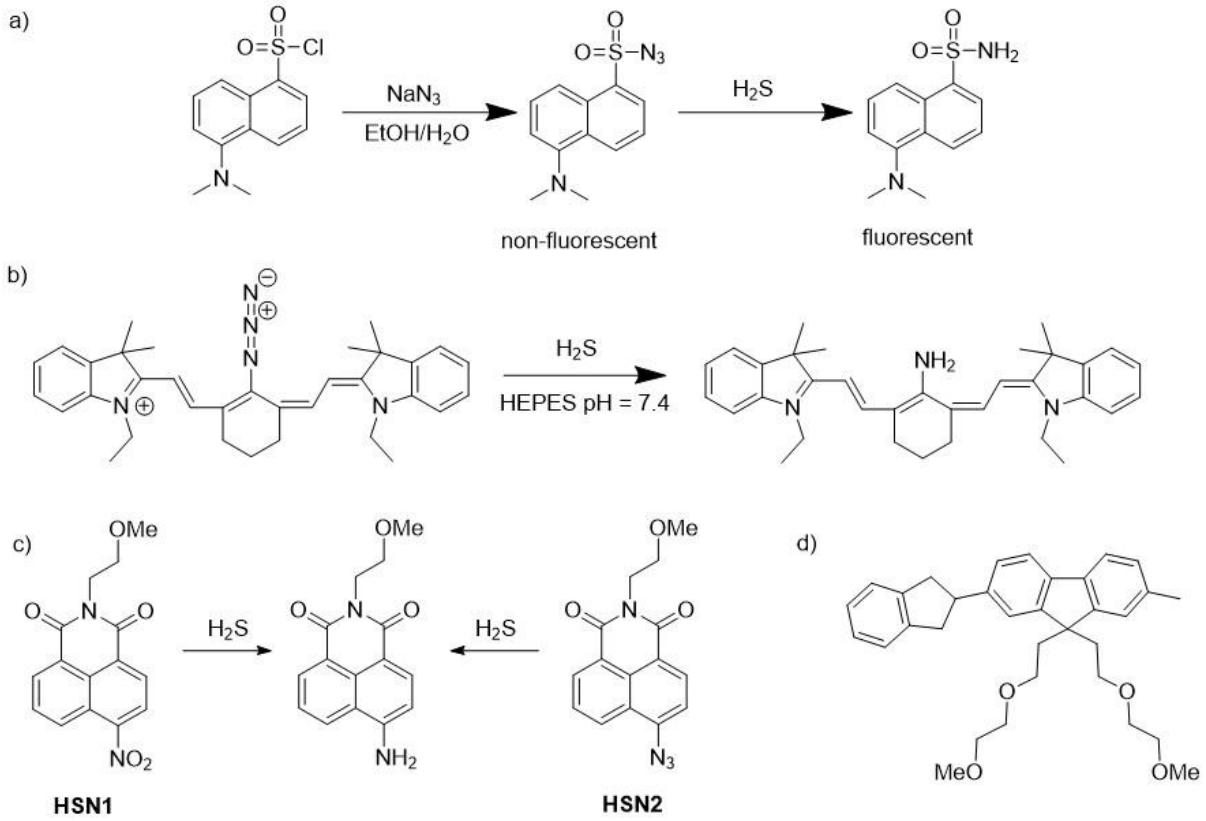


Figure 1 - 20 A summary of some of the key fluorescent probes for H_2S. a) a dansyl fluorophore with a sulfonyl azide[90]; b) an azido-heptamethine cyanine dye;[92] c) HSN1 and HNS2 and their interaction with H_2S[93]; and d) FS1[94]

Other options are a hydrosulfide naphthalimide-1 probe named HSN1 and a 4-azido-1,8-naphthalimide probe known as HSN2 which selectively react to create a turn-on response and can operate in living cells with a suitable signal-to-noise ratio (**Figure 1 - 20c**).[93] Both are weakly fluorescent in their unreacted state prior to H_2S addition, and post-treatment are both converted to fluorescent amines, though HSN2 shows a four times greater turn-on than HSN2 (60-fold after 45 min for HSN2 compared to 15-fold after 90 min for HSN1). HSN2 also showed less degradation in sensitivity tests when reacted with other reactive ROS, RNS, and RSS, and released a stronger intensity change when imaging in live cells.

A two-photon probe has also been generated using an azide-modified benzothiazole-fluorene[94] known as FS1 which has been used to image the presence of H_2S in slices of the rat hippocampus 90-190 µM deep (**Figure 1 - 20d**). Selectivity tests on this probe showed a higher selectivity for H_2S over other biologically significant RSS, RNS, ROS, and biological substrates including glutathione, cysteine, and 2-mercaptoethanol. These can be seen in **Figure 1 - 21**. Within cells, FS1 was also shown to be responsive to endogenously produced H_2S, showing substantial increase in two photon excited fluorescence when precursors of H_2S such as cysteine or glutathione were added.

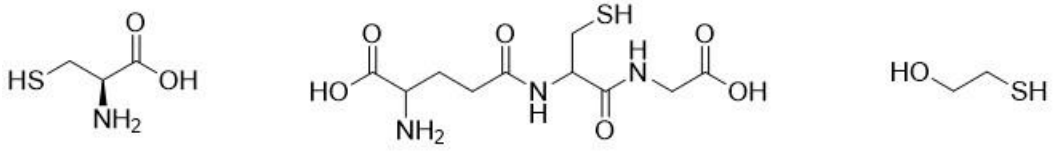


Figure 1 - 21 From left to right: cysteine, glutathione, 2-mercaptoethanol

An overall summation can be made that use of nitrogen within a structure is elemental to sensitivity to H_2S and other moieties including RNS, ROS, and other RSS species. However, variation within these structures indicates the overarching versatility of H_2S-sensing probes using azides as the key functional trigger has emerged. This has demonstrated the highest

sensitivity and fluorescence as opposed to NO_2 and other variants. Despite these promising attributes its ability to provide information on the mechanisms of hydrogen sulfide is limited, and more novel H_2S-releasing drugs are required to provide insight into this process.[90] Throughout this research, and by using and expanding this concept, it is possible to further modulate several factors including emission colours, imaging modalities, reactivity, and targetability.[87]

One alternative method of interacting with H_2S is through trapping it via nucleophilic addition and allowing detection of the analyte by the probe acting as an electrophile.[95] In the initial steps of nucleophilic addition, a thiol is generated which undergoes a second nucleophilic addition at a secondary electrophilic site causing cyclisation as seen in **Figure 1 - 22**.[96] This eventually generates a fluorescent molecule with strong fluorescence signal that is selective for H_2S over other biologically significant molecules like glutathione and cysteine. Another reaction pathway is through using a disulfide and ester group as two reaction sites for electrophilic interactions with H_2S.

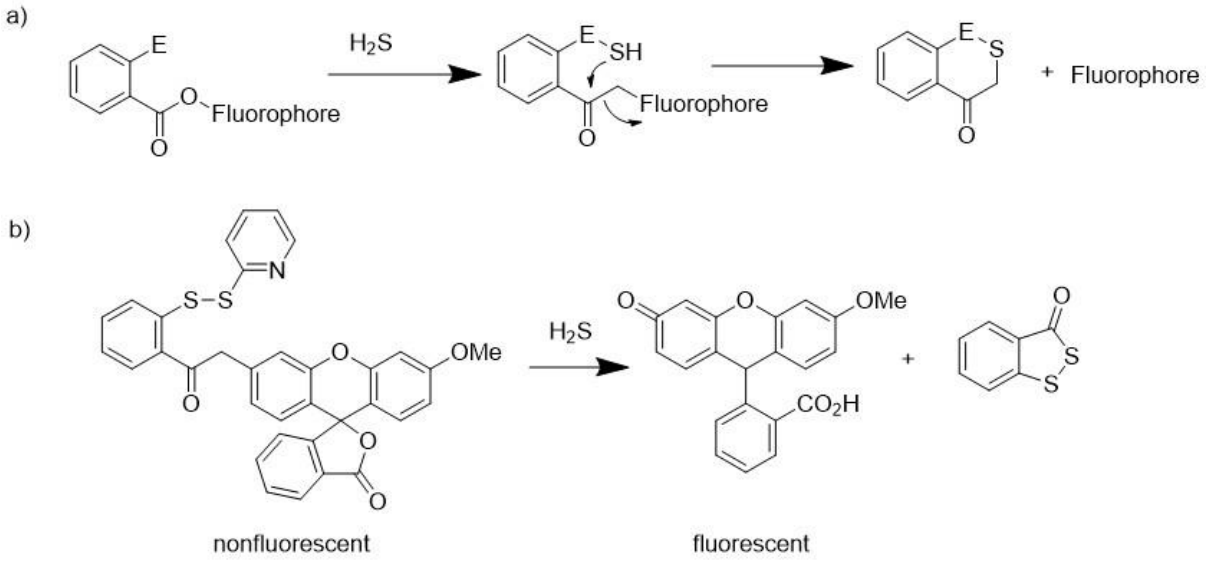


Figure 1 - 22 a) Interaction of a probe with H_2S showing generation of a thiol followed by cyclisation. E represents the electrophile; b) Example of a fluorescent probe reacting with H_2S through a Michael addition-cyclisation sequence to generate a fluorophore[96]

In particular, this probe is able to detect H_2S both quantitatively and qualitatively, as concentration was found to be linearly related to the fluorescence signal. Under fluorescent light, combinatory solutions of the probe and H_2S were seen to be highly fluorescent in colour. From this probe, further research can be made to investigate more H_2S-specific targetable fluorescent probes based on this structure.

When using 2-thiopyridine, a persulfide results when the ester is attacked by the terminal sulfur. This forms a benzodithiolone through cyclisation, releasing methoxyfluorescein in the process. This generates a probe that is capable of reacting with 50-500 µM H_2S when in bovine plasma, and 250 µM in cells.[87] *In vitro*, this shows H_2S selectivity over other thiols as displacing a thiopyridine with a substituted thiol, resulting in a non-cyclable disulfide. Additional probes have since been generated, also releasing methoxyfluorescein when reacting with H_2S, some examples of which can be seen in **Figure 1 - 23**.[97]

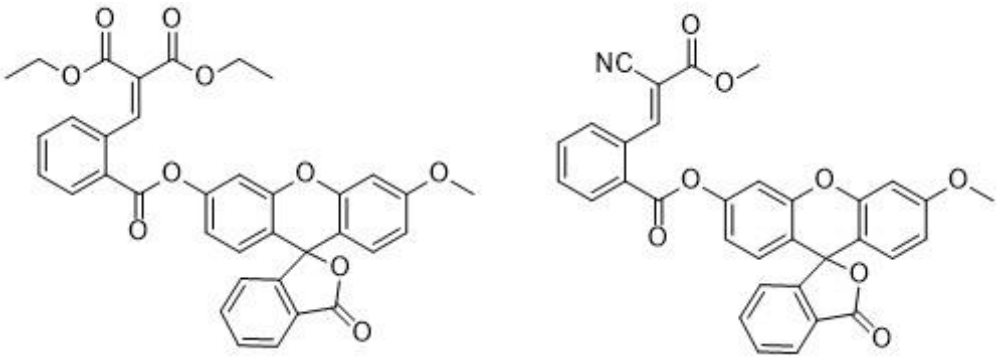


Figure 1 - 23 Michael acceptor-based fluorescent probes[97]

It is possible for biological processing of H_2S to use copper to detect it through fluorescence responses. One example was synthesised by Nagano,[98] which used a cyclen macrocycle attached to fluorescein where upon binding of Cu^{2+} to the cyclen the receptor quenches probe fluorescence. Examples of this structure can be seen **Figure 1 - 24a**. Fluorescence can also be observed with this biological probe via reacting with a sulfide donor (e.g., Na_2S, NaHS),

causing the precipitates CuS and unbound cyclen-AF to form. This probe is capable of rapid detection of sulfide *in vitro* down to 10 µM. A similar process was utilised by Zeng and Bai[99] to synthesise a sulfide probe via combination of fluorescein and a pendant 8-hydroyquinoline ligand to engage copper binding (**Figure 1 - 24b**). This coordination results in quenched fluorescence and induces a spectral shift upon conversion to a copper metal complex.

An advantage to using copper in combination with sulfur species is that combination of these elements generates formation of a stable CuS species. This shows more promise than other chemosensors, most of which developed for detection of sulfide ions are not of particular interest compared against anions including but not limited to fluoride and other sulfate forms. Alternative forms of probes include utilisation of metal-ion affinity, but these are generally irreversible and can cause potential issues in biological systems.[99]

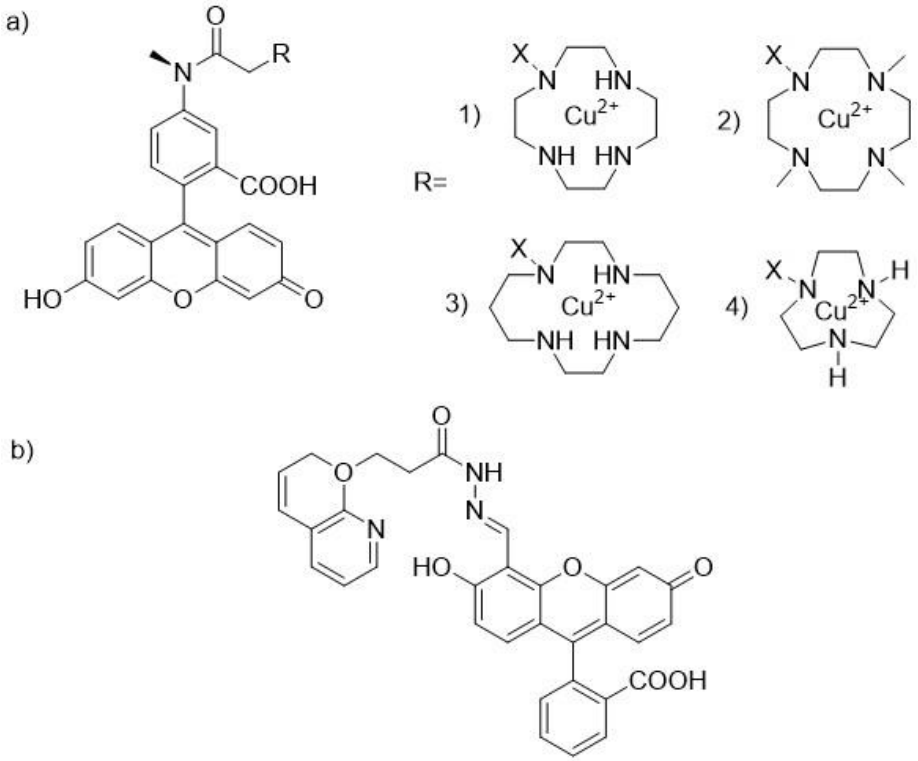


Figure 1 - 24 a) Macrocyclic fluorescein-Cu^{2+} complexes, where R = macrocycle + Cu^{2+} and X = macrocycle binding site. R1 = Cyclen-AF+Cu^{2+} (HSip-1), R2 = TMCyclen-AF+Cu^{2+}, R3 = Cyclam-AF+Cu^{2+}, R4 = TACN-AF+Cu^{2+};[98] 11b) a fluorescent sensor based on an 8-hydroxyquinoline receptor and fluorescein[99]

1.10.2.2 H_2S THERAPEUTICS

Whilst understanding and application of H_2S and its related sulfide groups has steadily grown and improved over the years, detailed understanding about the extent of its potential application in treatments and therapeutics is still required. Development of such treatments comes with concern with using H_2S or its various salt forms, however, with complications like its malodorous and volatile nature posing some of the most obvious concerns. Additionally, the delicate balance between protective and toxic concentration levels combined with the narrow therapeutic window means that doses of H_2S-based treatments must be administered in precise doses at specific times. This is further complicated by the body's maintenance of H_2S homeostasis through complex mechanisms.[78]

Treatments have been investigated regarding overdosing, intoxication, and toxic levels of H_2S. *In vitro* studies have determined that endogenous production of free radicals and oxidant species may be involved with sulfide's cytotoxic effects, which is potentially related to the *in vivo* toxicity H_2S demonstrates. In these *in vivo* situations, induced methaemoglobinaemia and sodium nitrite dosage have demonstrated protective effects against this toxicity.[100] Another option is preventative action through use of sodium hydrogen carbonate ($NaHCO_3$) which is thought to alter the inhibition of carbonic anhydrase by H_2S.[101]

Oxidised glutathione is another option for toxicity reduction, which is thought to occur via interruption of hydrosulfide reactions within 'key enzymatic disulfide groups'. In cases where sulfide intoxication is observed, oxygen therapy is used which demonstrates potential treatment against toxic H_2S doses given the consistent benefits reported in animals who have been dosed.[83] Two possible methods of dose administration are single bolus doses, or sustained and constant dosage. The bolus method, however, comes with some limitations. **Figure 1 - 25** visually demonstrates the pharmacokinetics of these dosage types.

Administration of a single dose would only result in a spike of H_2S and when redox chemistry is considered, it is possible it will change the cellular redox states. This effect could then potentially extend past the H_2S-specific functions and impact others. Distribution of H_2S and its sulfide relatives must also be taken into consideration, as distribution of the various sulfur states can vary dramatically from the physiologic state[78] and it is well known that persulfides can influence other biological processes on their own. Some suggestions have been made that polysulfides and thiosulfates are the active molecules responsible for persulfide formation rather than H_2S, but this has yet to be confirmed.

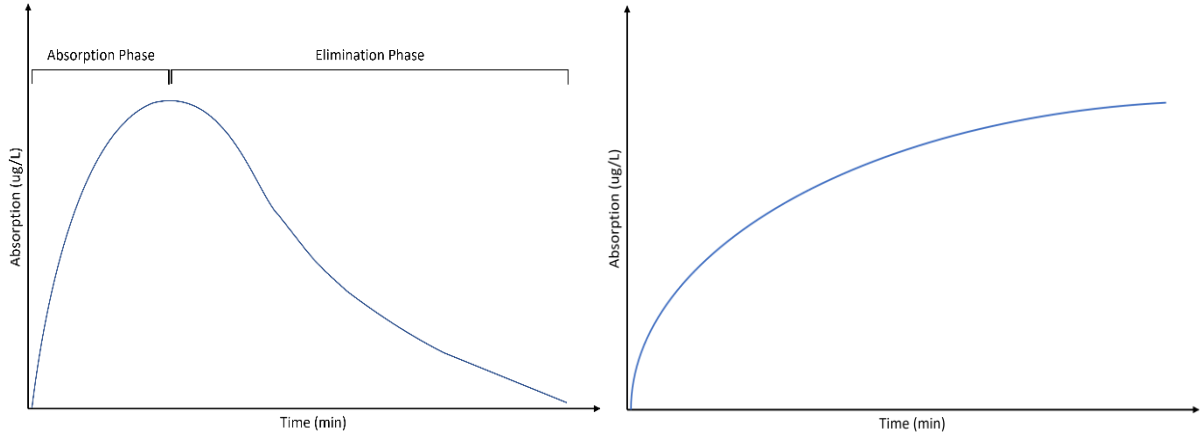


Figure 1 - 25 Pharmacokinetics of a bolus dosage (left) and steady state dosage (right)

The concentration of each sulfur species could also be problematic, as using different H_2S donors at the same concentration does not mean they will end up equal. Release rates and oxidation states of each molecule play a significant role in this natural variation. This could interfere, making studies on them difficult, and any results physiologically irrelevant. Ideally, pure polysulfide donors would be used, but synthesising these compounds at high purities has proved a challenge for scientists. The variations in concentration also pose a problem as the ideal concentration range for sulfide compounds in physiology and therapeutics is not known, and homeostasis-inducing endogenous H_2S concentration limits are still under scrutiny.[78] Current studies have reported levels between 0.1 and 300 µM, but specifics are

still unknown. Conservative estimates guess healthy levels of plasma H_2S to be between high nanomolar to low micromolar concentrations.

One condition of using sulfide treatments is that sulfide is an endogenous compound, which means that any exogenous sulfide delivery systems would need to pass strict safety and efficacy in preclinical animal studies before tests move to human subjects. Another possible hurdle is inferior efficacy when compared to pre-existing therapies, side effects limiting dosage levels, issues with manufacturing and formulation, and low therapeutic index.[83] A possible method of developing these treatments is to link sulfide-releasing moieties with existing drugs, or exploitation of sulfide-precursors or prodrugs that induce sulfide production. For neurodegenerative diseases like Alzheimer's, Parkinson's, Huntington's, and ALS treatments are focused on delaying or stopping advancement of the inflammation associated with these diseases.

1.10.3 Nitrobenzene (NO_2) and Reactive Nitrogen Species (RNS)

Nitroaromatics are a class of compound being more frequently used and investigated in industrial and biological applications. Identified by the presence of at least one nitrogen dioxide (-NO_2) group attached to an aromatic ring, they are primarily synthetic in nature. In recent years, however, studies have shown the presence of some organic structures with this functional group as well. Metabolism of structures possessing this functional group remains of tantamount significance as whilst they are attached valuable economic importance, they have potential to be hazardous to human health and must be thoroughly investigated.

RNS include species like nitric oxide (NO), nitroxyl (HNO), NO_2, and peroxynitrite ($ONOO^-$). $ONOO^-$ is a more recent addition to this list, and is formed through reaction of NO with superoxide O_2^-,[102] whilst its protonated ONOOH form (also written as HNO_3) decomposes over

time to generate NO_2 and OH^-. These RNS species can be interconverted or reacted with ROS to generate other RNS or ROS species, as described by Kwon *et al.* in 2021 and seen in **Figure 1 - 26.**[102] NO can also be generated endogenously by nitric oxide synthases and requires a precise homeostasis to be maintained. Failure to maintain this can result in cancer, stroke, and neurodegenerative diseases.[103] Damage to cells by RNS is found to be possible through induced nitrosative stress, though $ONOO^-$ can also impart damage through oxidation of DNA, proteins and lipids.[102]

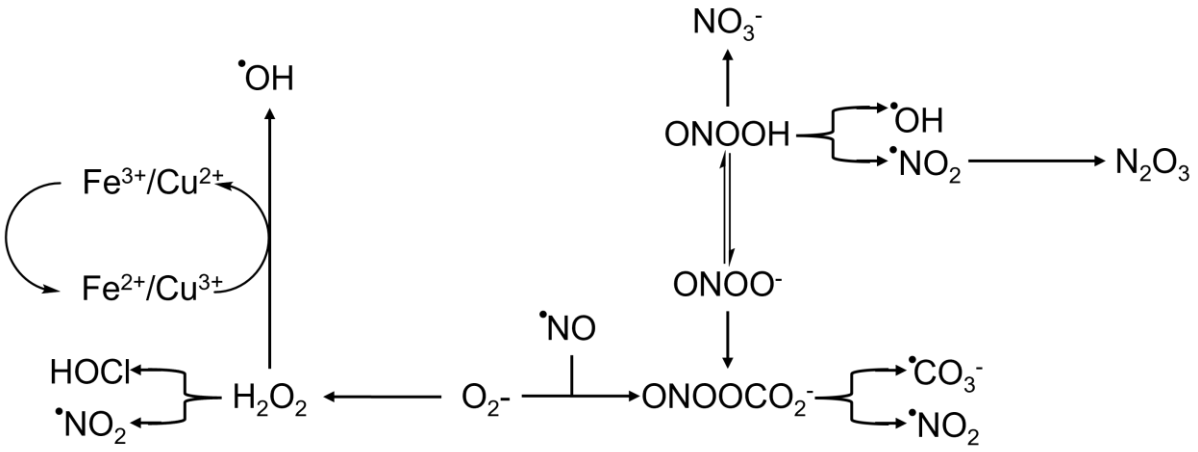


Figure 1 - 26 Selected conversion pathways of ROS and RNS, modified from Kwon *et al.* 2021[102]

This nitroaromatic component is known to show strong deactivation towards electrophilic aromatic substitution of benzene, as when the nitro group is attached to said aromatic it delocalises the π-electrons of the ring in order to balance its inherent charge deficiency. In this pairing, the electronegativity of this nitro group originates from the combined actions of the oxygen atoms, which are found to be electron deficient and bonded to the nitrogen atom. This results in partial positive charges at *ortho* and *para* positions that repel electrophiles and directs attacks to open *meta* positions, allowing for targeted binding.[104] When attached to a benzene ring specifically, the nitro group delocalises the π-electrons to neutralise its inherent charge deficiency,[104] providing the molecule with charge and inducing properties in the subsequent structures that make it a useful synthetic tool.

Synthetic xenobiotic compounds that are released into the biosphere can prove problematic for organisms due to the potential inclusion of unusual chemical bonds or functional groups,[105] which can render such structures resistant to the progressive microbial degradation found in natural organic compounds. Studies on nitro-substituted compounds initially found few naturally occurring structures, as most were found in antibiotics. This class of compound is an important intermediate in the synthetic process of several thousand consumer products, with estimates of up to 10% of sales within the chemical industry involving at least one step with a nitroaromatic structure.[106] As an example, combustion of fossil fuels involves the generation of polycyclic nitroaromatic structures, which are frequently highly mutagenic in nature.

Production of plastics, dyes, and other rubber-based chemicals utilise nitrobenzene and dinitrobenzene derivatives, whilst pentachloronitrobenzene is used in fungicide. The result of these processes is a bio-source of nitroaromatic compounds derived almost exclusively anthropogenic in nature.[105] Additionally, lingering effects from the war industry prevail, with heavy contamination of soil by nitroaromatics still present at sites of former World War II manufacturing and storage facilities.[105] This is most notably found in the United States and Europe.

It is feasible to accomplish bioremediation of these compounds by targeting the more water-soluble solvents and pesticides containing these nitroaromatics, though several barriers to their use are found. This includes but is not limited to their toxicity to microorganisms and low bioavailability due to insolubility. These must be taken into consideration and dealt with to ensure effective treatment via biodegradation.

Bioremediation of these compounds is especially important as their toxicity includes but is not limited to carcinogenicity, skin and eye irritation, allergic reactions, and mutagenicity. The mechanisms of the biological activities of such compounds is imperative, and one method through which this is achieved is through study of the reduction potential.[107] This is often defined as the measure of their ability to accept electrons, as a greater reduction potential means a higher propensity for electron affinity. This reduction of nitroaromatic compounds in particular is linked to potential activation of their toxic and mutagenic properties,[108, 109] or conversely remediating the compound and reducing these properties, indicating that their reduction potential is of tantamount importance.

When reducing different nitro-based compounds, this is often achieved with ammonium sulfide, or hydrogen sulfide in an alcoholic solution that also contains ammonia. Depending on the reducing agent chosen, the conditions and overall rate of reduction differ which subsequently alters the products formed. This is also influenced by the number such nitro-based substituents, with mononitro derivatives of aromatic hydrocarbons attacking slowly at standard temperatures, whilst 1,3-dinitrobenzene is readily and completely reduced to give monoamino-compounds. The latter also demonstrates an observable increase in reduction rate parallel to the rise in temperature, though it is noteworthy that tarry products are formed when too much ammonia is used, affecting the yield.[110]

Comparison of these structures could lead to the conclusion that as the number of nitro groups increases, so does the rate of reduction, however this is not always observed, as dinitro- and trinitro-*m*-xylenes, and dinitromesitylene (examples of which can be seen in **Figure 1 - 27**) are only able to be reduced after prolonged exposure to ammonium sulfide at high temperatures. The reduction in this reaction pathway timing can be attributed to the

presence of the additional methyl groups combined with the presence of amino groups rendering the nucleus more basic, causing the nitro groups to be less inclined to be reduced.[110]

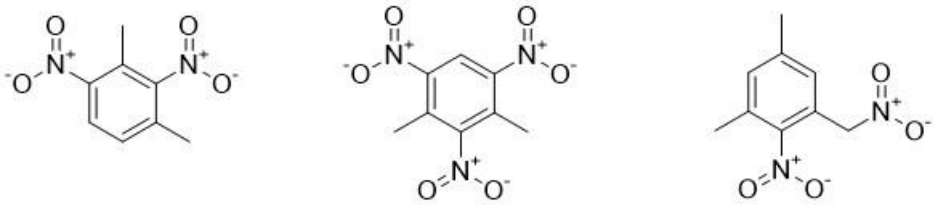


Figure 1 - 27 From left to righ: 2,4-dinitro-m-xylene, 2,4,6-trinitro-m-xylene, and dinitromesitylene

Both the nitro group and its reduced amine counterpart exhibit stability in nature, however interconversion between these two functional groups creates very reactive intermediates named nitroso and hydroxylamino derivatives respectively. These are often more toxic than their predecessors, however polycyclic nitroaromatics do not exhibit high levels of toxicity or carcinogenicity. These polycyclics are activated by both reduction by intestinal microflora, but also through mediated oxidation of the aromatic ring by cytochrome P-450.[105]

Nitrobenzene in particular has been extensively studied in previous years, with analysis using mice and rat for *in vivo* studies showing a correlation between the dose and disposition of nitrobenzene with the severity of the resulting lesions found on the spleen, central nervous system, testes, and liver.[106] From this, it was eventually determined that a key step in the metabolism of nitrobenzene is nitro reduction, with nearly all of this reduction occurring in the intestinal microflora.

1.10.3.1 Nitro Compounds and Hypoxia

Cells in hypoxic conditions are known to be more resistant to radiation than their oxygenated counterparts, which has been considered a contributing factor to failure in radiotherapy.[111] Radiosensitisers were suggested as a means of overcoming this problem, as these compounds

were able to selectively increase the radiosensitivity of hypoxic cells exclusively. This ability is possible due to their reduction potential, or electron affinity.[109]

Many hypoxia-activated compounds are based off the 1-methyl-2-nitroimidazole group which acts as the bio-reductant of the structure.[112] O'Connor *et al.* in 2016 designed and synthesised an important intermediate in the synthesis of these compounds to facilitate easier overall synthesis.[112] This intermediate can be seen in **Figure 1 - 28**. Most previously reported work within the bio-reductive field uses reductive groups capable of selectively activating alkylating agents. This generally damages DNA and/or can induce nonspecific cytotoxicity.

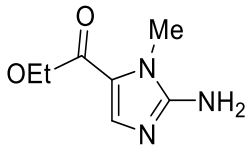


Figure 1 - 28 The intermediate synthesised by O'Connor et al. in 2016[112]

Pimonidazole, seen in **Figure 1 - 29**, is an exogenous 2-nitroimidaole-based probe capable of binding to SH-containing cellular macromolecules such as peptides, proteins, and amino acids through covalent linkage.[113, 114] This is oxygen dependent and occurs in hypoxic regions located in histological sections of tumours specifically, allowing for highly targeted use of this probe.[115] The adducts that form after this can be detected through methods such as immunohistochemistry. Using this to target hypoxia markers has the advantage that tissues from human tissues can be studied for the relationships between hypoxia and already-studied physiological parameters. In particular, the histological sections of this method also permit the study of distribution of hypoxia and other factors such as blood vessels and angiogenesis.[116]

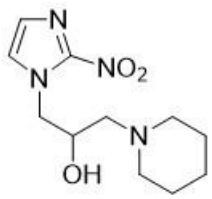


Figure 1 - 29 Pimonidazole

1.10.3.2 NITROBENZENE DERIVATIVES

The most widely used protecting group in biochemistry and photolithography is 2-nitrobenzyl, as it is photoremovable and can be used to determine physiological response times to bioagents like neurotransmitters.[117] Often, decay of these compounds is used to detect the release rate of the protected agents, and this is primarily used through their main photoreaction of intramolecular proton transfer (H-atom). This gives rise to *aci*-nitro tautomers which have a strong absorption at around 400 nm, allowing for easy detection. A known problem with this structure, however, is that successful release of the bioactive compound also causes the formation of 2-nitrosobenzaldehyde, which can potentially give rise to further harmful photoreactions. It may alternatively inactivate the biological methods of production.[117] **Figure 1 - 30** provides the chemical structures of these compounds and a generalised example of *aci*-nitro tautomerism.

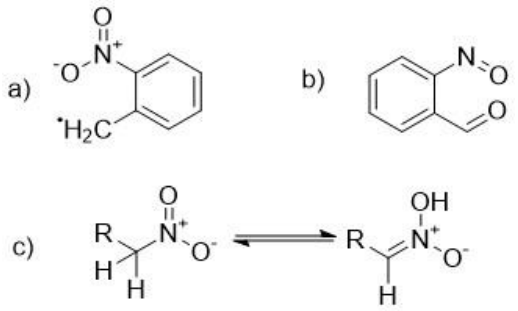


Figure 1 - 30 a) 2-nitrobenzyl, b) 2-nitrosobenzaldehyde, c) an example of *aci*-nitro tautomerism

Nitroimidazole-based drugs are often used to treat diseases caused by anaerobic protozoan infections and bacterium, with drugs like ornidazole (ONZ) active against such protozoa and anaerobic bacteria, and metronidazoles (MNZ) used to prevent and treat susceptible protozoal and anaerobic bacterial infections. Chemical structures of both can be found in

Figure 1 - 31.[118] The problem with these, however, is that their use can lead to drug resistance, and when drugs like MNZ accumulate in the human body, malign effects such as seizures and peripheral neuropathy can result. Other drugs such as dimetridazole are suspected of possessing carcinogenic and mutagenic properties.[118]

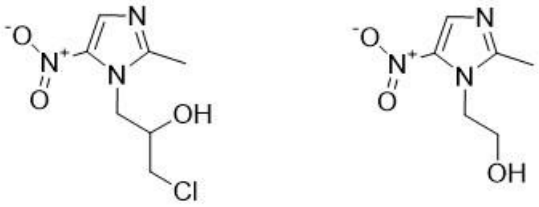


Figure 1 - 31 ONZ (left) and MNZ (right)

Methods for determination of MNZ have been developed in recent years, including polarography, thin layer chromatography, and electrochemical sensors among others. In particular, there is attention of electrochemical sensors and spectrophotometry due to their recognition capabilities, high sensitivity/selectivity, real-time detection functionality, and their rapid responses. Their use is also attributed with drawbacks in terms of stability, reproducibility, and the vulnerability of the drugs to exterior influences such as local pH and surface poisoning.[118]

Some nitrobenzene derivatives are capable of performing as antiparasitic or antibiotic agents. One such example is benznidazole (BNZ – see

Figure 1 - 32) which is used as an antiparasitic in the treatment of Chaga's Disease, an infection caused by *trypanosoma cruzi*.[119] Its use in clinical treatment has received controversy due to its limited effectiveness and potential for toxic side effects, however it still remains more effective than alternative drugs such as Posaconazole when administered in the acute (initial) stage of infection.[120, 121] This acute phase is usually self-limited, however

when untreated can develop into chronic and potentially lifelong illness – at this stage risk of developing cardiac and/or digestive problems increases substantially.

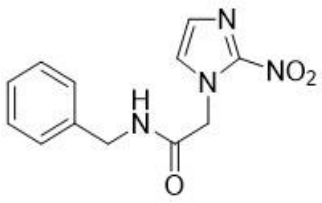


Figure 1 - 32 Benznidazole

Treatment of acute cases of Chaga's with combination treatments has been reported as more effective than use of BNZ alone.[120] In combination with ketoconazole, a greater higher response rate was observed in murine models and suggests that whilst more research is needed into monotherapeutic treatments, combination therapy proves a potentially viable alternative. This is especially promising as data suggests that BNZ is capable of crossing the blood-brain barrier, which would allow for possible treatment of parasitic cases within the central nervous system.[121]

1.11 AIMS OF THE PROJECT

This project aims at designing and synthesising structurally related systems capable of responding to changes in different, selected biomarkers relating to redox stress. The focus has been on luminescence studies and the response and selectivity of these probes to oxygen, H_2S, and select metals in monometallic lanthanide structures. Comparison of different lanthanides has been undertaken to explore the difference in sensitivity and luminescence in these structures. The work divides into four related chapters:

- Synthesis and investigations on systems bearing an anthryl chromophore that react with singlet oxygen;
- Exploration of potential routes to bimetallic systems that incorporate an anthryl chromophore;
- Preparation and evaluation of azidophenacyl-DO3A derived complexes that react with sodium hydrosulfide (NaHS) and an active metal such as zinc; and
- Exploration of the behaviour of nitrophenacyl-DO3A derivatives to determine their reactivity with an active metal, and explore whether conversion of different molecules to the same product can be used to distinguish physiological processes

1.12 REFERENCES

1. Gillen, R.; Clark, S. J.; Robertson, J., Nature of the electronic band gap in lanthanide oxides. *Physical Review B* **2013,** *87* (12), 125116.
2. Bünzli, J.-C. G.; Piguet, C., Taking advantage of luminescent lanthanide ions. *Chemical Society Reviews* **2005,** *34* (12), 1048-1077.
3. Weissman, S. I., Intramolecular Energy Transfer The Fluorescence of Complexes of Europium. *The Journal of Chemical Physics* **1942,** *10* (4), 214-217.
4. Bünzli, J.-C. G., Lanthanide Luminescence for Biomedical Analyses and Imaging. *Chemical Reviews* **2010,** *110* (5), 2729-2755.
5. Song, B.; Vandevyver, C. D. B.; Chauvin, A.-S.; Bünzli, J.-C. G., Time-resolved luminescence microscopy of bimetallic lanthanide helicates in living cells. *Organic & Biomolecular Chemistry* **2008,** *6* (22), 4125-4133.
6. Allen, M. J., Aqueous Lanthanide Chemistry in Asymmetric Catalysis and Magnetic Resonance Imaging. *Synlett* **2016,** *27* (09), 1310-1317.
7. Sørensen, T. J.; Faulkner, S., Multimetallic Lanthanide Complexes: Using Kinetic Control To Define Complex Multimetallic Arrays. *Accounts of Chemical Research* **2018,** *51* (10), 2493-2501.
8. Hemmilä, I.; Laitala, V. J. J. o. F., Progress in Lanthanides as Luminescent Probes. *Journal of Fluorescence* **2005,** *15* (4), 529-542.
9. Faulkner, S.; Natrajan, L. S.; Perry, W. S.; Sykes, D., Sensitised luminescence in lanthanide containing arrays and d–f hybrids. *Dalton Transactions* **2009,** (20), 3890-3899.
10. Faulkner, S.; Pope, S. J. A.; Burton-Pye, B. P., Lanthanide Complexes for Luminescence Imaging Applications. *Applied Spectroscopy Reviews* **2005,** *40* (1), 1-31.
11. Beeby, A.; Bushby, L. M.; Maffeo, D.; Gareth Williams, J. A., Intramolecular sensitisation of lanthanide(iii) luminescence by acetophenone-containing ligands: the critical effect of para-substituents and solvent. *Journal of the Chemical Society, Dalton Transactions* **2002,** (1), 48-54.
12. Beeby, A.; Faulkner, S.; Parker, D.; Williams, J. A. G., Sensitised luminescence from phenanthridine appended lanthanide complexes: analysis of triplet mediated energy transfer processes in terbium, europium and neodymium complexes. *Journal of the Chemical Society, Perkin Transactions 2* **2001,** (8), 1268-1273.
13. Horrocks, W. D.; Bolender, J. P.; Smith, W. D.; Supkowski, R. M., Photosensitized Near Infrared Luminescence of Ytterbium(III) in Proteins and Complexes Occurs via an Internal Redox Process. *Journal of the American Chemical Society* **1997,** *119* (25), 5972-5973.
14. Lazarides, T.; Sykes, D.; Faulkner, S.; Barbieri, A.; Ward, M. D., On the Mechanism of d–f Energy Transfer in RuII/LnIII and OsII/LnIII Dyads: Dexter-Type Energy Transfer Over a Distance of 20 Å. *Chemistry - A European Journal* **2008,** *14* (30), 9389-9399.
15. Latva, M.; Takalo, H.; Mukkala, V.-M.; Matachescu, C.; Rodríguez-Ubis, J. C.; Kankare, J., Correlation between the lowest triplet state energy level of the ligand and lanthanide(III) luminescence quantum yield. *Journal of Luminescence* **1997,** *75* (2), 149-169.
16. Faulkner, S.; Pope, S. J. A., Lanthanide-Sensitized Lanthanide Luminescence: Terbium-Sensitized Ytterbium Luminescence in a Trinuclear Complex. *Journal of the American Chemical Society* **2003,** *125* (35), 10526-10527.
17. Mikhnenko, O.; Blom, P.; Nguyen, T.-Q., Exciton Diffusion in Organic Semiconductors. *Energy and Environmental Science* **2015,** *8*.
18. Braslavsky, S. E., Glossary of terms used in photochemistry. *Pure and Applied Chemistry* **2007,** *79* (3), 293-465.
19. Beeby, A.; M. Clarkson, I.; S. Dickins, R.; Faulkner, S.; Parker, D.; Royle, L.; S. de Sousa, A.; A. Gareth Williams, J.; Woods, M., Non-radiative deactivation of the excited states of europium, terbium and ytterbium complexes by proximate energy-matched OH, NH and CH oscillators: an improved luminescence method for establishing solution hydration states. *Journal of the Chemical Society, Perkin Transactions 2* **1999,** (3), 493-504.

20. Horrocks, W. D.; Sudnick, D. R., Lanthanide ion probes of structure in biology. Laser-induced luminescence decay constants provide a direct measure of the number of metal-coordinated water molecules. *Journal of the American Chemical Society* **1979,** *101* (2), 334-340.
21. Horrocks, W. D.; Sudnick, D. R., Lanthanide ion luminescence probes of the structure of biological macromolecules. *Accounts of Chemical Research* **1981,** *101*, 384-392.
22. Hall, J.; Häner, R.; Aime, S.; Botta, M.; Faulkner, S.; Parker, D.; S. de Sousa, A., Relaxometric and luminescence behaviour of triaquahexaazamacrocyclic complexes, the gadolinium complex displaying a high relaxivity with a pronounced pH dependence. *New Journal of Chemistry* **1998,** *22* (6), 627-631.
23. Rinehart, J. D.; Long, J. R., Exploiting single-ion anisotropy in the design of f-element single-molecule magnets. *Chemical Science* **2011,** *2* (11), 2078-2085.
24. Kaltsoyannis, N.; Scott, P. R., *The F Elements*. Oxford University Press: 2007.
25. Peters, J. A.; Huskens, J.; Raber, D. J., Lanthanide induced shifts and relaxation rate enhancements. *Progress in Nuclear Magnetic Resonance Spectroscopy* **1996,** *28* (3), 283-350.
26. Bleaney, B., Nuclear magnetic resonance shifts in solution due to lanthanide ions. *Journal of Magnetic Resonance (1969)* **1972,** *8* (1), 91-100.
27. Bleaney, B.; Dobson, C. M.; Levine, B. A.; Martin, R. B.; Williams, R. J. P.; Xavier, A. V., Origin of lanthanide nuclear magnetic resonance shifts and their uses. *Journal of the Chemical Society, Chemical Communications* **1972,** (13), 791b-793.
28. Aime, S.; Botta, M.; Ermondi, G., NMR study of solution structures and dynamics of lanthanide(III) complexes of DOTA. *Inorganic Chemistry* **1992,** *31* (21), 4291-4299.
29. Polášek, M.; Kotek, J.; Hermann, P.; Císařová, I.; Binnemans, K.; Lukeš, I., Lanthanide(III) Complexes of Pyridine-N-Oxide Analogues of DOTA in Solution and in the Solid State. A New Kind of Isomerism in Complexes of DOTA-like Ligands. *Inorganic Chemistry* **2009,** *48* (2), 466-475.
30. Placidi, M. P.; Natrajan, L. S.; Sykes, D.; Kenwright, A. M.; Faulkner, S., Bimetallic Lanthanide Complexes Derived from Macrocycle-Appended m-Xylyl Derivatives: Synthesis and Spectroscopic Properties. *Helvetica Chimica Acta* **2009,** *92* (11), 2427-2438.
31. Abergel, R. J.; D'Aléo, A.; Ng Pak Leung, C.; Shuh, D. K.; Raymond, K. N., Using the Antenna Effect as a Spectroscopic Tool: Photophysics and Solution Thermodynamics of the Model Luminescent Hydroxypyridonate Complex [EuIII(3,4,3-LI(1,2-HOPO))]−. *Inorganic Chemistry* **2009,** *48* (23), 10868-10870.
32. Atkinson, P.; Findlay, K. S.; Kielar, F.; Pal, R.; Parker, D.; Poole, R. A.; Puschmann, H.; Richardson, S. L.; Stenson, P. A.; Thompson, A. L.; Yu, J., Azaxanthones and azathioxanthones are effective sensitisers for europium and terbium luminescence. *Organic & Biomolecular Chemistry* **2006,** *4* (9), 1707-1722.
33. Polasek, M.; Caravan, P., Is Macrocycle a Synonym for Kinetic Inertness in Gd(III) Complexes? Effect of Coordinating and Noncoordinating Substituents on Inertness and Relaxivity of Gd(III) Chelates with DO3A-like Ligands. *Inorganic Chemistry* **2013,** *52* (7), 4084-4096.
34. Gallo-Bernal, S.; Patino-Jaramillo, N.; Calixto, C. A.; Higuera, S. A.; Forero, J. F.; Lara Fernandes, J.; Góngora, C.; Gee, M. S.; Ghoshhajra, B.; Medina, H. M., Nephrogenic Systemic Fibrosis in Patients with Chronic Kidney Disease after the Use of Gadolinium-Based Contrast Agents: A Review for the Cardiovascular Imager. *Diagnostics (Basel)* **2022,** *12* (8).
35. Cheong, B. Y.; Muthupillai, R., Nephrogenic systemic fibrosis: a concise review for cardiologists. *Texas Heart Institute Journal* **2010,** *37* (5), 508-15.
36. Cheng, R. H.; Chen, J. M.; Chen, Y. W.; Cai, H.; Cui, X.; Hwang, D.; Chen, Z.; Ding, S., Macromolecular Crowding May Significantly Affect the Performance of an MRI Contrast Agent: A 1H NMR Spectroscopy, Microimaging, and Fast-Field-Cycling NMR Relaxometry Study. *ChemistryOpen* **2018,** *7*.
37. Reisfeld, R.; Levchenko, V.; Lazarowska, A.; Mahlik, S.; Grinberg, M., Intensification of luminescence of Europium-EDTA complex in polyvinyl pyrrolidone films by copper nanoparticles. *Optical Materials* **2016,** *59*, 3-7.

38. Fusaro, L.; Mocci, F.; Muller, R. N.; Luhmer, M., Insight into the Dynamics of Lanthanide-DTPA Complexes As Revealed by Oxygen-17 NMR. *Inorganic Chemistry* **2012,** *51* (15), 8455-8461.
39. Hueting, R.; Tropiano, M.; Faulkner, S., Exploring energy transfer between pyrene complexes and europium ions – potential routes to oxygen sensors. *RSC Advances* **2014,** *4* (83), 44162-44165.
40. Ward, M. D., Mechanisms of sensitization of lanthanide(III)-based luminescence in transition metal/lanthanide and anthracene/lanthanide dyads. *Coordination Chemistry Reviews* **2010,** *254* (21), 2634-2642.
41. Bottrill, M.; Kwok, L.; Long, N. J., Lanthanides in magnetic resonance imaging. *Chemical Society Reviews* **2006,** *35* (6), 557-571.
42. Pinto, S. M.; Tomé, V.; Calvete, M. J. F.; Castro, M. M. C. A.; Tóth, É.; Geraldes, C. F. G. C., Metal-based redox-responsive MRI contrast agents. *Coordination Chemistry Reviews* **2019,** *390*, 1-31.
43. New, E. J.; Parker, D., The mechanism of cell uptake for luminescent lanthanide optical probes: the role of macropinocytosis and the effect of enhanced membrane permeability on compartmentalisation. *Organic & Biomolecular Chemistry* **2009,** *7* (5), 851-855.
44. Junker, A. K. R.; Sørensen, T. J., Illuminating the Intermolecular vs. Intramolecular Excited State Energy Transfer Quenching by Europium(III) Ions. *European Journal of Inorganic Chemistry* **2019,** *2019* (9), 1201-1206.
45. Nesmerak, K., Lanthanide/Actinide Toxicity. In *Encyclopedia of Metalloproteins*, Kretsinger, R. H.; Uversky, V. N.; Permyakov, E. A., Eds. Springer New York: New York, NY, 2013; pp 1098-1103.
46. Faulkner, S.; Blackburn, O. A., The Chemistry of Lanthanide MRI Contrast Agents. In *The Chemistry of Molecular Imaging*, 2014; pp 179-197.
47. Haley, T. J., Pharmacology and Toxicology of the Rare Earth Elements. *Journal of Pharmaceutical Sciences* **1965,** *54* (5), 663-670.
48. Heffern, M. C.; Matosziuk, L. M.; Meade, T. J., Lanthanide Probes for Bioresponsive Imaging. *Chemical Reviews* **2014,** *114* (8), 4496-4539.
49. Blackburn, O. A.; Edkins, R. M.; Faulkner, S.; Kenwright, A. M.; Parker, D.; Rogers, N. J.; Shuvaev, S., Electromagnetic susceptibility anisotropy and its importance for paramagnetic NMR and optical spectroscopy in lanthanide coordination chemistry. *Dalton Transactions* **2016,** *45* (16), 6782-6800.
50. J R Alger, a.; Frank, J. A., The Utilization of Magnetic Resonance Imaging in Physiology. *Annual Review of Physiology* **1992,** *54* (1), 827-846.
51. Oudkerk, M.; Sijens, P. E.; Van Beek, E. J. R.; Kuijpers, T. J. A., Safety and Efficacy of Dotarem (Gd-DOTA) versus Magnevist (Gd-DTPA) in Magnetic Resonance Imaging of the Central Nervous System. *Investigative Radiology* **1995,** *30* (2).
52. Young, L. K.; Matthew, S. Z.; Houston, J. G., Absence of potential gadolinium toxicity symptoms following 22,897 gadoteric acid (Dotarem®) examinations, including 3,209 performed on renally insufficient individuals. *European Radiology* **2019,** *29* (4), 1922-1930.
53. Desreux, J. F., Nuclear magnetic resonance spectroscopy of lanthanide complexes with a tetraacetic tetraaza macrocycle. Unusual conformation properties. *Inorganic Chemistry* **1980,** *19* (5), 1319-1324.
54. Tweedle, M. F., The ProHance story: the making of a novel MRI contrast agent. *European Radiology* **1997,** *7* (5), S225-S230.
55. Vogler, H.; Platzek, J.; Schuhmann-Giampieri, G.; Frenzel, T.; Weinmann, H.-J.; Radüchel, B.; Press, W.-R., Pre-clinical evaluation of gadobutrol: a new, neutral, extracellular contrast agent for magnetic resonance imaging. *European Journal of Radiology* **1995,** *21* (1), 1-10.
56. Parmelee, D. J.; Walovitch, R. C.; Ouellet, H. S.; Lauffer, R. B., Preclinical evaluation of the pharmacokinetics, biodistribution, and elimination of MS-325, a blood pool agent for magnetic resonance imaging. *Investigative Radiology* **1997,** *32* (12), 741-747.

57. Pubanz, D.; Gonzalez, G.; Powell, D. H.; Merbach, A. E., Unexpectedly Large Change of Water Exchange Rate and Mechanism on [Ln(DTPA-BMA)(H_2O)] Complexes along the Lanthanide(III) Series. *Inorganic Chemistry* **1995,** *34* (17), 4447-4453.
58. Sørensen, T. J.; Kenwright, A. M.; Faulkner, S., Bimetallic lanthanide complexes that display a ratiometric response to oxygen concentrations. *Chemical Science* **2015,** *6* (3), 2054-2059.
59. Amelia, M.; Lavie-Cambot, A.; McClenaghan, N. D.; Credi, A., A ratiometric luminescent oxygen sensor based on a chemically functionalized quantum dot. *Chemical Communications* **2011,** *47* (1), 325-327.
60. Kilbourn, B. T., The role of the lanthanides in applied catalysis. *Journal of the Less Common Metals* **1986,** *126*, 101-106.
61. Zhao, N.; Xin, H.; Zhang, L., Advanced Biomedical Applications of Reactive Oxygen Species-Based Nanomaterials in Lung Cancer. *Frontiers in Chemistry* **2021,** *9* (124).
62. Auten, R. L.; Davis, J. M., Oxygen Toxicity and Reactive Oxygen Species: The Devil Is in the Details. *Pediatric Research* **2009,** *66* (2), 121-127.
63. Beeby, A.; Faulkner, S.; Williams, J. A. G., pH Dependence of the energy transfer mechanism in a phenanthridine-appended ytterbium complex. *Journal of the Chemical Society, Dalton Transactions* **2002,** (9), 1918-1922.
64. Liou, G.-Y.; Storz, P., Reactive oxygen species in cancer. *Free Radical Research* **2010,** *44* (5), 479-496.
65. Hayyan, M.; Hashim, M. A.; AlNashef, I. M., Superoxide Ion: Generation and Chemical Implications. *Chemical Reviews* **2016,** *116* (5), 3029-3085.
66. Mani, S.; Cao, W.; Wu, L.; Wang, R., Hydrogen sulfide and the liver. *Nitric Oxide : Biology and Chemistry* **2014,** *41*, 62-71.
67. Callaghan, S.; Senge, M. O., The good, the bad, and the ugly – controlling singlet oxygen through design of photosensitizers and delivery systems for photodynamic therapy. *Photochemical & Photobiological Sciences* **2018,** *17* (11), 1490-1514.
68. Yang, B.; Chen, Y.; Shi, J., Reactive Oxygen Species (ROS)-Based Nanomedicine. *Chemical Reviews* **2019,** *119* (8), 4881-4985.
69. Song, B.; Wang, G.; Tan, M.; Yuan, J., A Europium(III) Complex as an Efficient Singlet Oxygen Luminescence Probe. *Journal of the American Chemical Society* **2006,** *128* (41), 13442-13450.
70. Staszak, K.; Wieszczycka, K.; Marturano, V.; Tylkowski, B., Lanthanides complexes – Chiral sensing of biomolecules. *Coordination Chemistry Reviews* **2019,** *397*, 76-90.
71. Qiu, Z.; Shu, J.; Liu, J.; Tang, D., Dual-Channel Photoelectrochemical Ratiometric Aptasensor with up-Converting Nanocrystals Using Spatial-Resolved Technique on Homemade 3D Printed Device. *Analytical Chemistry* **2019,** *91* (2), 1260-1268.
72. Luo, Z.; Zhang, L.; Zeng, R.; Su, L.; Tang, D., Near-Infrared Light-Excited Core–Core–Shell UCNP@Au@CdS Upconversion Nanospheres for Ultrasensitive Photoelectrochemical Enzyme Immunoassay. *Analytical Chemistry* **2018,** *90* (15), 9568-9575.
73. Payne, S. J.; Fiore, G. L.; Fraser, C. L.; Demas, J. N., Luminescence Oxygen Sensor Based on a Ruthenium(II) Star Polymer Complex. *Analytical Chemistry* **2010,** *82* (3), 917-921.
74. Gruhlke, M. C. H.; Slusarenko, A. J., The biology of reactive sulfur species (RSS). *Plant Physiology and Biochemistry* **2012,** *59*, 98-107.
75. Módis, K.; Coletta, C.; Asimakopoulou, A.; Szczesny, B.; Chao, C.; Papapetropoulos, A.; Hellmich, M. R.; Szabo, C., Effect of S-adenosyl-l-methionine (SAM), an allosteric activator of cystathionine-β-synthase (CBS) on colorectal cancer cell proliferation and bioenergetics in vitro. *Nitric Oxide : Biology and Chemistry* **2014,** *41*, 146-156.
76. Szabo, C.; Coletta, C.; Chao, C.; Módis, K.; Szczesny, B.; Papapetropoulos, A.; Hellmich, M. R., Tumor-derived hydrogen sulfide, produced by cystathionine-β-synthase, stimulates bioenergetics, cell proliferation, and angiogenesis in colon cancer. *Proceedings of the National Academy of Sciences* **2013,** *110* (30), 12474.

77. Zheng, Y.; Yu, B.; De La Cruz, L. K.; Roy Choudhury, M.; Anifowose, A.; Wang, B., Toward Hydrogen Sulfide Based Therapeutics: Critical Drug Delivery and Developability Issues. *Medicinal Research Reviews* **2018,** *38* (1), 57-100.
78. Li, L.; Hsu, A.; Moore, P. K., Actions and interactions of nitric oxide, carbon monoxide and hydrogen sulfide in the cardiovascular system and in inflammation — a tale of three gases! *Pharmacology & Therapeutics* **2009,** *123* (3), 386-400.
79. Giuffrè, A.; Vicente, J. B., Hydrogen Sulfide Biochemistry and Interplay with Other Gaseous Mediators in Mammalian Physiology. *Oxidative Medicine and Cellular Longevity* **2018,** *2018*, 6290931.
80. Dombkowski, R. A.; Russell, M. J.; Olson, K. R., Hydrogen sulfide as an endogenous regulator of vascular smooth muscle tone in trout. *American Journal of Physiology-Regulatory, Integrative and Comparative Physiology* **2004,** *286* (4), R678-R685.
81. Donnarumma, E.; Trivedi, R. K.; Lefer, D. J., Protective Actions of H2S in Acute Myocardial Infarction and Heart Failure. In *Comprehensive Physiology*, pp 583-602.
82. Szabó, C., Hydrogen sulfide and its therapeutic potential. *Nature Reviews Drug Discovery* **2007,** *6* (11), 917-935.
83. Lippert, A. R.; New, E. J.; Chang, C. J., Reaction-Based Fluorescent Probes for Selective Imaging of Hydrogen Sulfide in Living Cells. *Journal of the American Chemical Society* **2011,** *133* (26), 10078-10080.
84. Shefa, U.; Kim, M.-S.; Jeong, N. Y.; Jung, J., Antioxidant and Cell-Signaling Functions of Hydrogen Sulfide in the Central Nervous System. *Oxidative Medicine and Cellular Longevity* **2018,** *2018*, 1873962-1873962.
85. Lin, V. S.; Lippert, A. R.; Chang, C. J., Chapter Four - Azide-Based Fluorescent Probes: Imaging Hydrogen Sulfide in Living Systems. *Methods in Enzymology*, Cadenas, E.; Packer, L., Eds. Academic Press: 2015; Vol. 554, pp 63-80.
86. Lin, V. S.; Chang, C. J., Fluorescent probes for sensing and imaging biological hydrogen sulfide. *Current Opinion in Chemical Biology* **2012,** *16* (5), 595-601.
87. Pang, L.; Wang, D.; Zhou, J.; Zhang, L.-H.; Ye, X.-S., Synthesis of neamine-derived pseudodisaccharides by stereo- and regio-selective functional group transformations. *Organic & Biomolecular Chemistry* **2009,** *7*, 4252-66.
88. Tropiano, M.; Faulkner, S., A lanthanide based sensor for the time-gated detection of hydrogen sulfide. *Chemical Communications* **2014,** *50* (36), 4696-4698.
89. Peng, H.; Cheng, Y.; Dai, C.; King, A. L.; Predmore, B. L.; Lefer, D. J.; Wang, B., A Fluorescent Probe for Fast and Quantitative Detection of Hydrogen Sulfide in Blood. *Angewandte Chemie, International Edition in English* **2011,** *50* (41), 9672-9675.
90. Li, L.; Bhatia, M.; Zhu, Y. Z.; Zhu, Y. C.; Ramnath, R. D.; Wang, Z. J.; Anuar, F. B. M.; Whiteman, M.; Salto-Tellez, M.; Moore, P. K., Hydrogen sulfide is a novel mediator of lipopolysaccharide-induced inflammation in the mouse. *FASEB Journal* **2005,** *19* (9), 1196-1198.
91. Yu, F.; Li, P.; Song, P.; Wang, B.; Zhao, J.; Han, K., An ICT-based strategy to a colorimetric and ratiometric fluorescence probe for hydrogen sulfide in living cells. *Chemical Communications* **2012,** *48* (23), 2852-2854.
92. Montoya, L. A.; Pluth, M. D., Selective turn-on fluorescent probes for imaging hydrogen sulfide in living cells. *Chemical Communications* **2012,** *48* (39), 4767-4769.
93. Das, S. K.; Lim, C. S.; Yang, S. Y.; Han, J. H.; Cho, B. R., A small molecule two-photon probe for hydrogen sulfide in live tissues. *Chemical Communications* **2012,** *48* (67), 8395-8397.
94. Yu, F.; Han, X.; Chen, L., Fluorescent probes for hydrogen sulfide detection and bioimaging. *Chemical Communications* **2014,** *50* (82), 12234-12249.
95. Liu, C.; Pan, J.; Li, S.; Zhao, Y.; Wu, L. Y.; Berkman, C. E.; Whorton, A. R.; Xian, M., Capture and Visualization of Hydrogen Sulfide by a Fluorescent Probe. *Angewandte Chemie International Edition* **2011,** *50* (44), 10327-10329.

96. Liu, C.; Peng, B.; Li, S.; Park, C.-M.; Whorton, A. R.; Xian, M., Reaction Based Fluorescent Probes for Hydrogen Sulfide. *Organic Letters* **2012,** *14* (8), 2184-2187.
97. Sasakura, K.; Hanaoka, K.; Shibuya, N.; Mikami, Y.; Kimura, Y.; Komatsu, T.; Ueno, T.; Terai, T.; Kimura, H.; Nagano, T., Development of a Highly Selective Fluorescence Probe for Hydrogen Sulfide. *Journal of the American Chemical Society* **2011,** *133* (45), 18003-18005.
98. Hou, F.; Huang, L.; Xi, P.; Cheng, J.; Zhao, X.; Xie, G.; Shi, Y.; Cheng, F.; Yao, X.; Bai, D.; Zeng, Z., A Retrievable and Highly Selective Fluorescent Probe for Monitoring Sulfide and Imaging in Living Cells. *Inorganic Chemistry* **2012,** *51* (4), 2454-2460.
99. Beauchamp, R. O.; Bus, J. S.; Popp, J. A.; Boreiko, C. J.; Andjelkovich, D. A.; Leber, P., A Critical Review of the Literature on Hydrogen Sulfide Toxicity. *CRC Critical Reviews in Toxicology* **1984,** *13* (1), 25-97.
100. Almeida, A. F.; Guidotti, T. L., Differential sensitivity of lung and brain to sulfide exposure: a peripheral mechanism for apnea. *Toxicological Sciences : An Official Journal of the Society of Toxicology* **1999,** *50* (2), 287-93.
101. Kwon, N.; Kim, D.; Swamy, K. M. K.; Yoon, J., Metal-coordinated fluorescent and luminescent probes for reactive oxygen species (ROS) and reactive nitrogen species (RNS). *Coordination Chemistry Reviews* **2021,** *427*, 213581.
102. Bove, P. F.; van der Vliet, A., Nitric oxide and reactive nitrogen species in airway epithelial signaling and inflammation. *Free Radical Biology and Medicine* **2006,** *41* (4), 515-527.
103. Ju, K.-S.; Parales, R., Nitroaromatic Compounds, from Synthesis to Biodegradation. *Microbiology and Molecular Biology Reviews* **2010,** *74*, 250-72.
104. Spain, J. C., BIODEGRADATION OF NITROAROMATIC COMPOUNDS. *Annual Review of Microbiology* **1995,** *49* (1), 523-555.
105. Rickert, D. E., Metabolism of Nitroaromatic Compounds. *Drug Metabolism Reviews* **1987,** *18* (1), 23-53.
106. Gooch, A.; Sizochenko, N.; Sviatenko, L.; Gorb, L.; Leszczynski, J., A quantum chemical based toxicity study of estimated reduction potential and hydrophobicity in series of nitroaromatic compounds. *SAR And QSAR In Environmental Research* **2017,** *28* (2), pp133-150.
107. Rafii, F.; Selby, A. L.; Newton, R. K.; Cerniglia, C. E., Reduction and mutagenic activation of nitroaromatic compounds by a Mycobacterium sp. *Applied and Environmental Microbiology* **1994,** *60* (12), 4263-4267.
108. Adams, G. E.; Stratford, I. J.; Wallace, R. G.; Wardman, P.; Watts, M. E., Toxicity of nitro compounds toward hypoxic mammalian cells in vitro: dependence on reduction potential. *Journal of the National Cancer Institute* **1980,** *64* (3), 555-60.
109. Cohen, J. B.; McCandlish, D., CXXVII.—The mechanism of the hydrogen sulfide reduction of nitro-compounds. *Journal of the Chemical Society, Transactions* **1905,** *87* (0), 1257-1272.
110. Skwarska, A.; Calder, E. D. D.; Sneddon, D.; Bolland, H.; Odyniec, M. L.; Mistry, I. N.; Martin, J.; Folkes, L. K.; Conway, S. J.; Hammond, E. M., Development and pre-clinical testing of a novel hypoxia-activated KDAC inhibitor. *Cell Chemical Biology* **2021,** *28* (9), 1258-1270.e13.
111. O'Connor, L. J.; Cazares-Körner, C.; Saha, J.; Evans, C. N. G.; Stratford, M. R. L.; Hammond, E. M.; Conway, S. J., Design, synthesis and evaluation of molecularly targeted hypoxia-activated prodrugs. *Nature Protocols* **2016,** *11* (4), 781-794.
112. Wilson, W. R.; Hay, M. P., Targeting hypoxia in cancer therapy. *Nature Reviews. Cancer* **2011,** *11* (6), 393-410.
113. Ragnum, H. B.; Vlatkovic, L.; Lie, A. K.; Axcrona, K.; Julin, C. H.; Frikstad, K. M.; Hole, K. H.; Seierstad, T.; Lyng, H., The tumour hypoxia marker pimonidazole reflects a transcriptional programme associated with aggressive prostate cancer. *British Journal of Cancer* **2015,** *112* (2), 382-390.
114. Aguilera, K. Y.; Brekken, R. A., Hypoxia Studies with Pimonidazole in vivo. *Bio Protocol* **2014,** *4* (19).

115. Varia, M. A.; Calkins-Adams, D. P.; Rinker, L. H.; Kennedy, A. S.; Novotny, D. B.; Fowler, W. C.; Raleigh, J. A., Pimonidazole: A Novel Hypoxia Marker for Complementary Study of Tumor Hypoxia and Cell Proliferation in Cervical Carcinoma. *Gynecologic Oncology* **1998,** *71* (2), 270-277.
116. Il'ichev, Y. V.; Schwörer, M. A.; Wirz, J., Photochemical Reaction Mechanisms of 2-Nitrobenzyl Compounds: Methyl Ethers and Caged ATP. *Journal of the American Chemical Society* **2004,** *126* (14), 4581-4595.
117. Dong, B.-X.; Pan, Y.-M.; Liu, W.-L.; Teng, Y.-L., An Ultrastable Luminescent Metal–Organic Framework for Selective Sensing of Nitroaromatic Compounds and Nitroimidazole-Based Drug Molecules. *Crystal Growth and Design* **2018,** *18* (1), 431-440.
118. Wardman, P., Nitroimidazoles as hypoxic cell radiosensitizers and hypoxia probes: misonidazole, myths and mistakes. The *British Journal of Radiology* **2019,** *92* (1093), 20170915.
119. Morillo, C. A.; Waskin, H.; Sosa-Estani, S.; del Carmen Bangher, M.; Cuneo, C.; Milesi, R.; Mallagray, M.; Apt, W.; Beloscar, J.; Gascon, J.; Molina, I.; Echeverria, L. E.; Colombo, H.; Perez-Molina, J. A.; Wyss, F.; Meeks, B.; Bonilla, L. R.; Gao, P.; Wei, B.; McCarthy, M.; Yusuf, S.; Morillo, C.; Sosa-Estani, S.; Waskin, H.; Meeks, B.; Yusuf, S.; Diaz, R.; Acquatella, H.; Lazzari, J.; Roberts, R.; Traina, M.; Meeks, B.; Bonilla, L. R.; Gao, P.; Taylor, A.; Holadyk-Gris, I.; Whalen, L.; Bangher, M. C.; Romero, M. A.; Prado, N.; Hernández, Y.; Fernandez, M.; Riarte, A.; Scollo, K.; Lopez-Albizu, C.; Cuneo, C. A.; Gutiérrez, N. C.; Milesi, R. R.; Berli, M. A.; Mallagray, M. H.; Cáceres, N. E.; Beloscar, J. S.; Petrucci, J. M.; Colombo, H.; Dellatorre, M.; Prado, A.; Apt, W.; Zulantay, I.; Echeverría, L. E.; Isaza, D.; Reyes, E.; Wyss, F. S.; Figueroa, A.; Guzmán Melgar, I.; Rodríguez, E.; Gascon, J.; Aldasoro, E.; Posada, E. J.; Serret, N.; Molina, I.; Sánchez-Montalvá, A.; Perez-Molina, J. A.; López-Vélez, R.; Reyes-López, P. A., Benznidazole and Posaconazole in Eliminating Parasites in Asymptomatic T. Cruzi Carriers: The STOP-CHAGAS Trial. *Journal of the American College of Cardiology* **2017,** *69* (8), 939-947.
120. Perin, L.; Silva, R. M. d.; Fonseca, K. d. S.; Cardoso, J. M. d. O.; Mathias, F. A. S.; Reis, L. E. S.; Molina, I.; Correa-Oliveira, R.; Vieira, P. M. d. A.; Carneiro, C. M., Pharmacokinetics and Tissue Distribution of Benznidazole after Oral Administration in Mice. *Antimicrobial Agents and Chemotherapy* **2017,** *61* (4), e02410-16.

2 Redox Active Luminescent Lanthanide Complexes

2.1 INTRODUCTION

Europium has been previously tested and proven as a redox-responsive MRI agent in Eu^{2+} chelate complexes and has been used in diagnosis of blood flow and strokes.[71] Other lanthanides such as dysprosium (Dy^{3+}) have been investigated regarding its potential as a contrast agent with high magnetic field properties. Other uses of these lanthanide complexes extend potentially to X-Ray PDT cancer treatment, and other more specific functions such as identification of specific proteins.

Previous fluorescent probes have been crafted using anthracene bound into a xanthene ring. These give sensitive fluorescent responses, however they are limited to higher pH values[70] and by steady-state investigations. Oxygen sensors work based on collision between the ligand triplet state and the oxygen ground state, which converts the triplet state to ground state and generates an ROS as seen in the following Equation 2.1:

$$S_1 + {}^3O_2 \leftrightarrow S_0 + {}^1O_2 \qquad \textbf{Equation 2.1}$$

Complexes such as $Ru(bpy)_3^{2+}$ are quenched by oxygen through exploitation of the interactions observed between the triplet ground state and the triplet excited state of molecular oxygen.[59] These complexes can quantify oxygen which has two potential pathways that can lead to ground state regeneration:[74] oxygen collision or phosphorescence as seen in **Figure 2 - 1**. Oxygenation is only possible if oxygen is present, and as the concentration of oxygen increases, the probability of the phosphorescence pathway decreases. Similar exchange pathways are observed in lanthanide complexes, where fast k_{et} means a Dexter

pathway and T_1 should quench before collision with oxygen can occur. This would result in no ROS generation.

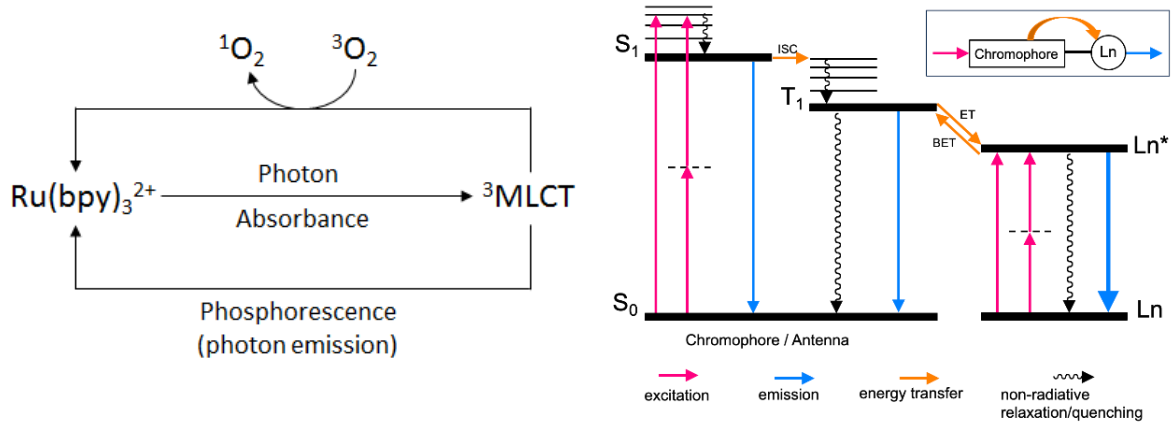


Figure 2 - 1 Possible pathways of action for Ru(bpy) (left) and a lanthanide complex (right)

In this report, studies on oxygen-responsive probes have utilised an anthryl chromophore to generate the ROS $^1O_2$. In the real world of PDT, however, visible light excitation of structures means the anthryl excited state will not be independently generated. This structure is not inherently luminescent, however reaction with the singlet ROS has been proven to generate a luminescent complex. In this reaction, the complex converts the oxygen triplet state to an excited state upon collision with a chromophore in its excited triplet state, thus preventing the triplet state from sensitising emission.

Instead, the complex reacts with the singlet oxygen through a Diels-Alder reaction to yield a sensitising group known as an endoperoxide. **Figure 2 - 2** presents the target complex of this chapter and demonstrates an example of how the probes studied in this chapter might react with singlet oxygen in this mechanism. Energy transfer subsequently occurs within this complex as it has a higher energy state (25,933 cm^{-1}) than the Tb^{3+} emissive state ($^5D_4$ = 20,500 cm^{-1}), and so emission can be sensitised. It is then possible for emission intensity to increase as exposure to UV light increases.

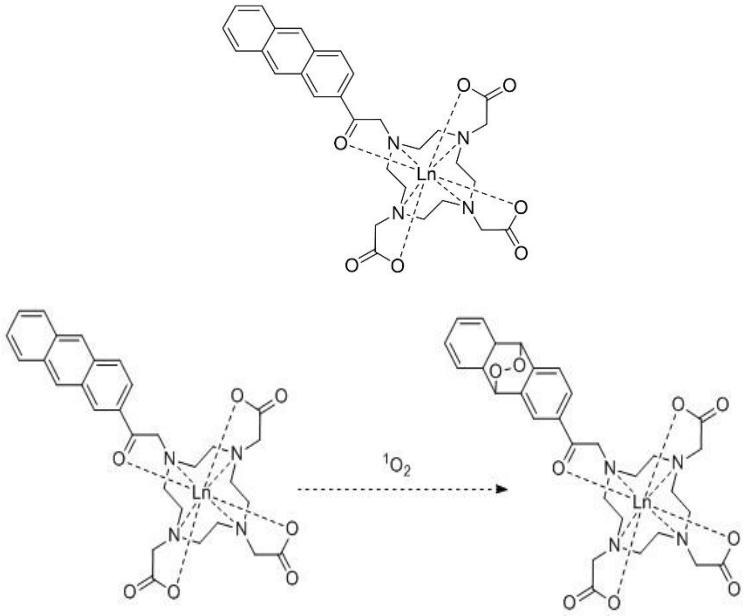
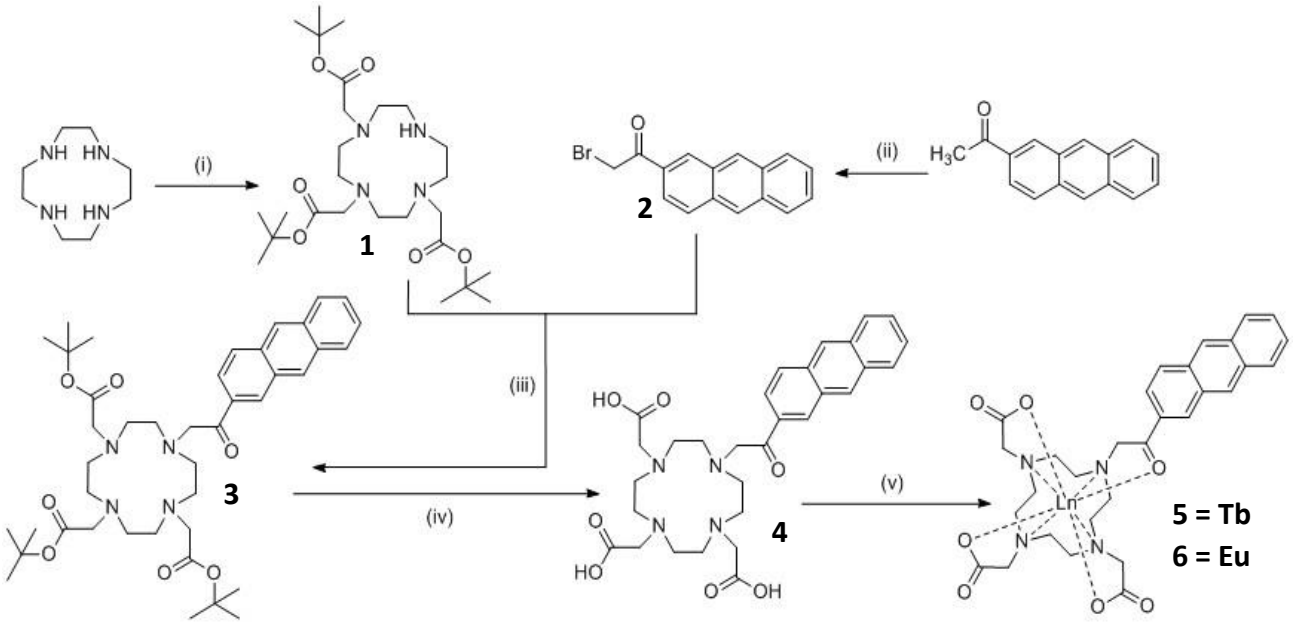


Figure 2 - 2 Top: Target complex structure. Bottom: Oxygen reactivity process of the lanthanide complex explored in this chapter

2.2 SYNTHESIS AND CHARACTERISATION

Synthesis and analysis has focused on monometallic complexes using an anthryl functionalised DO3A as the base structure, synthesised following previously recorded literature procedures[122]. This is summarised in **Scheme 2 - 1**. Analytical data was found to



Scheme 2 - 1 Synthesis of the monometallic lanthanide complex. Reaction conditions: (i) $C_6H_{11}BrO_2$, $NaHCO_3$, CH_3CN, N_2, r.t. (ii) $CHCl_3$:EtOAc (1:1), $CuBr_2$, 80 °C (iii) K_2CO_3, MeCN, 80 °C (iv) DCM, TFA, r.t. (v) $Ln(CF_3SO_3)_3$ where Ln = Tb or Eu, MeOH, 60 °C

correspond with those previously recorded and confirmed synthesis of the intermediates and final complexes. The chosen lanthanides of study were terbium and europium, which have been shown to be efficient quenchers.

1 was synthesised by combining cyclen with a tert-butyl bromoketone in acetonitrile (MeCN) to create the desired base DO3A structure. This was purified through excess washing with toluene over a two-day period. Synthesis was confirmed through comparison to previously reported literature.[123] The α-bromoketone **2** was then synthesised to form the ligand arm through bromination of 2-acetylanthracene using excess copper (ii) bromide. Whilst impurities are present in **2** as seen in **Figure 2 - 3**, as the next step of the synthetic method requires purification and the overall yield is quite high (95%) with quite small impurities in comparison to the product yield, it was deemed suitable to use the compound as is and purify after the next reaction.

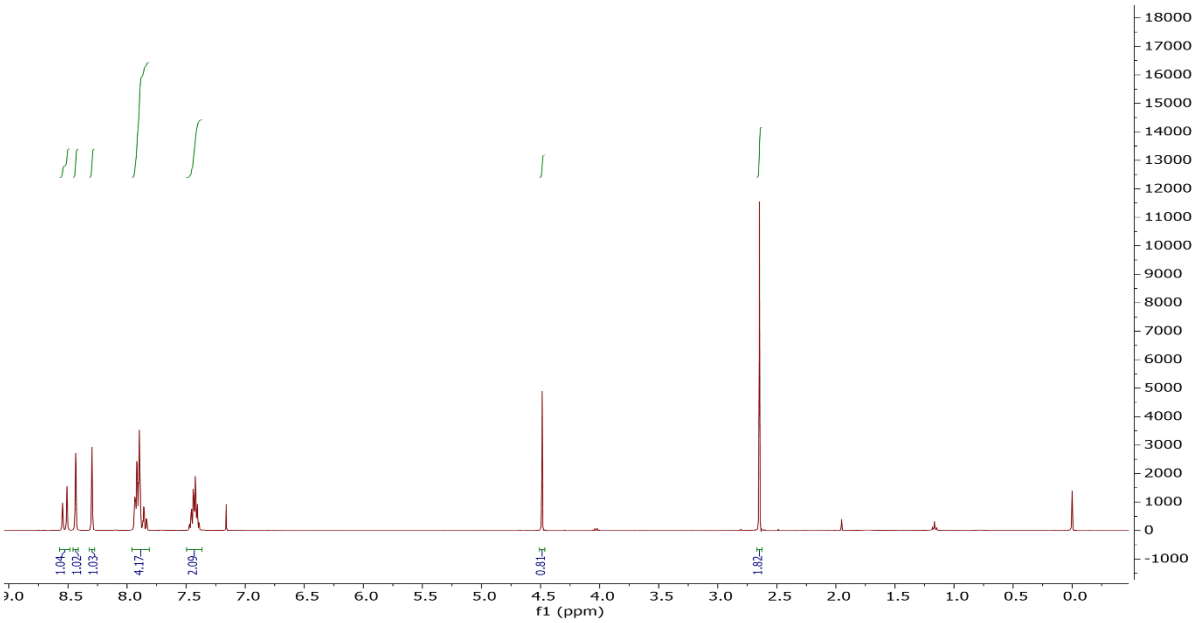


Figure 2 - 3 ^{1}H NMR Spectrum of 2

Triester and this bromoketone were then refluxed overnight in MeCN to generate **3**, which was filtered and dried. This was then purified using silica gel column chromatography with methanol (MeOH) and dichloromethane (DCM), and confirmed through characterisation via

NMR, UV-Visible (UV-Vis), and Infra-red (IR) spectroscopy. Purification in this step is necessary to remove excess bromoketone from **2** and its accompanying impurities, as well as excess unreacted **1** and any carbonate that was not removed in the filtration post-reflux. The higher level of peaks in the 2.5-3.5 ppm region in **Figure 2 - 4** is attributed to the broad nature of the cyclen peaks and represents the backbone of this chromophore-appended ligand.

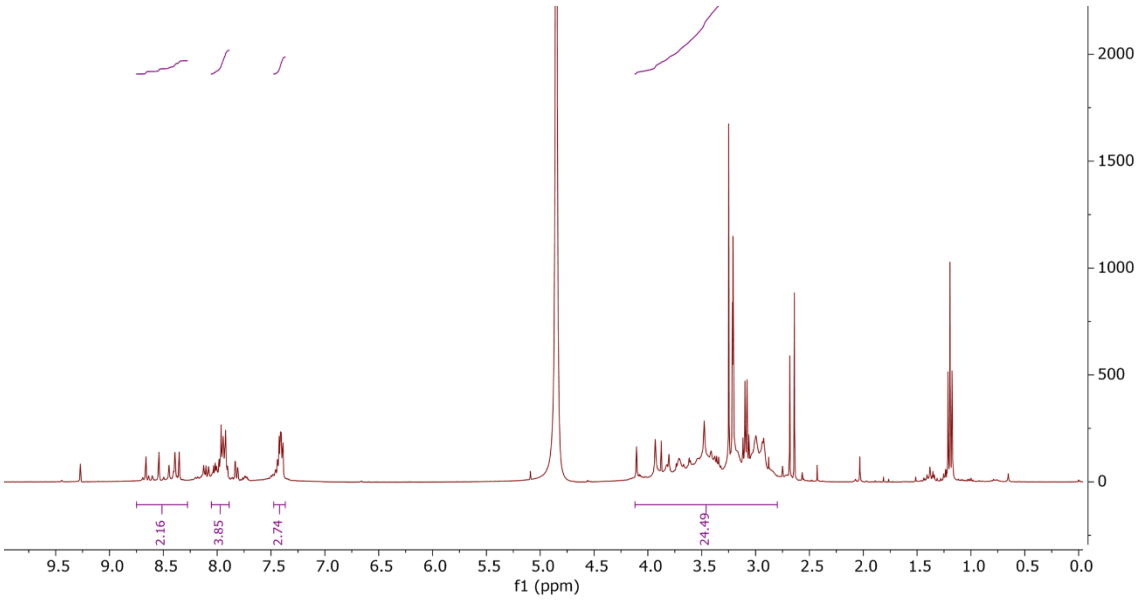


Figure 2 - 4 ^{1}H NMR Spectrum of 4

To remove the tert-butyl arms, **3** was reacted with TFA and DCM in a 1:1 ratio over a period of 48 hr and washed several times with DCM and MeOH to remove excess TFA and generate **4**. To further remove impurities, **4** was triturated with MeOH and diethyl ether (Et_2O). NMR suggests a successful separation of the tert-butyl arms, as evidenced by the disappearance of the peaks between 1.5-1.6 ppm that represent the tert-butyl peaks whilst retaining the remaining multidentate cyclen-based structure.

After deprotection was completed, **4** was reacted with a lanthanide salt in MeOH to induce complexation of the lanthanide into the cyclen pocket. The trifluoromethanesulfonate lanthanide complex was chosen for this purpose as removal of the excess unreacted lanthanide salt was easily achieved. These compounds were reacted together at 60 °C for 48

hr with adjustment of pH as required to maintain moderately acidic conditions of 4-5, after which pH was adjusted to 10 to remove the excess unreacted lanthanide salt as an insoluble hydroxide precipitate. This solid was removed via centrifugation to ensure full separation, the supernatant neutralised, and the solvent removed under reduced pressure to yield **5** and **6**. Further purification of the complex was achieved through trituration and dialysis to remove any excess salts formed during complexation.

Complexes were characterised by NMR, mass spectrometry, and luminescence. Mass spectrometry of **6** revealed the presence of the molecular ion, whilst NMR showed incorporation of the lanthanide and that the complex demonstrated broken symmetry. **Figure 2 - 5** provides the ^{1}H NMR of **6**. This means all protons are inequivalent axial ring protons in a broad sweep, and similar observations were found for **5**.

A predominantly SAP arrangement is seen in the peaks between 25-35 ppm with a minor TSAP geometric orientation also found. This is seen in the minor peaks found between 15-20 ppm. The remaining spectral peaks can be seen to move upfield in accordance with the increase in

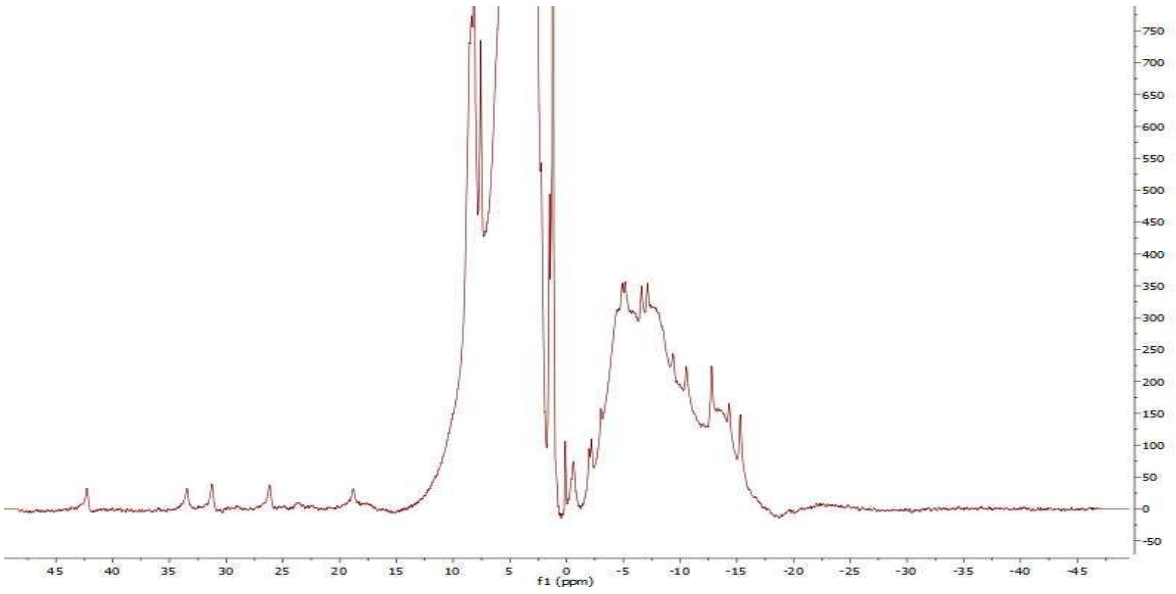


Figure 2 - 5 ^{1}H NMR Spectrum of 6

magnetic anisotropy because of changes to the ligand field. This is caused by the europium ion and suggests that protons within the structure reside in an equatorially favoured position rather than axial. Specific assignment of peaks is only possible in symmetric complexes, and in non-cyclen-based ligands, however a summation can be made that synthesis and combination of lanthanide and ligand has succeeded.

UV analysis of **5** and anthracene was performed at standard oxygenation levels in MeOH. Unsurprisingly, it was observed that the compound is sensitive to light when exposed to oxygen. This can be overcome, however, by carrying out synthesis in the dark to avoid premature conversion through light sensitivity. Storage of the complex in the dark is also highly advised to further avoid decomposition.

Analysis of UV absorption spectra of **5** in **Figure 2 - 6** reflects the anthryl chromophore which is known to absorb at λ = 252 nm; correlation is observed in this sample of anthracene. A similar peak is observed in **5**, though a slight shift in peak wavelength is noticeable. This is attributed to the reactivity with UV light and the interactions between the lanthanide and functionalised DO3A structure. The peaks at λ = 205 and λ = 300 nm can also be attributed to

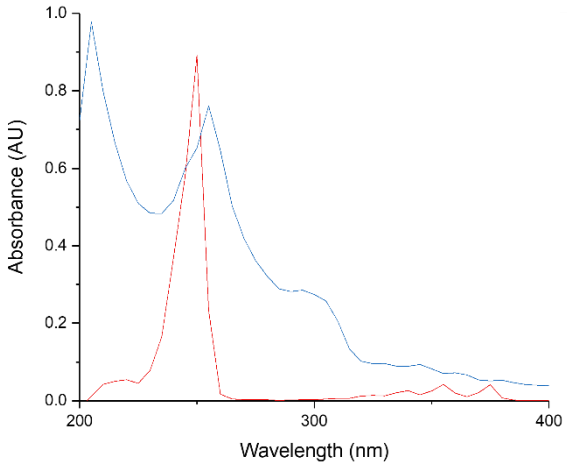


Figure 2 - 6 UV Spectra of 5 (blue) and anthracene (red)

the presence of terbium and its interactions with light, as these are only observed post-terbium/DO3A combination.

2.3 The Impact of Deuterated Solvent on Photophysical Properties

Low-energy excited states of lanthanides are easy to quench by oscillators including O-H, N-H and C-H and it can therefore be advantageous to minimise the exposure of lanthanide complexes to these quenchers. To potentially increase the visibility of any luminescent properties there are two ways to protect a lanthanide centre: encapsulate the lanthanide ion in a multidentate Schiff base to shield it from the exterior solvent system,[124] or to use a deuterated solvent system. With these solvents, emission can be found to be higher as O-D vibrations are less effective at quenching excited states than their protonated counterpart. It is also found that as solvent polarity increases, the relative intensity of the lanthanide can be found to decrease.[125]

Studies previously carried out on other structures such as curcumin[126] have also been undertaken to explore the effect of deuterated solvent on its photophysical properties and whether the shift in the spectra obtained was caused by the polarity effect, hydrogen transfer mechanism, or intermolecular hydrogen bonding. Exploration of several different solvents found the width of its fluorescence spectra diminished in deuterated solvents as opposed to non-deuterated. The suggestion has therefore been that when in deuterated solvents the interchanging of curcumin's various isomeric forms was partially inhibited, and that polarity of the solvent is an important factor in luminescence. From these conclusions it was decided

a brief investigation into the effect of deuterated solvent on the photophysical properties of the chosen complexes would be beneficial.

Luminescence studies were carried out to determine if there was a viable difference in the protonation of the solvent, and if this was a notable factor that affected its luminescence. The complex was dissolved in both deuterated methanol (MeOD) and MeOH to a concentration of 0.05 mM and the solutions degassed using liquid nitrogen and a customised degassing cuvette. Luminescence and UV-Vis scans were run on all samples. The samples were then oxygenated, and the same analysis run. Luminescence spectra were recorded at degassed and T = 0 minutes oxygenated. As prolonged exposure to oxygen over time results in degradation of the complex from its anthracene ligand into its oxygen-bonded counterpart as seen in **Figure 2 - 7**, solutions were only given an initial exposure to oxygen and then resealed to create a closed environment for the purpose of analysis.



Figure 2 - 7 Anthracene (left) and its oxygen-bonded counterpart (right) after interaction with singlet oxygen causes broken conjugation across the chromophore

The Diels-Alder reaction seen in this figure involves formation of two carbon-carbon bonds simultaneously to generate a cyclohexane in what is referred to as [4+2] cycloaddition.[127] For this to work two key structures are required: a conjugated diene in possession of 4 π electrons, and a dienophile (alkene or alkyne) that has 2 π electrons in a *cis* orientation.[128] This orientation is crucial as the *trans* orientation lacks the required proximity for the ends of the structure to react. **Figure 2 - 8** displays the mechanism through which these structures interact, transferring energy density from the HOMO of the diene to the dienophile's LUMO.

This is only possible when the molecular phases of these orbitals overlap and results in symmetry-allowed formation of σ-bonds inherently more stable than their π counterparts. When the dienophile has an electron withdrawing group, this reaction proceeds at even greater speeds.



Figure 2 - 8 The mechanism of the Diels-Alder reaction, showing formation and breaking of two bonds simultaneously

Reaction of anthracene in this chapter proves irreversible, as high temperatures equal to or exceeding 200 °C are required to engage in retro Diels-Alder synthesis,[128, 129] meaning the resultant product observed in this chapter upon reaction with singlet oxygen is highly stable and favoured in comparison to its reactant, both of which can be seen in **Figure 2 - 9.**

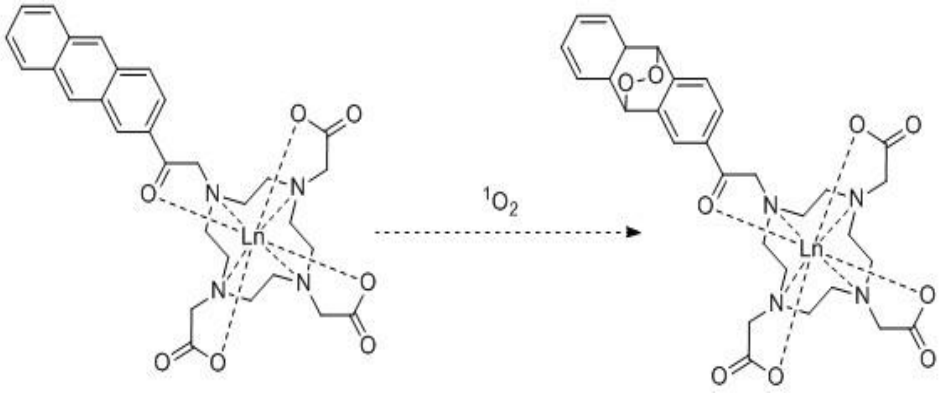


Figure 2 - 9 Reaction of the generalised lanthanide complex studied in this chapter with singlet oxygen, resulting in an acetophenone system with greater stability

Analysis of the fluorescence spectra in **Figure 2 - 10** indicates a large difference in intensity between the deuterated and standard methanol, with MeOH resulting in a much higher intensity than MeOD. The fluorescence spectrum also shows a clear difference between degassed and oxygenated levels, with **5** registering a 26% greater intensity in the degassed state compared to oxygenated. Phosphorescence shows a change as well, with the degassed

complex exhibiting phosphorescence 18% stronger than when oxygenated. When comparing to the deuterated solvent, an obvious difference can be seen, where fluorescence and phosphorescence of the complex in deuterated solvent registers at roughly 79% less than their protonated equivalent. Similar results are seen in **6**, though the difference between the solvent choices is less, with only a 60% decrease between protonated and deuterated methanol in both degassed and oxygenated states.

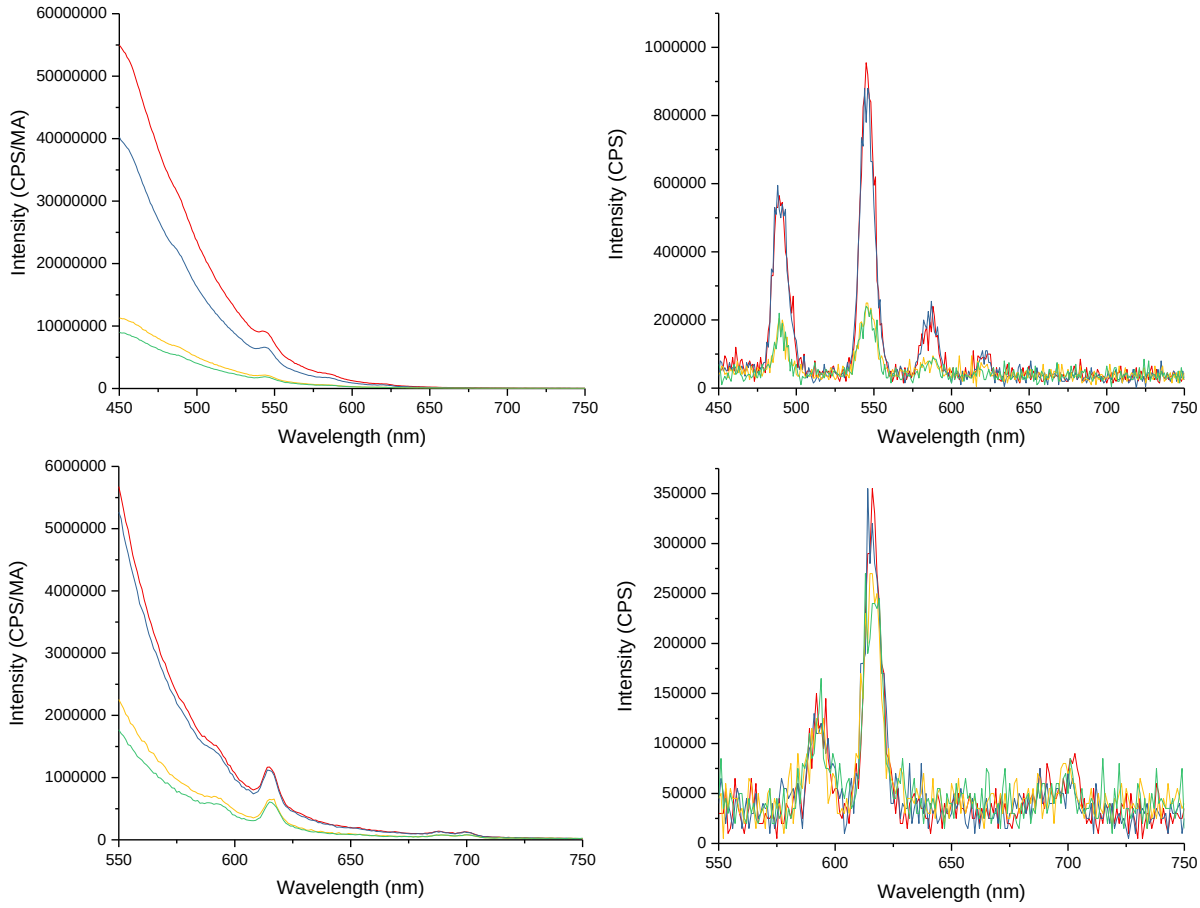


Figure 2 - 10 Top: Fluorescence (left) and phosphorescence (right) of 5. Bottom: Fluorescence (left) and phosphorescence (right) of 6. Scans are taken in MeOH at degassed (red) and oxygenated (blue) levels, and in MeOD at degassed (yellow) and oxygenated (green) levels

For europium, LMCT can quench the emissive state of the lanthanide, but for terbium this is not the case. As such, intramolecular quenching of europium emission is always likely to be the dominant pathway and collisional quenching of the donor triplet state is likely to result in the greater changes observed in **5**.

UV analysis corresponds with the selection of MeOH as the primary solvent of choice, as the intensity of absorbance observed is higher than is seen with MeOD. This is seen for both **5** and **6** as seen in **Figure 2 - 11**, which corresponds with the initial hypothesis that exposure of these complexes to oxygen results in an increase in luminescence, and suggests that solvent polarity may be an influencing factor in the photophysical properties of these complexes.

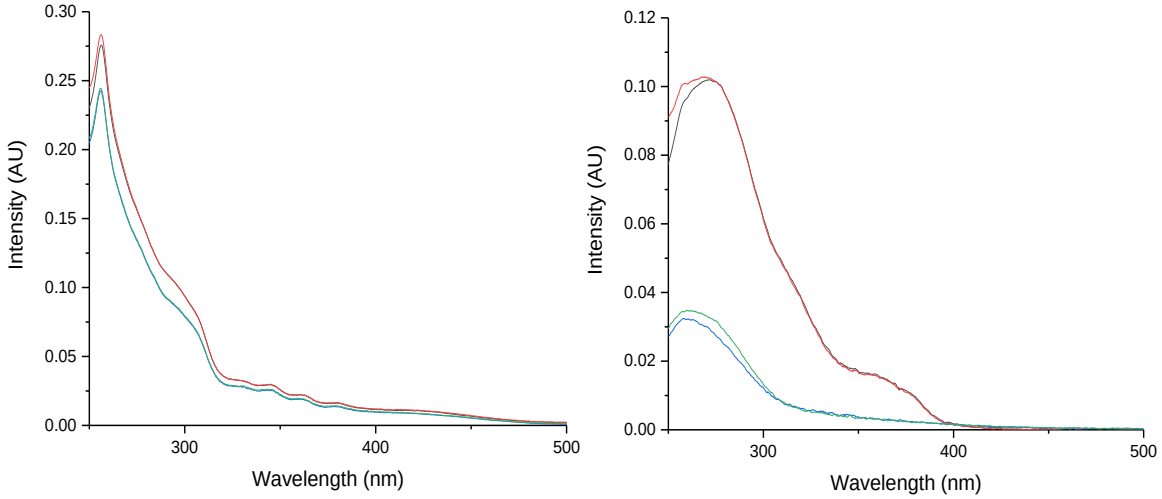


Figure 2 - 11 UV-Vis Spectra of 5 (left) and 6 (right) complexes in MeOH at degassed (black) and oxygenated (red) levels, and in MeOD at degassed (blue) and oxygenated (green) levels

It can be concluded from these studies that whilst deuterated solvents may play a role in increasing the luminescence intensity of a complex, in cases where a lanthanide ion is already enclosed in a multidentate Schiff base ligand structure the impact of the O-D oscillators is negligible. Hence, standard oxygenated MeOH proves more than sufficient for analysis of luminescent properties for these lanthanide-ligand structures.

2.4 The Impact of Oxygenation

Oxygen-sensitive luminescent molecular probes are not a novel concept and can prove advantageous in medicinal applications such as MRI contrast agents. In circumstances where tumours possess hypoxic regions, complexes that are sensitive to this differential are essential to detailed and accurate diagnoses. By synthesising oxygen-sensitive complexes, it is hoped

that quality of MRI and other imaging services that utilise such contrast agents can be improved, and such is the focus of this research project.

To investigate the luminescence potential of the complexes as standalones in a zero-input system, the impact of oxygen alone was analysed. Complexes were diluted to 0.05 mM in MeOH, and degassing performed using liquid nitrogen and a specially designed degassing cuvette. The complex was then analysed via luminescence and UV-Vis, after which the tap of the cuvette was opened to expose the solution to oxygen and shaken gently but thoroughly to ensure adequate mixing of solution and air. Standard MeOH was used as exposure to air deteriorates the quality of deuterated methanol over time and has already been proven in this thesis to be the superior solvent of choice. This was then re-analysed via luminescence and UV-Vis at 30-minute intervals from T = 0 to T = 3 hr to determine if there was any observable change to the luminescence of the complex.

To observe the data trend more clearly, selected data runs from degassed and T = 0, 1, 2, 3 hr were selected for comparison and are shown in **Figure 2 - 12**. Analysis of **6** shows an initial decrease in fluorescence in tandem with only a slight increase in phosphorescence upon initial oxygenation, with fluorescence decreasing by approximately 19% after 180 min and

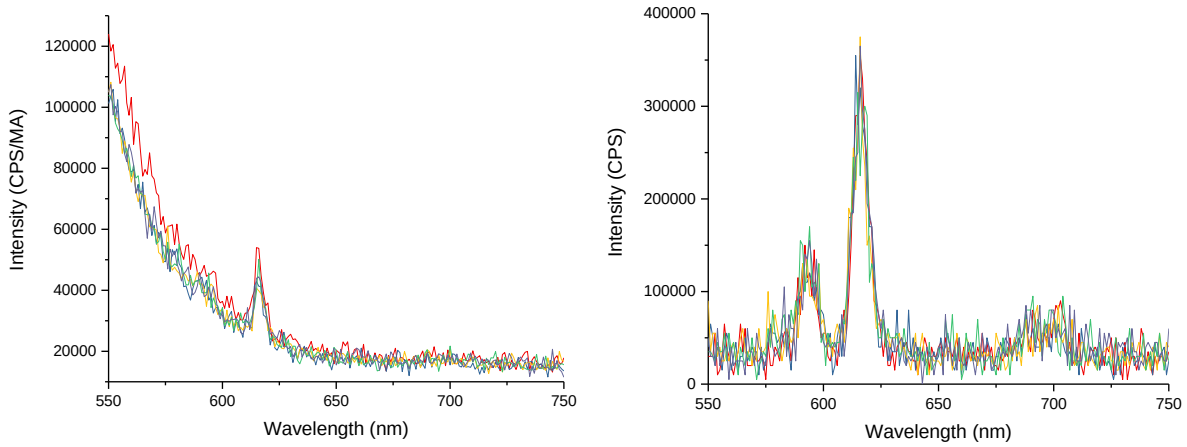


Figure 2 - 12 Fluorescence (left) and phosphorescence (right) of 6 at degassed (red), and T = 0 hr (blue), 1 hr (yellow), 2 hr (green), and 3 hr (black) in standard oxygenation conditions

phosphorescence increasing by only 3%. Analysis on the hourly mark shows only very slight changes in these luminescence scans over time. Oxygen can therefore be seen to impact the luminescence of the complex; however, the impact is only predominant in the initial exposure to oxygen and has a minimal impact in prolonged exposure. It can therefore be inferred that whilst oxygen does induce a change in the luminescence, additional stimuli to improve luminescence intensity is required.

The data for **6** indicates photo reactivity as the anthracene T_1 state is too low in energy to sensitise and so has little reaction time. This can be attributed to interaction of oxygen with the complex, as the redox mechanism takes precedence over the standard Dexter-type exchange due to the difference in energy required. Fluorescence also indicates a decrease in intensity upon oxygenation which continues to drop over time. This corresponds with the increase in phosphorescence as spin change occurs within the complex during oxygen quenching. Similar results are observed for **5** as seen in **Figure 2 - 13** with a decrease in both phosphorescence and fluorescence.

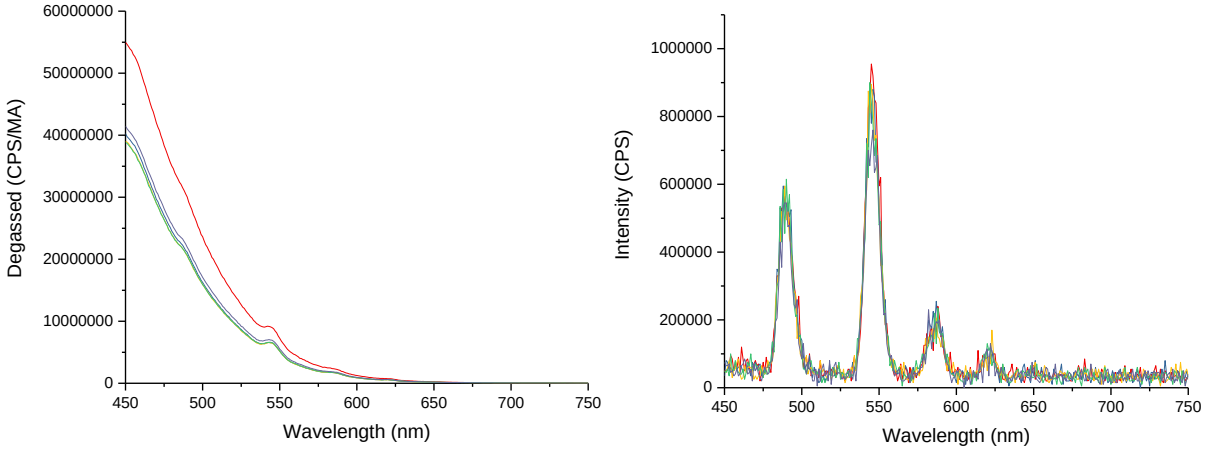


Figure 2 - 13 Fluorescence (left) and phosphorescence (right) of 5. Fluorescence (left) and phosphorescence (right) of 6 at degassed (red), and T = 0 hr (blue), 1 hr (yellow), 2 hr (green), and 3 hr (black) in standard oxygenation conditions

2.5 OXYGENATION AND IRRADIATION

To see if the level of photo reactivity could be influenced beyond the minimal input of oxygen alone, a similar study to the oxygenation experiment was run with the additional step of irradiation under a 365 nm lamp for 10-min intervals to a total accumulation of 60 min. Studies were completed in standard MeOH in accordance with previously discussed reasoning. Each complex was degassed using liquid nitrogen and a customised degassing cuvette, and degassed luminescence and UV-Vis run. The solution was then oxygenated and analysed before irradiation studies commenced.

Figure 2 - 14 summarises the luminescence data obtained. Analysis of **5** indicates that exposure to irradiation induces a greater shift than exposure to oxygen alone, with a decrease of 55% in fluorescence intensity at its maximum intensity, and an increase at λ = 616 nm of 45% after 60 min irradiation. Phosphorescence is also seen to increase by 91% at this wavelength, implying that in order to successfully initiate the photochemical Diels-Alder reaction necessary, both oxygen and irradiation are required stimulants. Similar results are observed in **6**, indicating that irradiation for both of these complexes results in a higher rate of broken conjugation across the anthryl chromophore, allowing for greater rates of spin change and inducing a larger shift in luminescence overall.

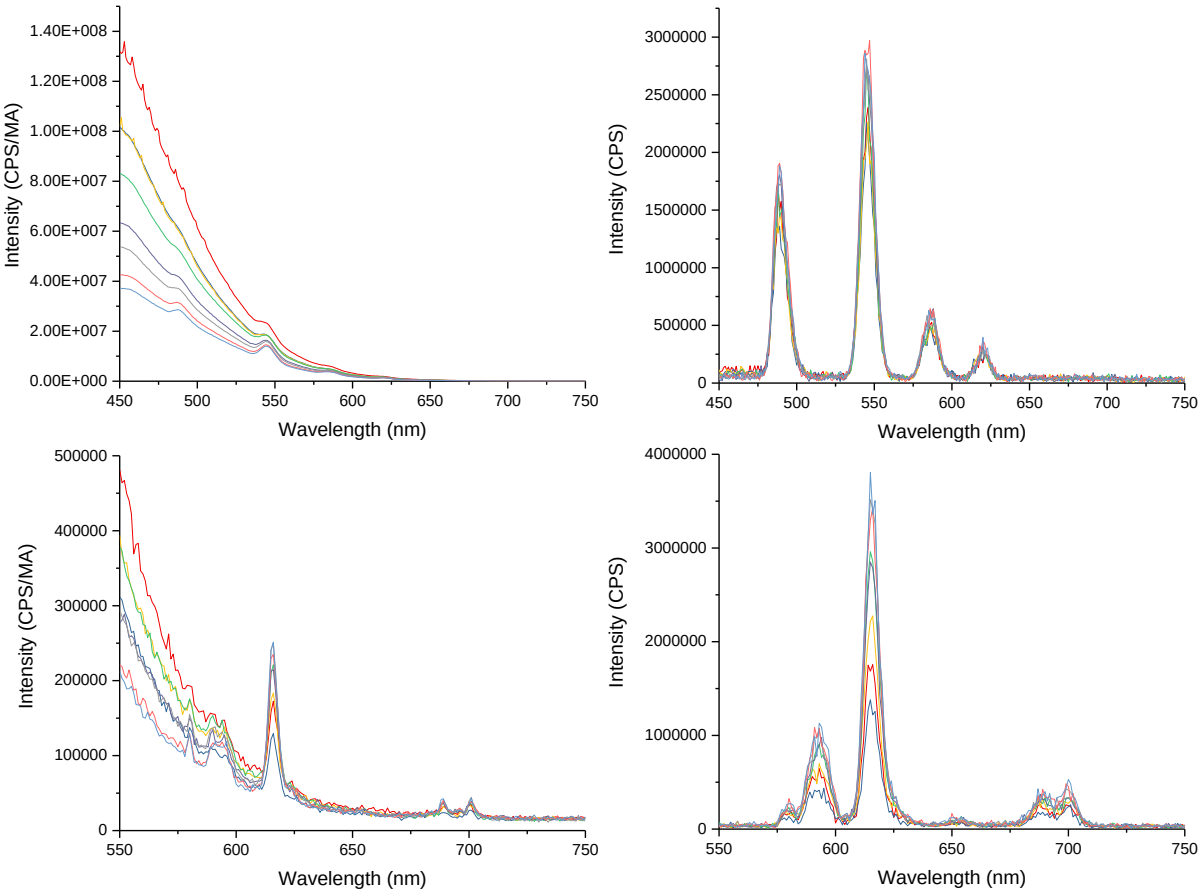


Figure 2 - 14 Top: Fluorescence (left) and phosphorescence (right) spectra of 5 during irradiation Bottom: Fluorescence (left) and phosphorescence (right) spectra of 6 during irradiation. Degassed = 10 min; Irradiation at 0 min = blue; 10 min = yellow; 20 min = green; 30 min = black; 40 min = grey; 50 min = pink; 60 min = cyan

Energy transfer from the triplet of the chromophore to that of the lanthanide seen in **Figure 2 - 15** is both rapid and irreversible which makes both the intensity and lifetime of the resulting luminescence independent from the input of oxygen.[37] When thermal repopulation of the triplet state of the chromophore from the lanthanide is easy, however, the intensity of this emission becomes subsequently dependent on the concentration of dissolved oxygen. This effect is heavily exploited in redox probes and has been previously investigated and confirmed,[37, 130] and implies in respect to the probes explored here that it is easier to generate the triplet state in the presence of oxygen. Quenching of this triplet state, however, is more facile when oxygen is present.

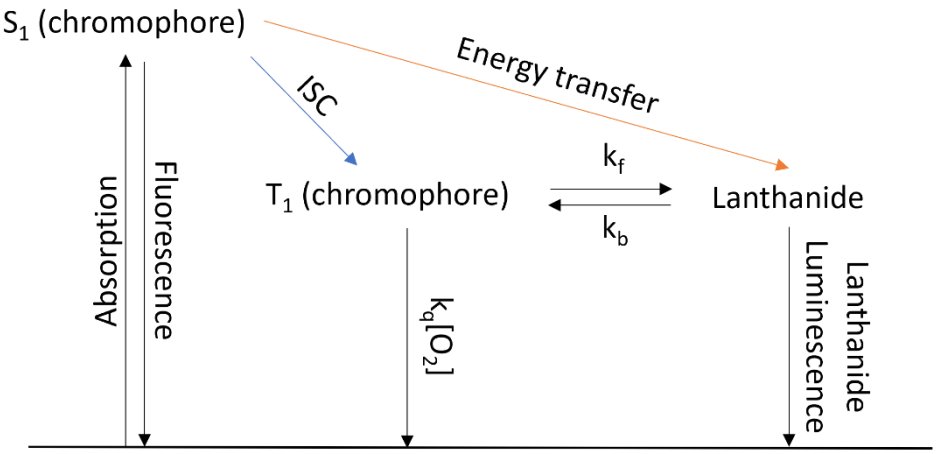


Figure 2 - 15 Energy transfer cascade for sensitised emission of a lanthanide, adapted from Hueting, Tropiano & Faulkner.[37] ISC is intersystem crossing, k_f and k_b are the energy constants for forward and backward energy transfer respectively

UV characterisation of **5** is shown in **Figure 2 - 16**, which demonstrates that irradiation induces a noticeable reduction in the anthryl attributed peak around λ = 252 nm as irradiation time increases, with a 34% reduction in absorbance after 60 min irradiation. A similar effect is seen in the large peak at λ = 300 nm caused by the Tb-DO3A component of the complex. This suggests that exposure to the UV light instigates an observable shift in luminescence from the anthryl chromophore to the lanthanide ion through the antenna effect, as luminescence is seen from both the chromophore and the lanthanide. A similar effect is seen in **6**, with a 29%

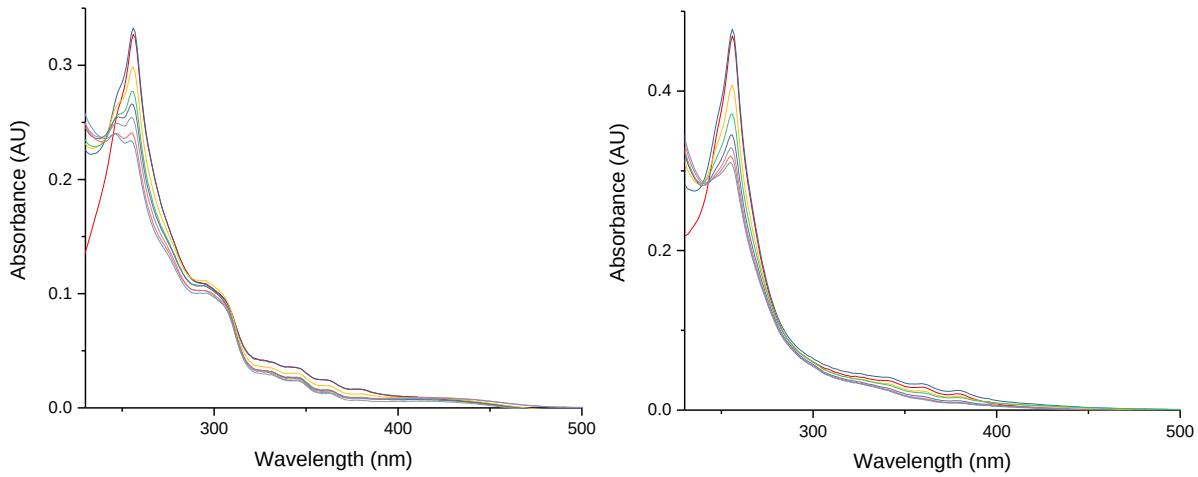


Figure 2 - 16 UV-Vis Spectra of 5 (left) and 6 (right). egassed = 10 min; Irradiation at 0 min = blue; 10 min = yellow; 20 min = green; 30 min = black; 40 min = grey; 50 min = pink; 60 min = cyan

drop in absorbance intensity, however this peak at λ = 300 nm is not observed. It is possible LMCT may play a role in quenching the excited state for this complex.

2.6 CONCLUSIONS

Photochemical generation for these complexes has been proven possible but the photo stability of these complexes can be problematic, and synthesis and storage must therefore be performed in the dark. Overall, these studies prove that reaction with the ROS results in generation of a more emissive product than the initial complex, and both show luminescence potential. Investigations into the deuterated solvent impact prove that when the lanthanide ion is encapsulated in a multidentate Schiff base the metal remains shielded from the solvent system and as such the positive effects a deuterated environment might offer become negligible. It can also be concluded that in oxygen chemistry terbium proves the more efficient of the two complexes overall as conversion and energy transfer occur through the triplet state yields a greater change in luminescence than europium's energy transfer mechanism of charge transfer.

2.7 REFERENCES

1. Staszak, K.; Wieszczycka, K.; Marturano, V.; Tylkowski, B., Lanthanides complexes – Chiral sensing of biomolecules. *Coordination Chemistry Reviews* **2019,** *397*, 76-90.
2. Qiu, Z.; Shu, J.; Liu, J.; Tang, D., Dual-Channel Photoelectrochemical Ratiometric Aptasensor with up-Converting Nanocrystals Using Spatial-Resolved Technique on Homemade 3D Printed Device. *Analytical Chemistry* **2019,** *91* (2), 1260-1268.
3. Luo, Z.; Zhang, L.; Zeng, R.; Su, L.; Tang, D., Near-Infrared Light-Excited Core–Core–Shell UCNP@Au@CdS Upconversion Nanospheres for Ultrasensitive Photoelectrochemical Enzyme Immunoassay. *Analytical Chemistry* **2018,** *90* (15), 9568-9575.
4. Song, B.; Wang, G.; Tan, M.; Yuan, J., A Europium(III) Complex as an Efficient Singlet Oxygen Luminescence Probe. *Journal of the American Chemical Society* **2006,** *128* (41), 13442-13450.
5. Sørensen, T. J.; Kenwright, A. M.; Faulkner, S., Bimetallic lanthanide complexes that display a ratiometric response to oxygen concentrations. *Chemical Science* **2015,** *6* (3), 2054-2059.
6. Payne, S. J.; Fiore, G. L.; Fraser, C. L.; Demas, J. N., Luminescence Oxygen Sensor Based on a Ruthenium(II) Star Polymer Complex. *Analytical Chemistry* **2010,** *82* (3), 917-921.
7. Ung, P.; Clerc, M.; Huang, H.; Qiu, K.; Chao, H.; Seitz, M.; Boyd, B.; Graham, B.; Gasser, G., Extending the Excitation Wavelength of Potential Photosensitizers via Appendage of a Kinetically Stable Terbium(III) Macrocyclic Complex for Applications in Photodynamic Therapy. *Inorganic Chemistry* **2017,** *56* (14), 7960-7974.
8. Dadabhoy, A.; Faulkner, S.; Sammes, P. G., Long wavelength sensitizers for europium(iii) luminescence based on acridone derivatives. *Journal of the Chemical Society, Perkin Transactions 2* **2002,** (2), 348-357.
9. Hui, Y.; Feng, W.; Wei, T.; Lü, X.; Song, J.; Zhao, S.; Wong, W.-K.; Jones, R. A., Adjustment of coordination environment of Ln3+ ions to modulate near-infrared luminescent properties of Ln3+ complexes. *Inorganic Chemistry Communications* **2011,** *14* (1), 200-204.
10. Chen, S.; Fan, R.-Q.; Gao, S.; Wang, X.; Yang, Y.-L., Synthesis, crystal structure and effect of deuterated solvents and temperature on visible and near infrared luminescence of N4-donor Schiff base lanthanide complexes. *Journal of Luminescence* **2014,** *149*, 75-85.
11. Barik, A.; Goel, N.; Priyadarsini, I.; Mohan, H., Effect of Deuterated Solvents on the Excited State Photophysical Properties of Curcumin. *Journal of Photoscience* **2004,** *11*.
12. Wessig, P.; Müller, G., The Dehydro-Diels−Alder Reaction. *Chemical Reviews* **2008,** *108* (6), 2051-2063.
13. Klein, D. R., *Organic Chemistry, 2nd Edition*. Wiley: 2013.
14. Martin, J. G.; Hill, R. K., Stereochemistry of the Diels-Alder Reaction. *Chemical Reviews* **1961,** *61* (6), 537-562.
15. Hueting, R.; Tropiano, M.; Faulkner, S., Exploring energy transfer between pyrene complexes and europium ions – potential routes to oxygen sensors. *RSC Advances* **2014,** *4* (83), 44162-44165.
16. Watkis, A.; Hueting, R.; Sørensen, T. J.; Tropiano, M.; Faulkner, S., Controlling energy transfer in ytterbium complexes: oxygen dependent lanthanide luminescence and singlet oxygen formation. *Chemical Communications* **2015,** *51* (86), 15633-15636.

3 Attempts on a Hetero-Metallic Luminescent Lanthanide Complex

3.1 Introduction

The systems of luminescent heterometallic complexes are less well known in modern research and can only be properly understood if both the metal ions are irreversibly bound in the appropriate binding pockets. Their properties are influenced by their structure, which enables synthetic chemists more control and exploitation of these characteristics in probe design. In these heterometallic complexes, only one energy transfer can occur per excitation event, which bears marked similarity to their monometallic analogues. When infused with lanthanide ions, these metal organic frameworks have demonstrated unique optical properties, and show promise as materials in sensing applications.[131]

Shielding of the *f*-orbitals in lanthanides is directly responsible for the bonding properties of lanthanide ions, causing their interactions with other elements to be mostly ionic in nature. The result of this is a ligand environment highly ineffective in influencing the lanthanide ion to which they are bound. This is reflected in the magnetic and luminescent properties of the lanthanides and has been shown to be unaffected by the type of ligand.[89] Their high coordination numbers also result in the usual atomic arrangement of a prismatic geometry.

Lanthanide luminescent bioprobes (LLBs) have shown potential as alternatives to organic dyes due to their reduced sensitivity to photobleaching and long-lived excited states. They also exhibit large Stokes shifts when the ligand is excited. Their reduced sensitivity is caused by the efficiency of deactivation of the ligand triplet state by the lanthanide excited state, whilst their excited state lifetimes lead to time-resolved detection of the metal centred

luminescence within the complex. This gives extremely low background and increased sensitivity.[132]

Design of an LLB is specific and well known, with several classes analysed including backbones of macrocycles derived from cyclen, cryptands, and other azacoronands (also known as 1-aza-crown ethers).[132, 133] **Figure 3 - 1** shows examples of these, where it can be noted that azacoronands include both cryptands and cyclen-based structures. These mostly rely on an induced fit to give the desired coordination environment. Ideally, this is rigid and saturated, minimising non-radiative losses.[132] Despite their advantages however, they remain at a disadvantage as their excitation wavelength is within the UV range between λ = 320-325 nm, whilst luminescence microscopy can be performed at λ = 360 nm excitation. As a result, the photophysical properties of the helicates are not used to their full potential.

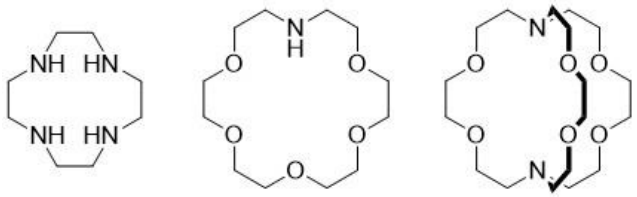


Figure 3 - 1 Cyclen, 1-aza-18-crown 6-ether as an example of an azacoronand, and 2,2,2-cryptand as an example of a cryptand

The kinetics of multi-metallic complexes rely on the stability of the ligand choice and the level of kinetic control, as when this cannot be regulated metal ions can become scrambled and form a mixture of undesired product. For a building block to be regarded as kinetically stable, low-rate constants (< 10^{-6} s^{-1}) in experimental conditions are required. Macrocyclic compounds therefore exhibit the greatest potential with a minimum of seven donor ligands required for stability. Larger chromophores also prove advantageous for stability, as lower bulkiness can translate to kinetic instability.[7, 33]

Multinuclear complexes that contain two or more lanthanide ions are generally quite rare in the field of macrocyclic chemistry, with most reported systems displaying high instability kinetically when derived from acyclic ligands. Their research focus has extended into bioassay applications and are able to be used with a variety of chromophores including but not limited to metal complexes and organic dye molecules.[134] Previous studies within the Faulkner research group have generated a trinuclear complex possessing three binding pockets featuring one ytterbium and two terbium ions. The structure of this complex can be found in **Figure 3 - 2**. When using a DTPA-like bridging ligand, it was noted that these complexes are usually *d-f* hybrids. This is due to the generally hard preparation required for synthesis of *f-f* mixed metal complexes.[16]

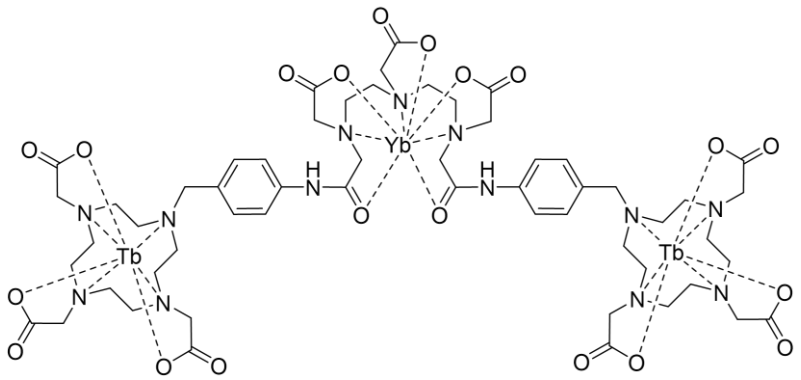


Figure 3 - 2 The trinuclear complex synthesised by Faulkner and Pope,[16] unnamed in the report

Across the lanthanide series there is a steady decrease in ionic radii as the atomic number increases.[135] The small change in this radius from one lanthanide to the next mean that whilst it is possible to distinguish those at the beginning or end of the lanthanide series (i.e. a large and small lanthanide ion) through specific ligand design, differentiation of lanthanides that possess comparable radii size is not.

There are two approaches that have been previously used to in preparation of these heterometallic complexes. The most common method involves thermodynamic control to convert more simplistic systems into complicated architecture.[30] Alternatively, complexes

which are inherently kinetically stable can be prepared through complexation with kinetic control. Both methods can generate heterometallic lanthanide complexes, though the latter method creates complexes that cannot be formed through thermodynamic control. In 1993, reports of the first instance of π-coordination in the CO ligand with an *f*-element by Beletskaya and co-workers for the trinuclear erbium complex $(EtOH)(H_2O)_4Er[Mo(CO)_3Cp]_3$ (seen in **Figure 3 - 3**) were reported. [136] This displayed a semi-bridging carbonyl and weak interaction between the erbium and molybdenum atoms.

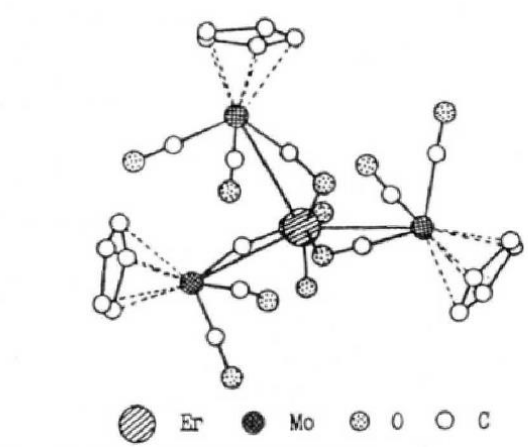


Figure 3 - 3 Ball and stick model of $(EtOH)(H_2O)_4Er[Mo(CO)_3Cp]_3$, taken from Beletskaya *et al.*[136]

It is essential in the design of a heterometallic complex that each lanthanide ion can reside in its own binding pocket with minimal dissociation. For this binding to be permanent, kinetic control is essential.[132] When working under kinetic control binding of a lanthanide ion is irreversible, and this irreversibility is key to making assembly of heterometallic lanthanide complexes possible. Any system under thermodynamic control, however, will produce a mixture of complexes that can prove challenging if not impossible to isolate and purify.

Interactions with DO3A have been previously well documented and have been performed using a wide array of substrates. Interactions between these structures have also been exploited to alter luminescence of lanthanides through solvent displacement via reactions with bidentate anions. When compared against DTPA complexes, they have proved two

orders of magnitude stronger and henceforth more stable, which can be attributed to their thermodynamic stability resulting from their "pre-organised macrocyclic structure and the higher basicity of donor groups".[133] Calculations of thermodynamic stability constants for EDTA, DOTA and DTPA in water determined that EDTA complexes have the lowest stability, whilst DOTA is the most stable.[133] Chemical structures of these backbones are seen in **Figure 3 - 4.**

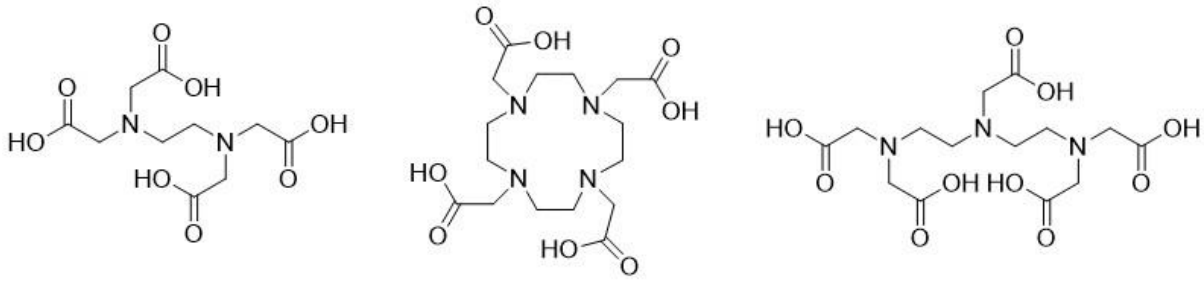


Figure 3 - 4 From left to right: EDTA, DOTA, DTPA

Formation of a lanthanide-DOTA complex is thought to occur via a three-step mechanism: coordination of the metal ion to the acetate arms, followed by coordination to two nitrogen atoms alongside simultaneous concerted proton transfer to two carboxylate arms. After this rapid deprotonation is complete, the lanthanide coordinates to the remaining nitrogen arms, giving the final combined product. This is strongly influenced by the pH of the solution in which the reactions take place, with optimal coordination occurring just below pH = 7.0.

Linkage of DO3A moieties results in formation of multi-metallic complexes that possess an inherent kinetic stability. Linkage of these moieties is achieved through a 'bridging ligand' which allows for connection of the two DO3A structures. These complexes are usually chiral in nature, and this can be utilised through experiments with circularly polarised luminescence. Time resolved luminescence spectroscopy can also be run to further understand the local environment surrounding the lanthanide ions. Previous studies have been run on such

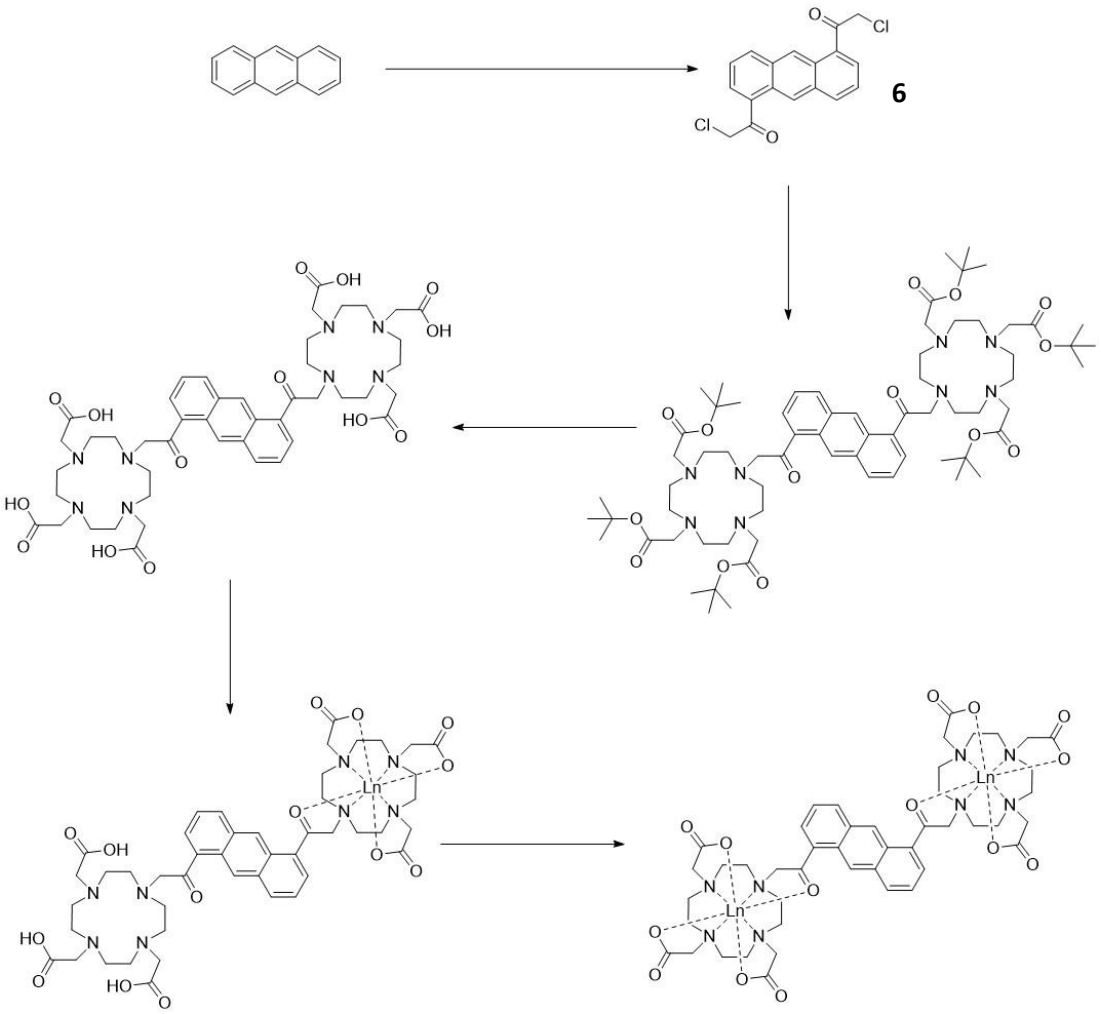
complexes with near-IR lanthanide ytterbium, where it was reported to have two distinct lanthanide environments present on the luminescence timescale.[137]

3.2 Synthesis and Attempted Isomer Separation

Synthesis was attempted using an anthryl bridging ligand to create an anthryl-bis(DOTA) backbone that contains a selection of chosen lanthanides. The predominant focus was on mixtures of europium and terbium. Cyclen was to be used as the base structure for the ligand, as it forms stable cationic complexes with protons and metal ions.[138] It was hypothesised in these complexes that addition of a second binding pocket would allow for more selective reactions with oxygen, as increasing the quantity of lanthanide within the complex would allow for more efficient deactivation, and increased sensitivity. This would also potentially allow for determination of the cause of emission, as in monometallic complexes, the presence of only one chromophore creates an environment where it is unknown what is responsible for the emission weakness.[59]

Combining europium and terbium within a singular complex would lead to quenched terbium luminescence, leaving the europium ion free to interact with the oxygen, and remain unaffected. These complexes have been previously shown to have promise *in vivo* in imaging applications[16, 59] in both bi-nuclear and tri-nuclear forms, with a general focus on lanthanide ions with smaller energy gaps. These have included elements such as ytterbium, erbium, and neodymium, which emit closer to the NIR range. Europium and terbium were of particular focus as they possess particularly long luminescence lifetimes, which are favourable in bioassay, microscopy, and sensor development among other fields.

Synthetic protocol was based off the same procedure as the monometallic lanthanide complexes, but utilising a 2:1 ratio of complex:ligand as opposed to the current 1:1. This was to be achieved through combining the anthryl ligand arm with the DO3A-based backbone in a 1:2 ratio, creating a structure with two cyclen pockets linked by the anthryl bridge seen in **Scheme 3 - 1**.



Scheme 3 - 1 Overall proposed synthetic route for Ln(bisDOTA). Reaction conditions: (i) $AlCl_3$, CH_2Cl_2 (dry), chloroacetyl chloride, -50°C – r.t. (ii) Compound 1, K_2CO_3, MeCN, 80 °C(iii) DCM, TFA, (iv) $Ln(CF_3SO_3)_3$ where initial Ln = Tb or Eu, MeOH, 60 °C

Whilst in the monometallic synthesis combination of these structures was straightforward, complications arose in the bimetallic synthesis in the initial stage, as anthracene is by nature a wholly symmetrical structure, and attachment of the chloroacetyl arms, whilst possible, proved impossible to direct to a singular product. As a result, the chloroacetyl arms were

capable of binding in a multitude of positions and ratios to the anthryl body, generating a large variety of isomers including but not limited to the targeted orientation of **6** as demonstrated in **Figure 3 - 5**.

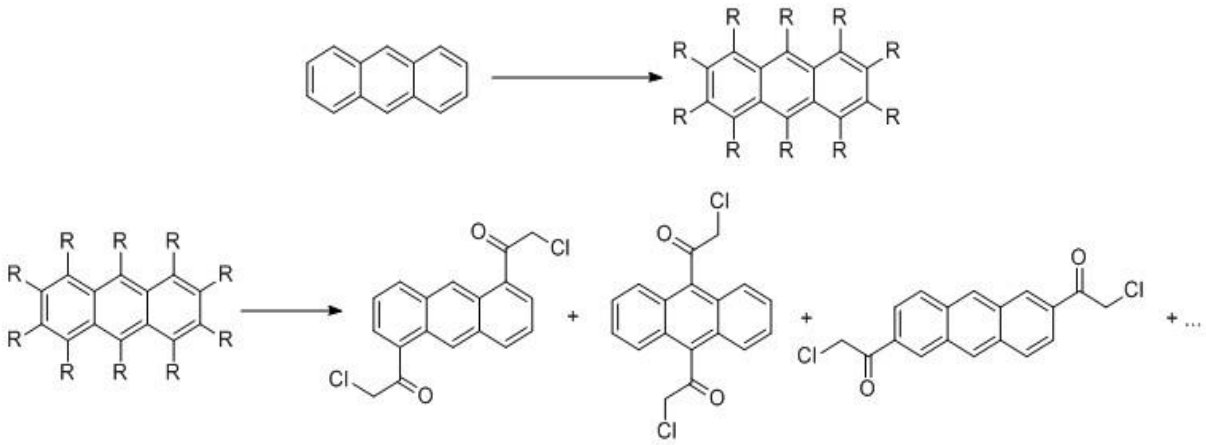


Figure 3 - 5 Potential binding points of anthracene, and some of the potential isomers that can subsequently result

The isomerisation problem could be eventually overcome through use of silica gel column chromatography through use of a slow gradient eluent across multiple columns, however the resultant NMR analysis proved difficult for most as due to the positioning of the arms, many exhibited high similarities to the point of incomprehension between the different structures as seen in **Figure 3 - 6**. The desired stereochemistry especially was of a very low yield (7% at the highest), which caused significant delays in progressing to the next step. Additional problems also arose at the next step when it could eventually be attempted, as purification issues once again resulted. This could be combated somewhat using silica gel column chromatography once more, however, again issues with purity and yield resulted as the reaction between the anthryl bridge and the DO3A pockets proved difficult to drive to completion and confirmation of synthesis could not be achieved.

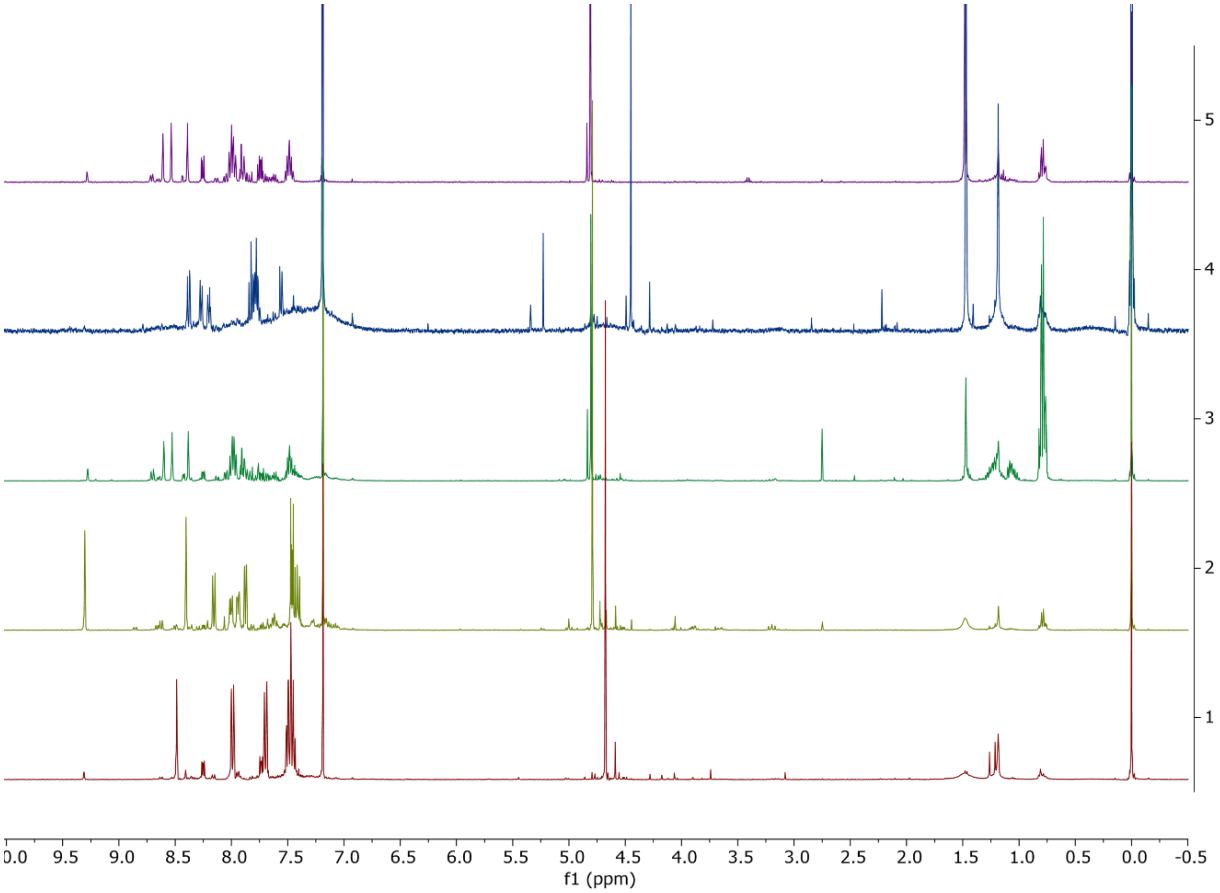
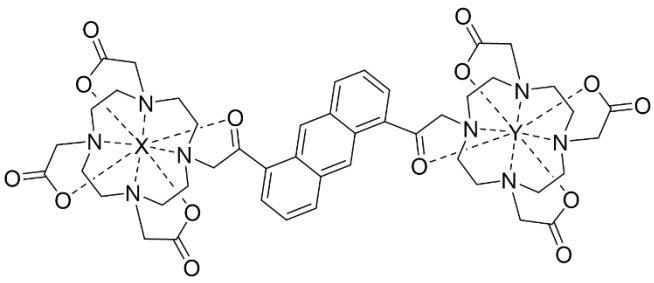


Figure 3 - 6 ^{1}H NMR Spectra of some of the different structural isomers found in synthesis of 6

Based on these problems, it was noted that purification of the final complex once both lanthanides are inserted into their respective pockets, that a hypothetical mixture of various ratios of Eu:Tb would occur, including 1:1, 2:0, 0:2, 1:0, 0:1, and 0:0, visualised in **Figure 3 - 7**. Separation of these complexes would prove difficult if not impossible even through HPLC as advised by now DPhil graduate Kezi Yao, as their respective masses and polarities would be exceptionally similar due to the identical backbone. At low yields as well, structure and presence of the lanthanide ions would be difficult to detect by NMR. Whilst work on this project was attempted for several years, success was highly limited, and it was eventually deemed the project should be discontinued, and other projects with a higher success rate focused on.



Variation	Lanthanide (X)	Lanthanide (Y)
1	N/A	N/A
2	Eu	N/A
3	N/A	Tb
4	Eu	Eu
5	Tb	Tb
6	Eu	Tb

Figure 3 - 7 The theorised final lanthanide-ligand structure, alongside a table depicting the different possible configurations. X = binding pocket 1, Y = binding pocket 2

3.3 Conclusion

In this chapter synthesis of a binuclear lanthanide complex using the same base ligand as that in the previous chapter was attempted. Previous literature dictates that synthesis of binuclear and even trinuclear complexes are possible, however complications for this class of molecule were found to arise in synthesis and purification. Development of these novel synthetic methods, whilst theoretically possible, generates various isomers and enantiomers of the base chromophore arm prior to attachment to the macrocyclic pocket. This problem extends into attachment of the two DO3A pockets and subsequent synthetic steps. Insertion of the lanthanide complexes would also prove tricky due to a potential mixture of ratiometric probes in various lanthanide ratios and the highly similar physical and chemical properties that would result.

3.4 REFERENCES

1. Wang, Y.; Wu, Y.; Zhou, C.; Cao, L.; Yang, H., A new bimetallic lanthanide metal-organic framework as a self-calibrating sensor for formaldehyde. *Inorganic Chemistry Communications* **2018,** *89*, 5-9.
2. Tropiano, M.; Faulkner, S., A lanthanide based sensor for the time-gated detection of hydrogen sulfide. *Chemical Communications* **2014,** *50* (36), 4696-4698.
3. Deiters, E.; Song, B.; Chauvin, A.-S.; Vandevyver, C. D. B.; Gumy, F.; Bünzli, J.-C. G., Luminescent Bimetallic Lanthanide Bioprobes for Cellular Imaging with Excitation in the Visible-Light Range. *Chemistry - A European Journal* **2009,** *15* (4), 885-900.
4. Faulkner, S.; Tropiano, M., Heterometallic Complexes Containing Lanthanides. *Luminescence of Lanthanide Ions in Coordination Compounds and Nanomaterials*, 2014.
5. Sørensen, T. J.; Faulkner, S., Multimetallic Lanthanide Complexes: Using Kinetic Control To Define Complex Multimetallic Arrays. *Accounts of Chemical Research* **2018,** *51* (10), 2493-2501.
6. Polasek, M.; Caravan, P., Is Macrocycle a Synonym for Kinetic Inertness in Gd(III) Complexes? Effect of Coordinating and Noncoordinating Substituents on Inertness and Relaxivity of Gd(III) Chelates with DO3A-like Ligands. *Inorganic Chemistry* **2013,** *52* (7), 4084-4096.
7. Werts, M. H. V.; Woudenberg, R. H.; Emmerink, P. G.; Van Gassel, R.; Hofstraat, J. W.; Verhoeven, J. W., A near-infrared luminescent label based on YbIII ions and its application in a fluoroimmunoassay. *Angewandte Chemie - International Edition* **2000,** *39* (24), 4542-4544.
8. Faulkner, S.; Pope, S. J. A., Lanthanide-Sensitized Lanthanide Luminescence: Terbium-Sensitized Ytterbium Luminescence in a Trinuclear Complex. *Journal of the American Chemical Society* **2003,** *125* (35), 10526-10527.
9. Cotton, S., *Lanthanide and Actinide Chemistry*. John Wiley & Sons: The Atrium, Southern Gate, Chichester, 2006.
10. Placidi, M. P.; Natrajan, L. S.; Sykes, D.; Kenwright, A. M.; Faulkner, S., Bimetallic Lanthanide Complexes Derived from Macrocycle-Appended m-Xylyl Derivatives: Synthesis and Spectroscopic Properties. *Helvetica Chimica Acta* **2009,** *92* (11), 2427-2438.
11. Beletskaya, I. P.; Voskoboynikov, A. Z.; Chuklanova, E. B.; Kirillova, N. I.; Shestakova, A. K.; Parshina, I. N.; Gusev, A. I.; Magomedov, G. K. I., Bimetallic lanthanide complexes with lanthanide-transition metal bonds. Molecular structure of $(C_4H_8O)(C_5H_5)2LuRu(CO)_2(C_5H_5)$. The use of 139La NMR spectroscopy. *Journal of the American Chemical Society* **1993,** *115* (8), 3156-3166.
12. Pope, S. J. A.; Kenwright, A. M.; Heath, S. L.; Faulkner, S., Synthesis and luminescence properties of a kinetically stable dinuclear ytterbium complex with differentiated binding sites. *Chemical Communications* **2003,** (13), 1550-1551.
13. Koike, T.; Gotoh, T.; Aoki, S.; Kimura, E.; Shiro, M., A new macrocyclic tetraamine, 2,4-dinitrophenylcyclen (= 1-(2,4-dinitrophenyl)-1,4,7,10-tetraazacyclododecane):synthesis, cation reporter properties, and recognition of 1-methylthymine by its zinc(II) complex. *Inorganica Chimica Acta* **1998,** *270* (1), 424-432.
14. Sørensen, T. J.; Kenwright, A. M.; Faulkner, S., Bimetallic lanthanide complexes that display a ratiometric response to oxygen concentrations. *Chemical Science* **2015,** *6* (3), 2054-2059.

4 Reducible Luminescent Lanthanide Complexes

4.1 Introduction

Whilst understanding and application of hydrogen sulfide (H_2S) and its related sulfide groups has steadily grown and improved over the years, detailed understanding about the extent of its potential application in treatments and therapeutics is still required. Development of such treatments comes with concern with using H_2S or its various salt forms, however, with complications like its malodorous and volatile nature posing some of the most obvious concerns. Additionally, the delicate balance between protective and toxic concentration levels combined with the narrow therapeutic window means doses of H_2S-based treatments must be administered in precise doses at specific times. This is further complicated by the body's maintenance of H_2S homeostasis through complex mechanisms.[78]

Treatments have been investigated regarding overdosing, intoxication, and toxic levels of H_2S. *In vitro* studies have determined that endogenous production of free radicals and oxidant species may be involved with sulfide's cytotoxic effects which is potentially related to the *in vivo* toxicity H_2S demonstrates.[100] Use of azides in a reductive manner activates the sensing group and induces a change in the efficiency of energy transfer between the lanthanide and the azide antenna chromophore. This was studied by Tropiano *et al.*[89] and analysis of the reduced amino structure that resulted indicated this was the only structure formed. The amino produce was also found to demonstrate high selectivity for NaHS when compared to other reducing agents like Cl^-, and HCO_3^-. These initial studies have since expanded to other fluorophore scaffolds.

One scientist reported developing a dansyl fluorophore with a sulfonyl azide[90] which was shown to react rapidly with H_2S at extremely low concentrations (down to 1 μM). Other examples include an azide-functionalised heptamethine cyanine fluorophore,[92] a hydrosulfide naphthalimide-1 probe named HSN1 and 4-azido-1,8-naphthalimide probe known as HSN2[93], and a two-photon probe using an azide-modified benzothiazole-fluorene known as FS1.[94]

An overall summation can be made that use of nitrogen within a structure is elemental for sensitivity to H_2S and other moieties including RNS, ROS, and other RSS species. However, variation within these structures indicates the overarching versatility of H_2S-sensing probes with azides as the key functional trigger. This demonstrates the highest sensitivity and fluorescence as opposed to NO_2 and other variants. Despite these promising attributes, its ability to provide information on the mechanisms of hydrogen sulfide is limited and more, novel H_2S-releasing drugs are required to provide insight into this process.[90] Throughout this research and by using and expanding this concept, it is possible to further modulate several factors including emission colours, imaging modalities, reactivity, and targetability.[87]

Synthesis in this report has focused on utilising the same core ligand structure as the monometallic and bimetallic oxygen probes functionalised with a benzo azide instead of anthracene to generate the structure seen in **Figure 4 - 1**. Azide complexes have been previously demonstrated to show high selectivity for H_2S and other sulfur species, and so it is hypothesised that reaction of this compound with a sulfide structure will induce a visible change in luminescence. This should then render the complex with potential for biological sulfide detection.

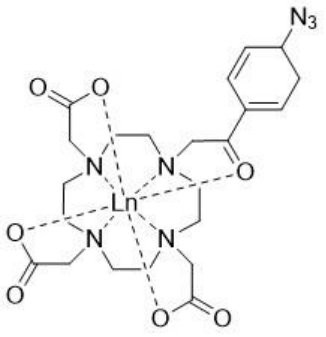
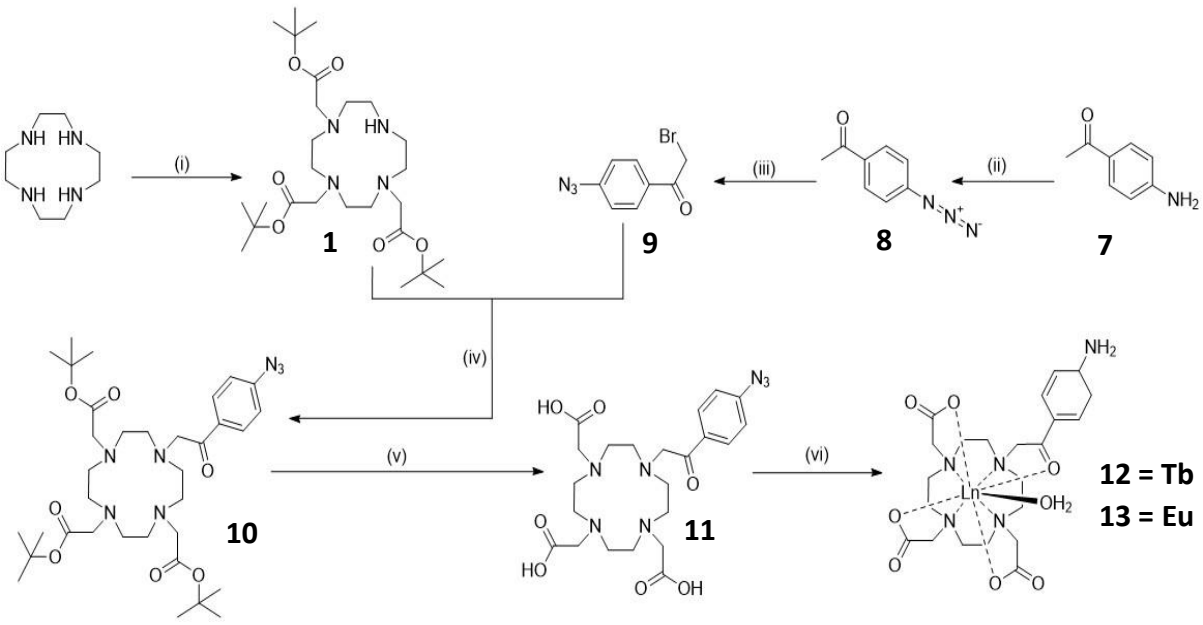


Figure 4 - 1 Target Ligand-Lanthanide structure

4.2 SYNTHESIS AND CHARACTERISATION

Synthesis was undertaken using previously reported literature procedures visualised in **Scheme 4 - 1**,[89] starting with reaction of the commercially available **7** with sodium azide through reflux to yield **8**. This was then reacted with bromine to generate **9** as reported.[89] ^{1}H NMR of this structure is seen in **Figure 4 - 3**. Slight impurities in this compound were ignored as they were small in comparison to the overall yield of product and purification was to occur in the next step. **1** was synthesised through functionalisation of cyclen according to literature[89, 123] and then reacted with **9** to generate the ligand backbone of **10**.



Scheme 4 - 1 Synthetic route for synthesis of azide probes. Reaction conditions: (i) $C_6H_{11}BrO_2$, $NaHCO_3$, CH_3CN, N_2, r.t.; (ii) 1. HCl (6M), 2. $NaNO_2$, 3. NaN_3, -15 °C; (iii) Br_2, Et_2O, dioxane, 4 °C; (iv) K_2CO_3, CH_3CN, 80 °C; (v) TFA, DCM, r.t.; (vi) $Ln(CF_3O_3S)_3$, MeOH, 60 °C

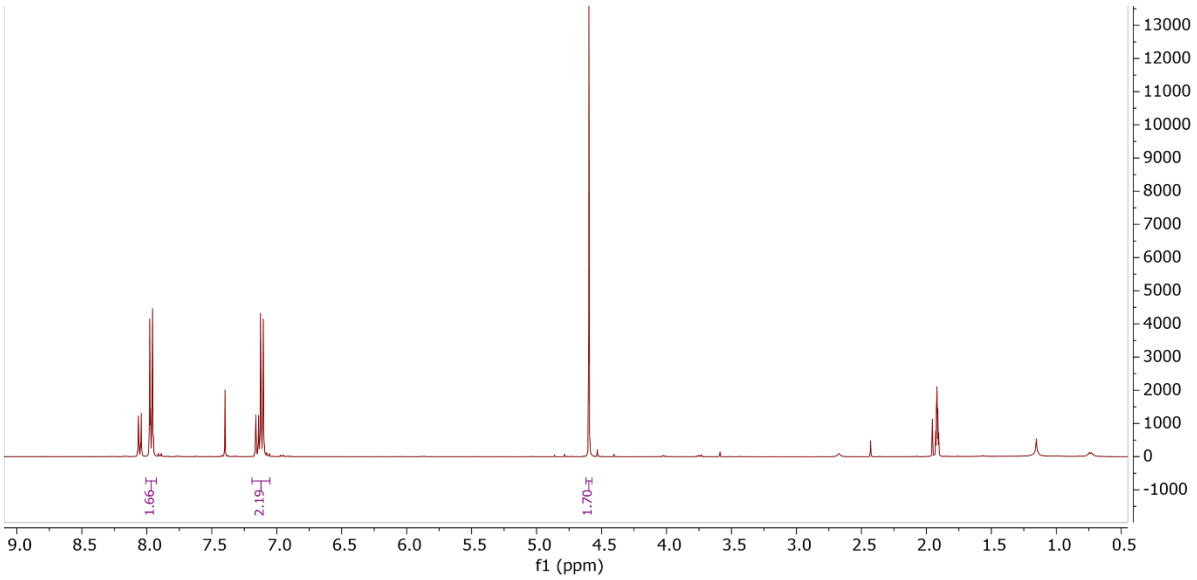


Figure 4 - 3 ^{1}H NMR Spectrum of 9

Purification of this complex was undertaken using silica gel column chromatography to separate this DO3A-benzoazide, NMR of which can be seen in **Figure 4 - 2**. Deprotection was performed using TFA and DCM in equal amounts to create a crude version of **11**, which was then purified by washing with DCM and MeOH. Further purification via trituration was then undertaken using MeOH and Et_2O to ensure a high purity **11** product. This was complexed with the appropriate lanthanide trifluoromethanesulfonate in MeOH for 48 hr before removing excess lanthanide salts as an insoluble hydroxide precipitate through adjustment of pH.

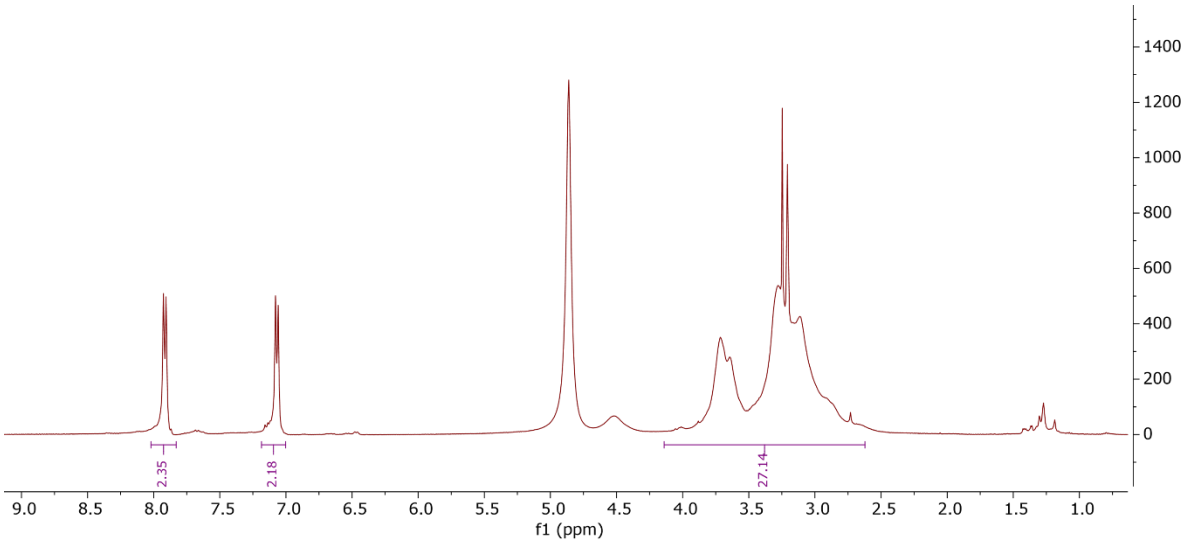


Figure 4 - 2 ^{1}H NMR Spectrum of 11

Purification was undertaken through trituration using MeOH and Et_2O, and then dialysis over 48 hr to yield **12** and **13.** This procedure was modified from initial attempts to follow the oxygen probe procedure to follow previously recorded literature,[89] however the steps in this procedure required modification to suit the need for low exposure to light.

These measures as required as azides are light-sensitive, and exposure can pre-emptively reduce it to its amine counterpart and/or promote degradation. Such preventative steps included refluxing in darkened conditions and drying to solid form whenever possible to minimise decomposition within the solvent. Sealing reaction vessels appropriately and creating stable anaerobic environments during reactions was also undertaken to minimise risk of product loss through evaporation. Reduction studies using sodium hydrosulfide and zinc were undertaken to explore the general reduction activity of the complexes. As azides exhibit light sensitivity and photodecomposition under laboratory light,[139] appropriate steps were taken to ensure minimal exposure of the azide functionality to light.

Complexes were characterised by NMR, MS, IR spectroscopy, and UV-Vis. NMR of **13** is shown in **Figure 4 - 4** and indicates clear incorporation of the lanthanide ion into the cyclen pocket, whilst mass spectrometry confirms the presence of the molecular ion. IR spectroscopy indicates the presence of both the expected cyclen amine-based structure and azide band stretching, overall confirming the successful synthesis of the complex. This corresponds with the previously reported literature.[89]

NMR spectra shows large peaks between 25-40 ppm with a minor additional geometric peak evident between 10-15 ppm, suggesting that SAP is the primary conformation of the molecule with a small percentage of TSAP present. As the remaining spectral peaks have evidently shifted to a higher chemical shift due to the pseudocontact shifts induced by the presence of the europium ion, it is suggested that most of these protons have obtained a more equatorial orientation than axial. Due to the molecule's anti-symmetric nature, specific spectral assignment is not possible, however it can overall be said that synthesis and insertion of the lanthanide into the cyclen pocket has been successful.

4.3 Reactivity with NaHS

Initial studies on the complex were run using an equivalent amount of sodium hydrosulfide (NaHS) in phosphate buffered saline (PBS) buffer using the method provided in 2014 by Tropiano and Faulkner, modified to a 1:1 ratio.[89] NaHS was dissolved in PBS buffer to 0.2 mM and added to a solution of 0.2 mM complex in buffer, thoroughly mixed, and the results observed via luminescence, UV, and MS over a short period of time. This was done to determine if a change was observable at this minimal concentration for the complexes

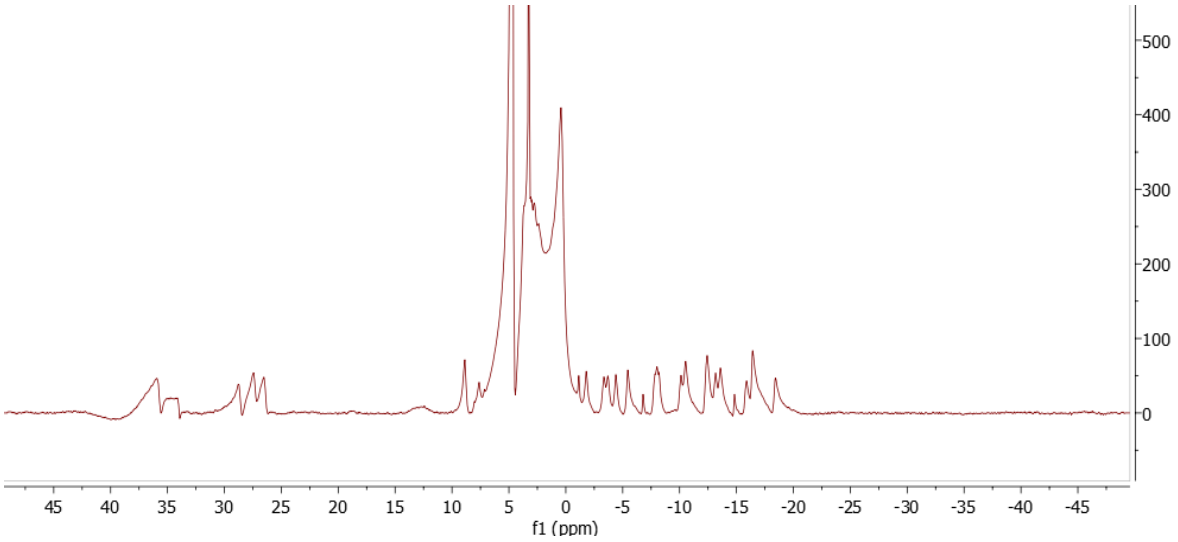


Figure 4 - 4 ^{1}H NMR Spectrum of 13

synthesised. The report only focuses on the europium derivative, however both europium and terbium complexes are studied in this thesis.

The 1:1 ratio study indicated that a change is observable upon initial addition of NaHS for both **12** and **13** as seen in **Figure 4 - 5**, with **12** demonstrating a 3% decrease in fluorescence and a 14% decrease in phosphorescence. **13** also shows an 8% decrease in fluorescence at the peak maximum, and a 10% phosphorescence increase. This was the only real change observed over time, as prolonged exposure after this initial addition shows no observable change in the luminescence beyond this point. It can therefore be confirmed that addition of NaHS induces a change in the luminescence of the azide complex upon initial combination, however any change after this introduction of sulfide is minimal and hence non-observable at this concentration. A larger concentration of NaHS, however, combined with additional external stimuli such as heat may also be required to generate a greater change in the luminescence intensity. This agrees with previous literature, which indicates a higher ratio is needed in order to generate an effective and observable reduction.[89] Overnight studies of this reaction also showed no change in luminescence.

While the previously reported literature used a 1:25 ratio of complex:NaHS in buffer, investigations were made into the suitability of different ratios to see if there was a more viable alternative. A similar procedure to the above experimental was followed, dissolving **13** to 10 µM in PBS buffer, and transferring 100 µL aliquots into 6 different vials in preparation for analysis. One of these was left to act as a control, whilst the remaining vials were reacted with 100, 200, 250, 400, and 500 µM NaHS. All vials were stirred at 37°C for 6 hr and analysed at T = 0, 3 and 6 hr to observe the clearest possible change within the complex. These concentration values were chosen to encircle the previously reported 250 µM, which chosen

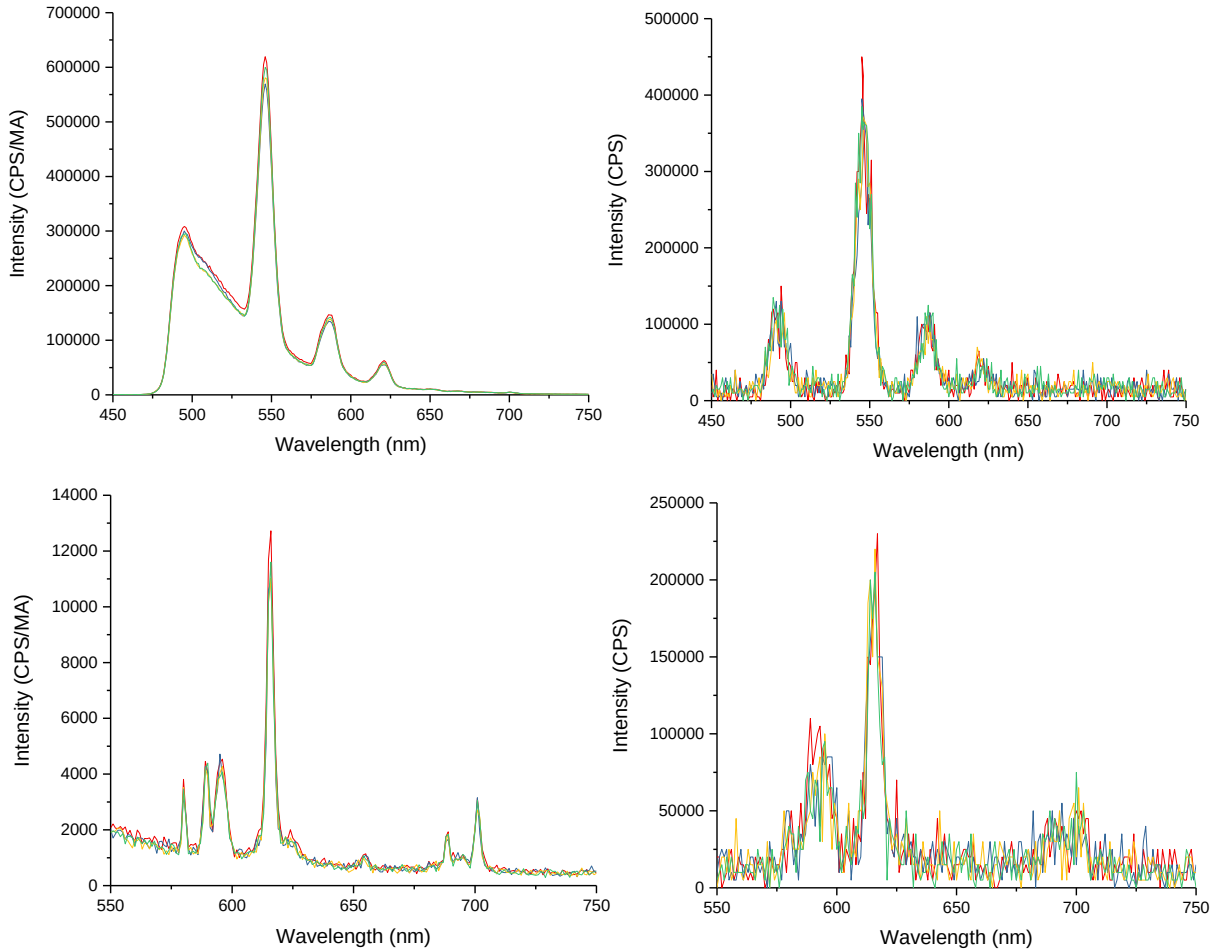


Figure 4 - 5 Top: Fluorescence (left) and phosphorescence (right) of 12. Bottom: Fluorescence (left) and phosphorescence (right) of 13. Red = 0 mM NaHS; Blue = 0.2 mM NaHS at T = 0 min; Yellow = 0.2 mM NaHS at T = 30 min; Green = 0.2 mM NaHS at T = 60 min

to create a 1:25 ratio between complex:NaHS. This reduction was observed via mass spectrometry as additional confirmation that structural changes were being induced and were thus the cause of any luminescence observations recorded after.

UV-Vis analysis at T = 6 hours shows that addition of the NaHS induces a large absorption peak in **13**, with a distinct peak formed at approximately λ = 227 nm that is not present in the control sample. This can be seen in **Figure 4 - 6**, and can is conceivably attributable to successful conversion of the azide to amine. The intensity of this peak differs according to the concentration, with a 60% increase observed when 400 µM NaHS is added in comparison to 100 µM. 500 µM appears to be an excess of NaHS, as the intensity begins to drop off by

approximately 6%. It is possible that at this higher concentration the level of NaHS begins to oversaturate the solution and interfere with the overall absorption intensity of the sample.

At higher concentrations a shift in the peak around λ = 300 nm can be seen to a higher wavelength approximating 350 nm. It can be therefore inferred that reduction of the azide complex occurs at a faster, more observable rate when a larger ratio of NaHS is present. This change can be seen to initially begin occurring at 250 µM NaHS that presents both the λ = 300 nm peak and a slight peak formation at λ = 350 nm. At 400 and 500 µM NaHS, this peak at λ = 300 nm disappears and only the peak at λ = 350 nm is seen, suggesting a more successful conversion rate at these higher concentrations whilst 250 µM indicates the beginning of an observable reduction phase.

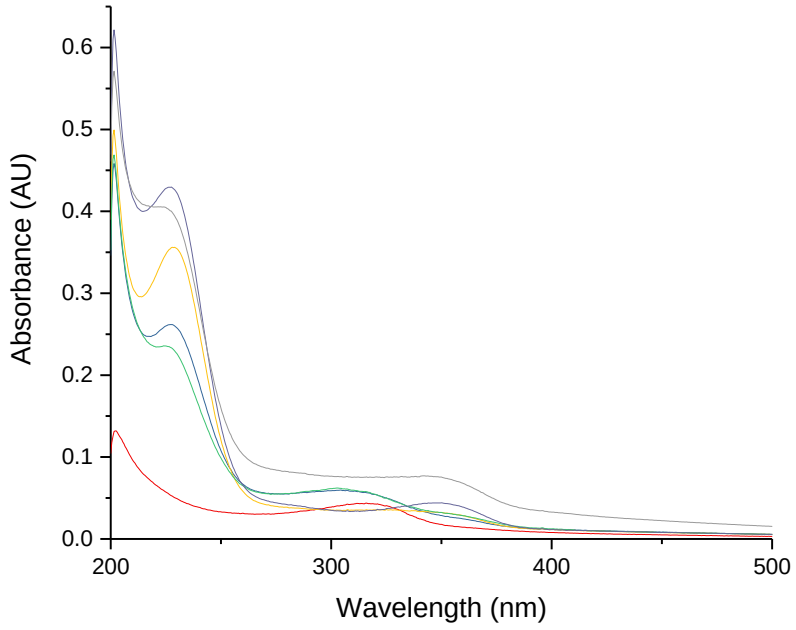


Figure 4 - 6 UV-Vis Spectrum of 13. Red = 0 µM NaHS; Blue = 100 µM NaHS; Yellow = 200 µM NaHS; Green = 250 µM NaHS; Black = 400 µM NaHS; Grey = 500 µM NaHS

This overall corresponds with the fluorescence data obtained seen in **Figure 4 - 7** which shows a clear observable increase in the absorption maxima of **13** as the concentration of NaHS increases to 400 µM. At this point, the intensity begins to decrease again as 500 µM is reached due to an excessive oversaturation of NaHS molecules causing interference in the absorption. The shift in fluorescence intensity observed is also similar to that observed in the UV-Vis, with the peak maxima at λ = 615 nm increasing by 112% with 100 µM, and 116 % with 400 µM. This is a clear indication that addition of NaHS induces a large shift in the fluorescence of the complex and is caused by conversion of the azide.

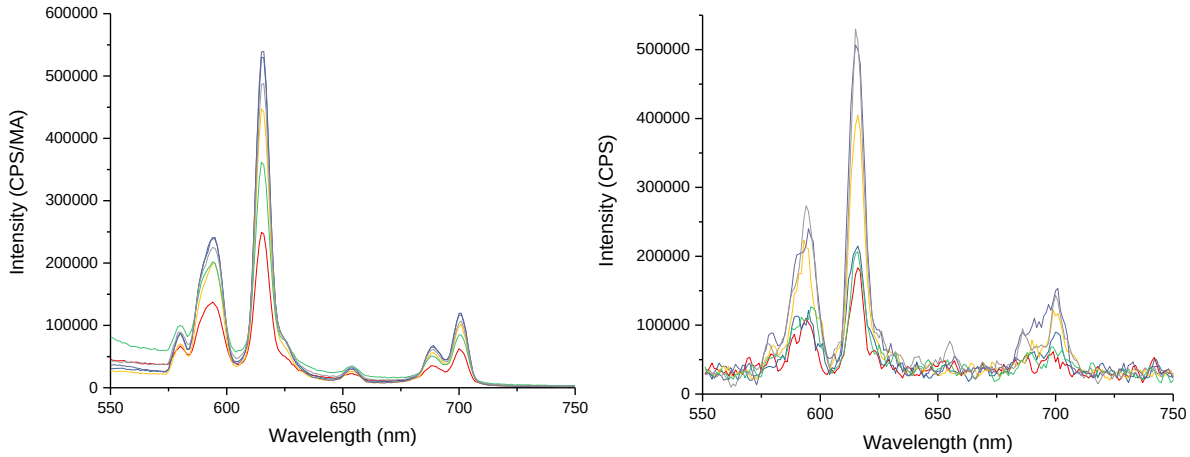


Figure 4 - 7 Fluorescence (left) and phosphorescence (right) spectra of 13. Red = 0 µM NaHS; Blue = 100 µM NaHS; Yellow = 200 µM NaHS; Green = 250 µM NaHS; Black = 400 µM NaHS; Grey = 500 µM NaHS

Similar observations are made for the phosphorescence data obtained, though the intensity in phosphoresce is observed to not change much between addition of 0, 100, and 250 µM NaHS as the maximum intensity does not shift. A much larger change is observed with addition of 200, 400, and 500 µM, and interestingly at 500 µM the phosphorescence intensity is not observed to decrease but rather continue to increase. The results indicate that 250 µM is a suitable concentration value, as it shows an obvious change between the different photophysical properties and has already been previously reported as an appropriate

concentration level. As a result, it was decided to continue research using this 1:25 ratio in accordance with previously reported literature.[89]

A final experiment was then run using this confirmed 1:25 ratio, using the same method as the previous experiment, however this time running both **12** and **13** to see if **12** would also reduce, and to confirm the previously reported experimental results for **13** when run on the same scale.[89] This was monitored by NMR and MS, and luminescence and UV-Vis analysis on the initial and final structures was run to observe any changes in the photophysical properties. Analysis was done in D_2O for ease of periodic analysis with regards to NMR.

Figure 4 - 8 shows the luminescence collected for **13** at T = 0 and T = 6 hr after reaction with NaHS. This shows an exceptionally clear difference between the azide and amine functionalities, as the azide in **13** pre-reduction shows a much lower fluorescence intensity at both time points with the maximum azide intensity of the peak at λ = 615 nm increasing by nearly 400% after conversion. This is further confirmation that the azide was successfully reduced and is also evidence that the amine possesses greater luminescence properties. Similar results are observed in the phosphorescence emission which shows an increase in the peak where λ = 595 nm of 157% for the amine when compared to the azide. This proves that

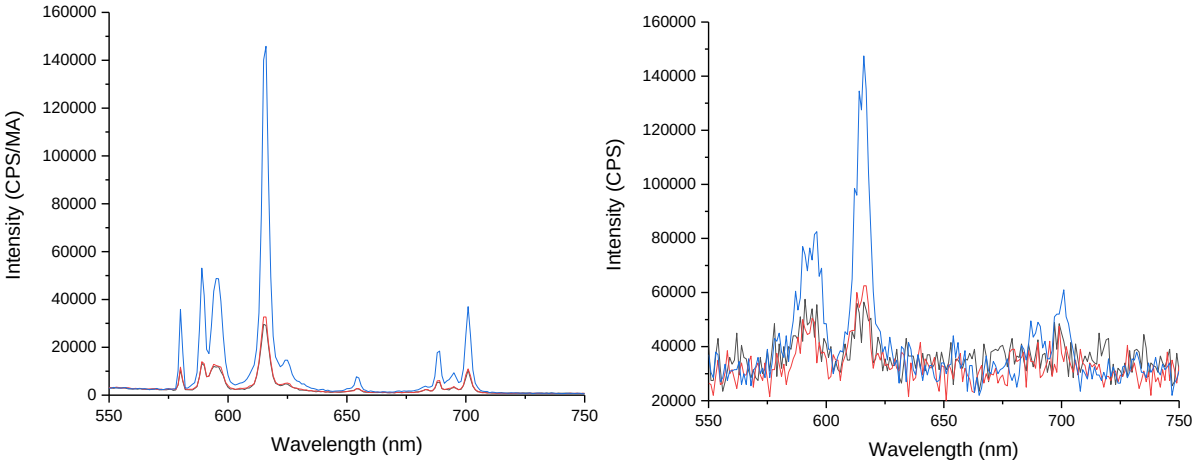


Figure 4 - 8 Fluorescence (left) and phosphorescence (right) of 13. Black = 0 hr; Red = Control at T = 6 hr; Blue = NaHS-added sample at T = 6 hr

as expected conversion of the azide to amine analogue through NaHS is possible and can be successfully performed and reproduced, and that the amine functionality results in a more luminescent complex overall.

Whilst analysis of the luminescent properties of **13** shows a clear difference between the azide and amine functionalised structures, **12** shows fewer clear distinctions. **Figure 4 - 9** shows the luminescence data collected for **12**, where addition of heat is seen to induce a change in the luminescence, increasing the luminescence by 25% at λ = 475 nm and 8% at λ = 545 nm in the control after 6 hr. After addition of NaHS, luminescence increases by 25% at λ = 475 nm accompanied by a 10% decrease at λ = 545 nm. When looking at phosphorescence, however, no visible change is observed, which suggests that when paired with terbium, fluorescence is the only measurable output as back energy transfer within the terbium complex causes quenching as the energy of the ligand triplet state is too similar to that of the terbium emissive state for effective emission.

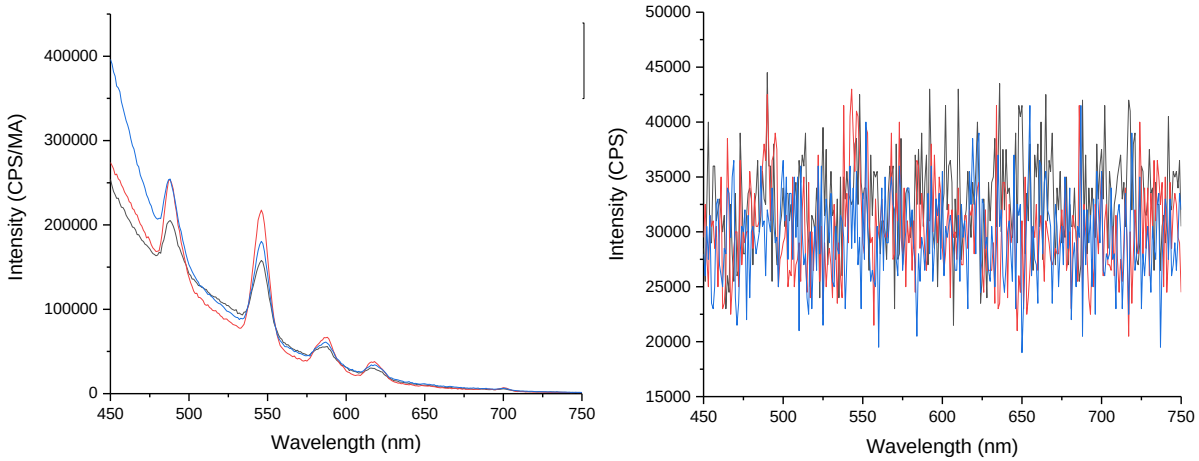


Figure 4 - 9 Fluorescence (left) and phosphorescence (right) of 12. Black = 0 hr; Red = Control at T = 6 hr; Blue = NaHS-added sample at T = 6 hr

4.4 Zinc Reduction of Azides

To further analyse the reduction potential of these complexes, investigations were made into the reactivity of azides with zinc. This has been previously proven to be an effective method of reducing this functionality using chemicals such as zinc borohydride[140] and zinc metal with ammonium chloride[141] to examine the reductive properties of this highly reactive species. For the purposes of this investigation, zinc metal was used in combination with ammonium chloride.

A simplified version of the reduction was run as an initial test to confirm that reduction of the azide was still possible with the extended ligand structure. 1 mg was dissolved in D_2O and combined with a small amount of zinc powder with ammonium chloride in solution, and the solution stirred at 37 °C for 24 hours. 10 µL aliquots were taken at hourly time points at T = 0 - 12, and T = 24 hr to observe the reaction via mass spectrometry, and the solution analysed via NMR at T = 0, 24 hr as a secondary method of confirmation. Luminescence spectra were also obtained at these time points.

Results from **13** indicate that reduction to the amine was successful, as an observable change in the NMR spectra around 35 ppm is seen that corresponds with the masses observed in mass spectrometry. NMR spectra can be found in **Figure 4 - 10**. A similarly pronounced change is seen in the NMR of **12**, though the changes within the spectra are more subtle as due to the low mass used against the wide sweep range required for terbium NMR detail is less pronounced. In particular, changes in the shifts between -50 and -100 ppm are observed as expected, as well as shifts within the axial ring protons between 150 and 350 ppm. Coupled with the mass spectrometry data this indicates that **12** also undergoes reduction which

suggests that in the presence of zinc, both are capable of reducing and suggesting that zinc is a more effective reductant than NaHS.

In this experiment, however, additional factors potentially contribute to the reduction of the azide as in addition to zinc, ammonium chloride and heat are added as additional factors in the promotion of reduction. To determine the reagent responsible, a more detailed reduction experimental was devised to observe any changes more clearly within the complexes. The complex was dissolved in D_2O to a concentration of 5 mg in solution and three 400 µL aliquots taken and transferred to separate mass spectrometry vials: one to act as a control, one to have 10% NH_4Cl added, and the final to have both 10% NH_4Cl, and zinc powder added. These were left to stir at 37 °C for 24 hr with NMR, mass spectrometry, and photophysical analysis performed at T = 0, 24 hr. To ensure removal of any excess unreacted zinc, solutions were filtered using a syringe filter prior to analysis. Additional time points were determined unnecessary during the simplified reduction study, and so the selected time points were reduced.

Analysis of the NMR of **13** shows a clear change in the axial ring protons around +25-40 ppm seen in **Figure 4 - 11**, with the zinc reduced sample showing a shift from +25-30 ppm, and loss of a peak around +35 ppm. This paired with the loss of peaks around +10 ppm and -13 ppm provide strong evidence that the azide structure has again been successfully reduced to its amine counterpart. As these changes are only observed upon reaction with zinc, it is clear the presence of NH_4Cl or heat are not influencing factors in this reduction and zinc is the sole reductant. This corresponds with the mass spectrometry data obtained in correlation, and similar results are observed in **12**.

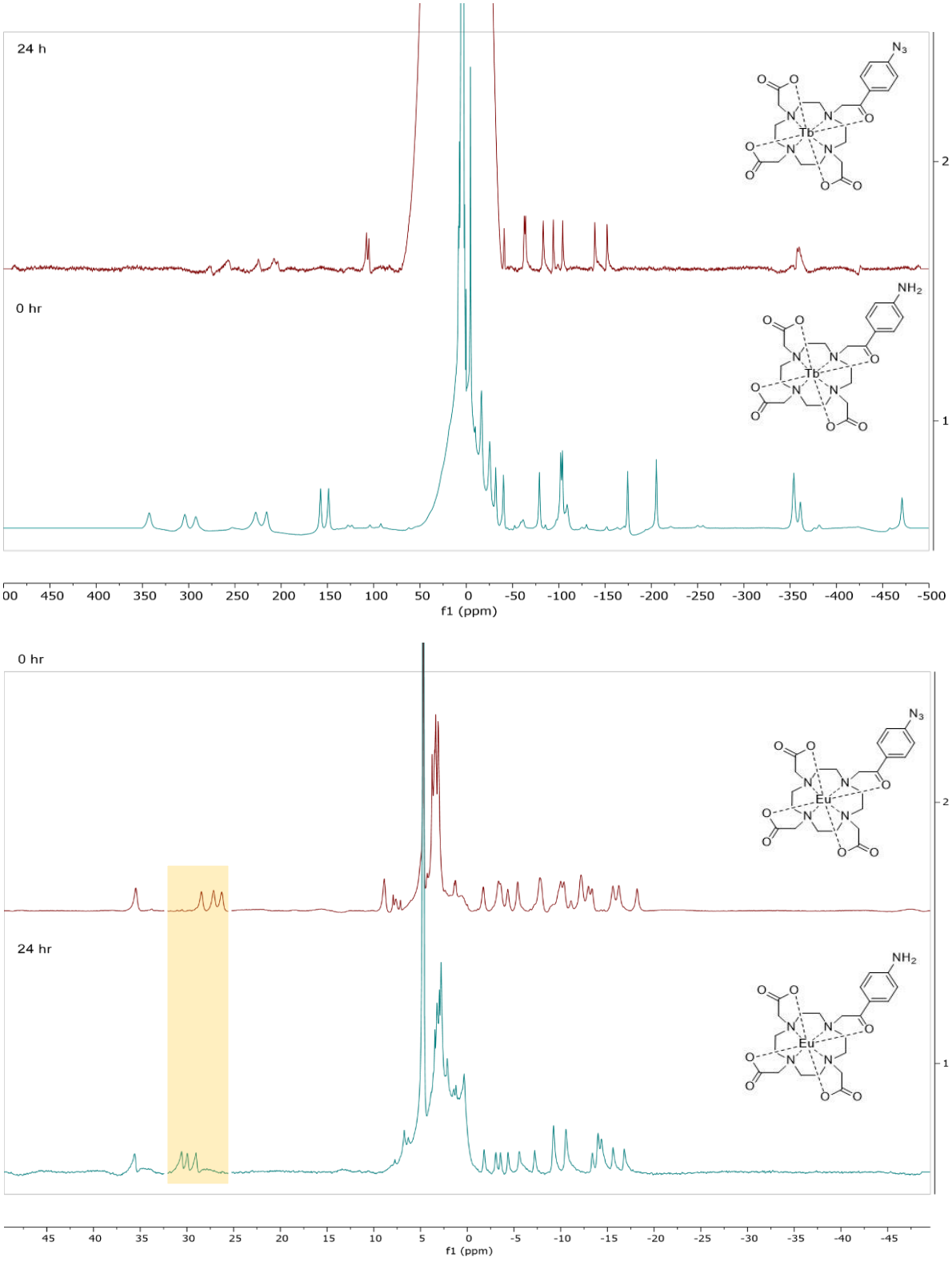


Figure 4 - 10 ^{1}H NMR spectra of 12 (top) and 13 (bottom) before and after reduction. Red = Control at T = 0 hr; Blue = Zinc + NH_4Cl at T = 24 hr.

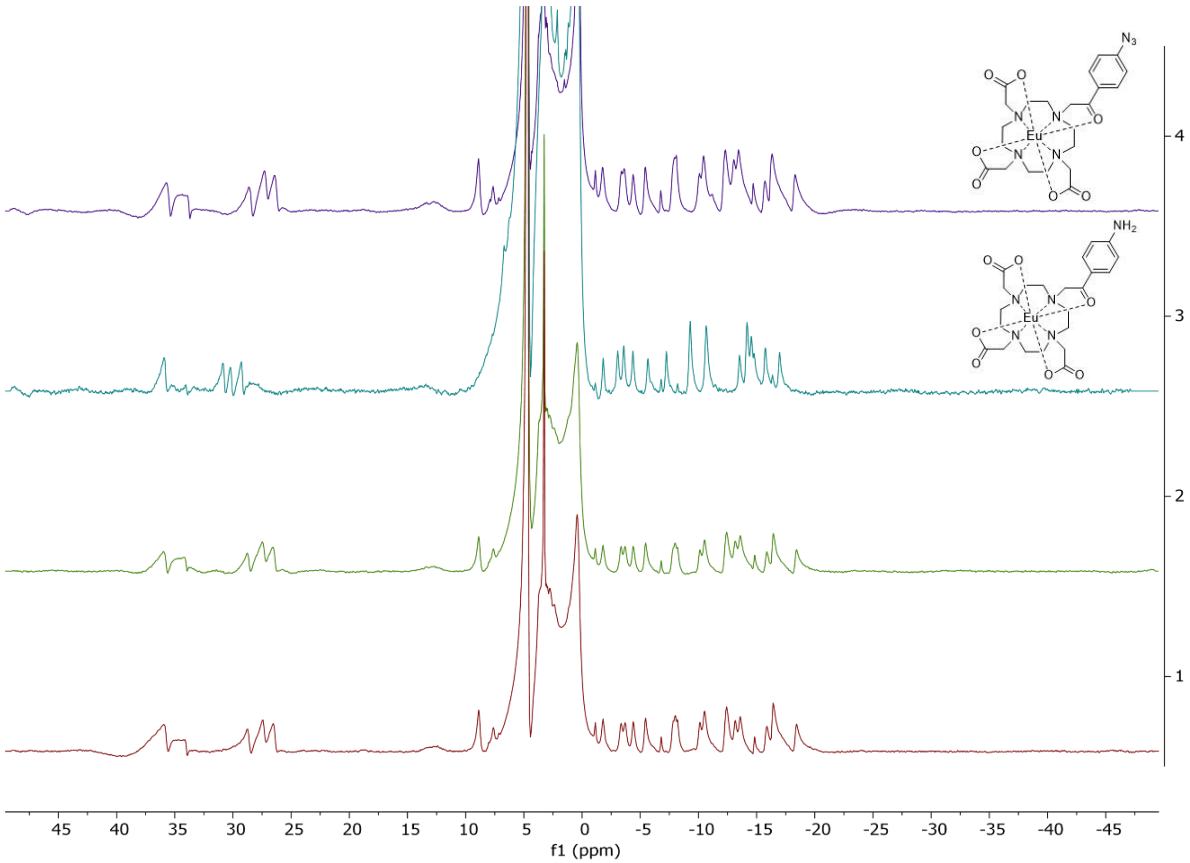


Figure 4 - 11 ^{1}H NMR spectrum of 13 after zinc reduction. Purple = Control at T = 0 hr; Blue = Zn+NH_4Cl at T = 24 hr; Green = NH_4Cl at T = 24 hr; Red = Control at T = 24 hr

Figure 4 - 12 describes the fluorescence and phosphorescence data obtained for both **12** and **13** after 24 hr reaction time and compares it against the initial luminescence data obtained. The data obtained shows a clear increase in fluorescence for **13**, with the peak at λ = 615 nm increasing by approximately 37% after 24 hr reacting with zinc. Interestingly, an even greater increase is seen in the NH_4Cl sample, which increases by 95%. It is possible that the presence of the ammonium component of this is contributing its own luminescence potential to the overall luminescence of the solution, eliciting a greater intensity than might otherwise be seen. The opposite is seen in the phosphorescence, which decreases by 27% after reaction with zinc, which works in tandem with the changes in fluorescence observed.

It is particularly interesting that the phosphorescence intensity of **12** is distinctly quenched when reacted with zinc or NH_4Cl, suggesting the amine counterpart has a distinctly reduced luminescence potential in comparison to the azide in this experimental setup. Conversely with **13**, a noticeable increase is seen, which could be in part influenced by the facile conversion properties of europium from europium III to europium II.

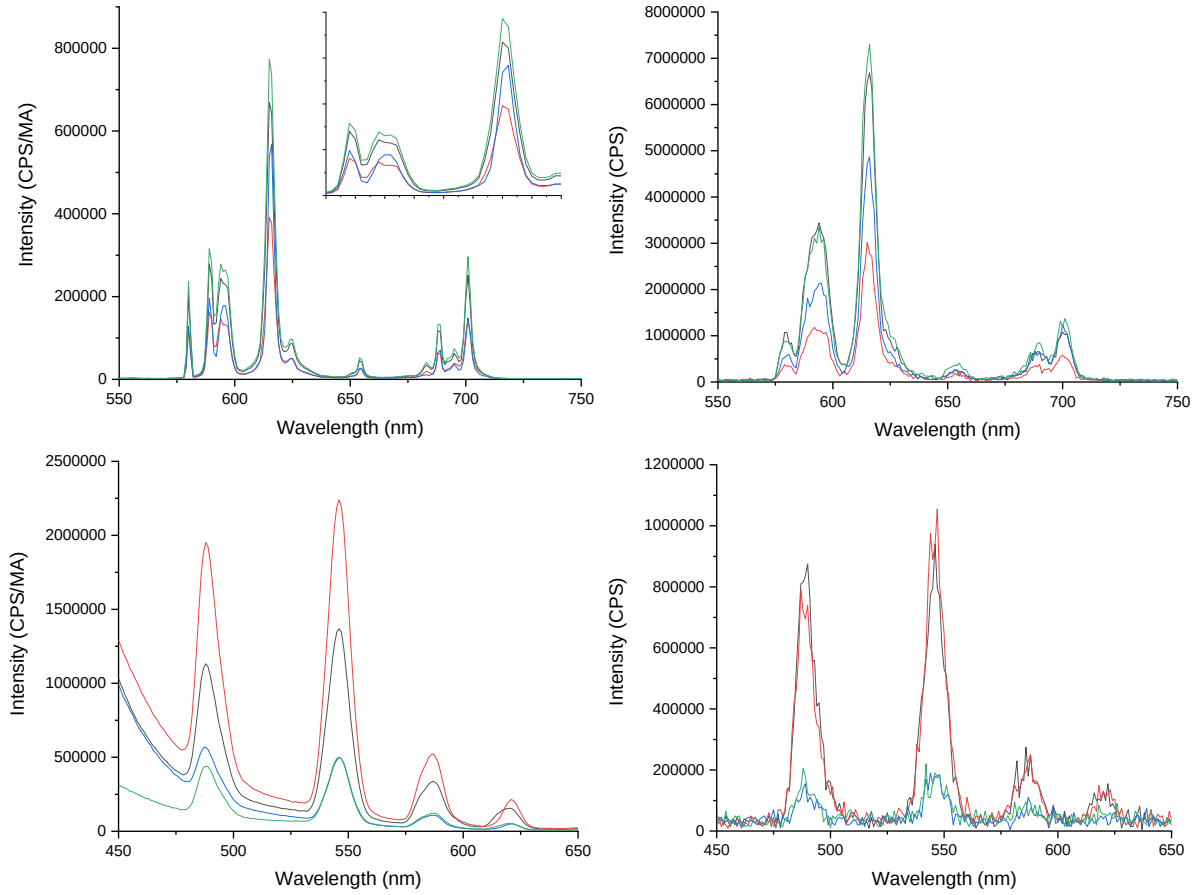


Figure 4 - 12 Top: Emission spectra of 13. Fluorescence (left) with zoomed perspective of λ = 580-620 nm, and phosphorescence (right) after zinc reduction. Bottom: Emission spectra of 12. Fluorescence (left) and phosphorescence (right). Black = Control at T = 0 hr; Red = Control at T = 24 hr; Blue = Zn + NH_4Cl at T = 24 hr; Green = NH_4Cl only at T = 24 hr

4.5 Degassed Solutions and Luminescence

Both azide and amine structures were analysed via luminescence to examine the fluorescence and phosphorescence patterns between conversion of said azide to amine. Only those reduced through the zinc-ammonium reduction were included here to allow for simpler analysis overall. Fluorescence scans of **13** and its amine reduced form indicates that as the azide is reduced, fluorescence decreases, however the expected increase of phosphorescence in the amine product was not observed. It is hypothesised that the cause of this is the triplet state of the ligand being too close to that of the metal, causing quenching of the luminescence in the amine equivalent. A similar problem was observed in **12** and its amine reduced form, where the fluorescence was expected to decrease for the azide to correspond with an increase in phosphorescence. The opposite was observed however as the peak intensity indicates an increase in fluorescence for the amine complex. For these complexes, it is expected that europium luminescence is quenched by the charge transfer mechanism, whilst terbium luminescence is quenched by the triplet states bearing too similar energy requirements.

This led to subsequent analysis via degassing and oxygenating of these complexes with the intent of determining if oxygen was playing a role in the lack of phosphorescence emission observed. Samples from before and after the zinc reduction were degassed in a solution of D_2O, and then phosphorescence emission and lifetime delay by decay scans run. The solutions were then aerated, and the same scans run again to see if a visible change was apparent. **Figure 4 - 13** provides the luminesce data obtained for both **12** and **13** at degassed and oxygenated levels.

13 demonstrates a clear change between these states, with the degassed complexes showing a higher level of phosphorescence compared to when in an aerobic state. This is strong evidence to support the hypothesis that the presence of oxygen inhibits the luminescence of the metal through oxidative quenching, which becomes prioritised over the standard energy transfer when in the presence of oxygen. A similar result is seen in **12**, showing that this predominance of quenching is apparent for both, however these changes could also indicate possible issues with the zinc reductant used in this experiment.

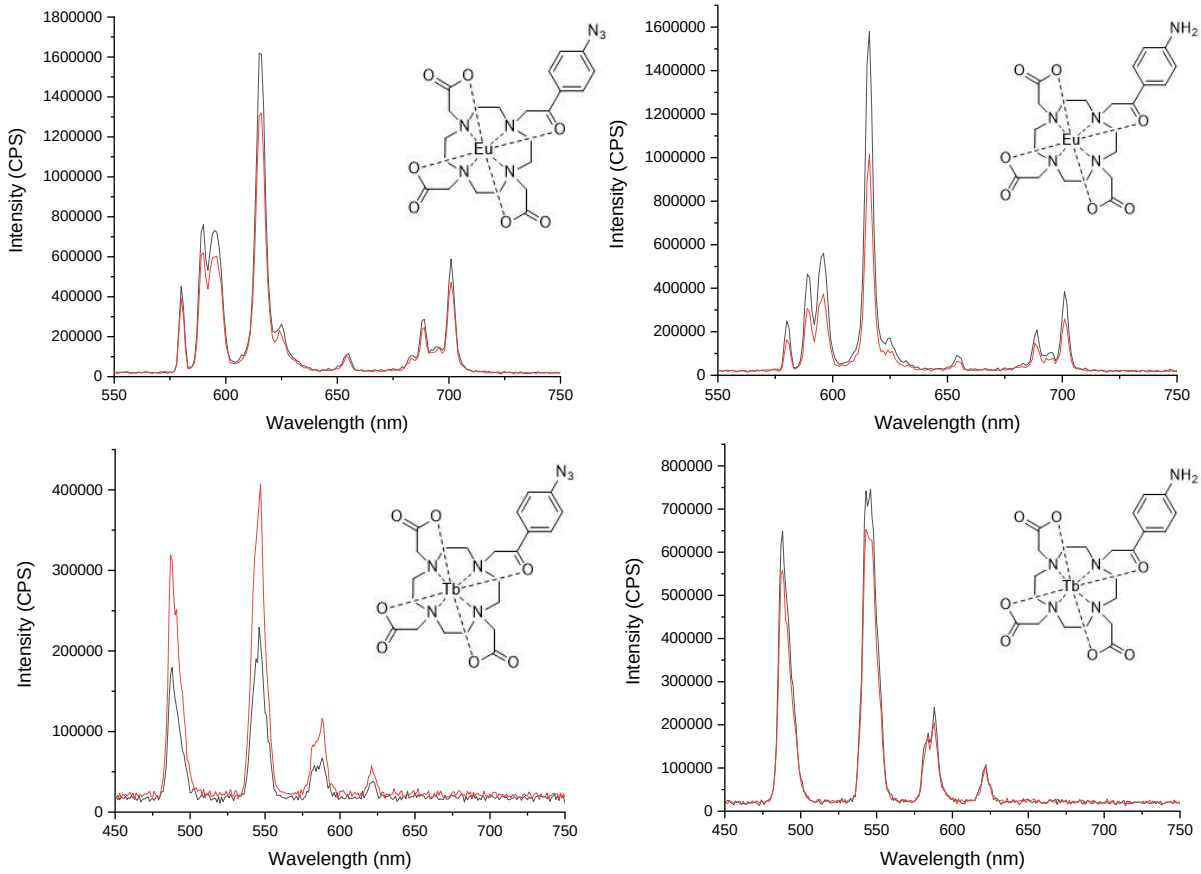


Figure 4 - 13 Phosphorescence emission spectra of 13 (top left) and the amine reduced form (top right), 12 (bottom left), and amine-reduced form (bottom right). Degassed levels are shown in black, whilst oxygenated levels are shown in red

4.6 CONCLUSION

This chapter has investigated the reduction and photophysical capabilities of a lanthanide complex in greater depth than has been previously reported,[89] allowing development of novel methods of analysis to greater understand the overall potential of the complex. The analysis of the reduction potential of the azide structures and the luminescence potential of their amine analogues, shows that azides bear a high potential for conversion to the amine through reductants of NaHS and zinc, with zinc proving a more efficient reductant. Conversion with these results in a complex that is more highly fluorescent than its predecessor. The azide functionality, however, demonstrates a much greater phosphorescent potential as both europium and terbium exhibit reduced phosphorescence when energy transfer occurs through the amine. It is also concluded that europium proves a more efficient lanthanide of choice than the terbium due to the lower energy of its excited triplet state.

4.7 REFERENCES

1. Zheng, Y.; Yu, B.; De La Cruz, L. K.; Roy Choudhury, M.; Anifowose, A.; Wang, B., Toward Hydrogen Sulfide Based Therapeutics: Critical Drug Delivery and Developability Issues. *Medicinal Research Reviews* **2018,** *38* (1), 57-100.
2. Beauchamp, R. O.; Bus, J. S.; Popp, J. A.; Boreiko, C. J.; Andjelkovich, D. A.; Leber, P., A Critical Review of the Literature on Hydrogen Sulfide Toxicity. *CRC Critical Reviews in Toxicology* **1984,** *13* (1), 25-97.
3. Tropiano, M.; Faulkner, S., A lanthanide based sensor for the time-gated detection of hydrogen sulfide. *Chemical Communications* **2014,** *50* (36), 4696-4698.
4. Peng, H.; Cheng, Y.; Dai, C.; King, A. L.; Predmore, B. L.; Lefer, D. J.; Wang, B., A Fluorescent Probe for Fast and Quantitative Detection of Hydrogen Sulfide in Blood. *Angewandte Chemie, International Edition in English* **2011,** *50* (41), 9672-9675.
5. Yu, F.; Li, P.; Song, P.; Wang, B.; Zhao, J.; Han, K., An ICT-based strategy to a colorimetric and ratiometric fluorescence probe for hydrogen sulfide in living cells. *Chemical Communications* **2012,** *48* (23), 2852-2854.
6. Montoya, L. A.; Pluth, M. D., Selective turn-on fluorescent probes for imaging hydrogen sulfide in living cells. *Chemical Communications* **2012,** *48* (39), 4767-4769.
7. Das, S. K.; Lim, C. S.; Yang, S. Y.; Han, J. H.; Cho, B. R., A small molecule two-photon probe for hydrogen sulfide in live tissues. *Chemical Communications* **2012,** *48* (67), 8395-8397.
8. Lin, V. S.; Chang, C. J., Fluorescent probes for sensing and imaging biological hydrogen sulfide. *Current Opinion in Chemical Biology* **2012,** *16* (5), 595-601.
9. Dadabhoy, A.; Faulkner, S.; Sammes, P. G., Long wavelength sensitizers for europium(iii) luminescence based on acridone derivatives. *Journal of the Chemical Society, Perkin Transactions 2* **2002,** (2), 348-357.
10. Abbenante, G.; Le, G. T.; Fairlie, D. P., Unexpected photolytic decomposition of alkyl azides under mild conditions. *Chemical Communications* **2007,** (43), 4501-4503.
11. Ranu, B. C.; Sarkar, A.; Chakraborty, R., Reduction of Azides with Zinc Borohydride. *The Journal of Organic Chemistry* **1994,** *59* (15), 4114-4116.
12. Lin, W.; Zhang, X.; He, Z.; Jin, Y.; Gong, L.; Mi, A., REDUCTION OF AZIDES TO AMINES OR AMIDES WITH ZINC AND AMMONIUM CHLORIDE AS REDUCING AGENT. *Synthetic Communications* **2002,** *32* (21), 3279-3284.

5 An Alternative Reducible Luminescent Lanthanide Complex

5.1 Introduction

While nitro aromatic compounds are generally stable in a chemical context, their biological reduction can potentially be harnessed in a number of ways. Previous analysis has shown that a key step in the metabolism of nitroaromatics is nitro reduction, which almost exclusively occurs in intestinal microflora.[105, 106] This reduction converts the nitro group to an amine, both of which are stable in nature. Interconversion between these groups, however, creates highly reactive intermediates such as nitroso and hydroxylamino derivatives.[105] Research has shown that reduction of NO_2 to NH_2 is possible, with the best mechanisms for this including an active metal such as stannous chloride ($SnCl_2$) with HCl through an acid-catalysed mechanism,[142] or other metals such as zinc in aqueous solutions containing chelating ethers.[143] This is a milder, more environmentally friendly method where the donor ether works both as a ligand and a solvent.

Nitroso and hydroxylamino derivatives are often more toxic than their predecessors, however complexes with a polycyclic nitroaromatic component do not exhibit this level of toxicity. This alternative selection can also be activated through both reduction by intestinal microflora,[105] and mediated oxidation of the aromatic ring by cytochrome P-450.[110] One previously documented mechanism classically utilises iron and hydrochloric acid (HCl) known as the Béchamp Reduction, which has proved effective and useful for reduction of nitroaromatics.[144] This reduction is important in industrial synthesis of medicinal supplies among others, and also bear the advantageous property of facile conversion to diazonium salts, which can be

substituted for a plethora of other functionalities. **Figure 5 - 1** demonstrates the mechanism of the Béchamp reduction.

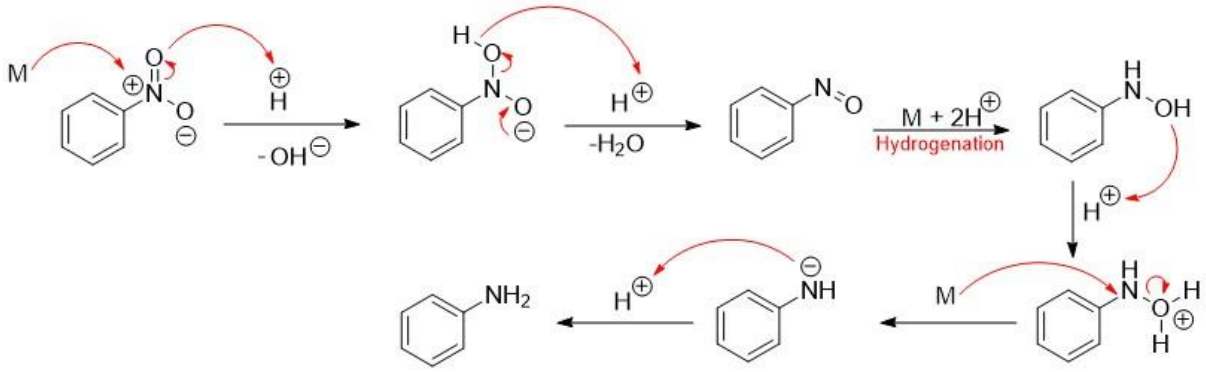


Figure 5 - 1 Mechanism of the Béchamp reduction

Other methods of chemical reduction have included investigations into alternative metal/acid combinations, and the influence of structure on the reduction potential. This includes titanium oxide-graphene hybrids, which showed that using hybrid photocatalysts generated higher yields of amino-aromatics than pure,[145] and gold-based nano-catalysts which offer high catalytic efficiency for nitroaromatic reduction with greener environmental synthetic implications.[146] Research has also extended towards carbon-supported nickel nanoparticles using silicon dioxide cores, which have showed excellent reduction capabilities of 4-nitrophenol, and proved capable of adhesion to histidine-rich proteins.[147]

Synthesis in this report was undertaken using the same core ligand structure as previously discussed complexes as seen in **Figure 5 - 2**, however instead functionalising with a nitrobenzene instead of anthracene or azidobenzene. Reduction of nitro-based compounds are often achieved with ammonium sulfide, or hydrogen sulfide paired with ammonia in an alcoholic solution.[110] Depending on the reducing agent chosen, the conditions and overall rate of reduction differ, subsequently altering the products formed.[110] It is hypothesised that reaction of this compound with the same zinc and ammonium chloride combination as the

azide reduction used will induce a reduction of this group it to an amine to generate the same product as reduction of the azide. It is hoped that this would eventually be useful as a method for identifying biological processes that reduce compounds to the same product through different mechanisms.

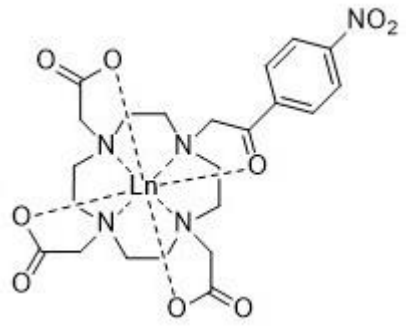
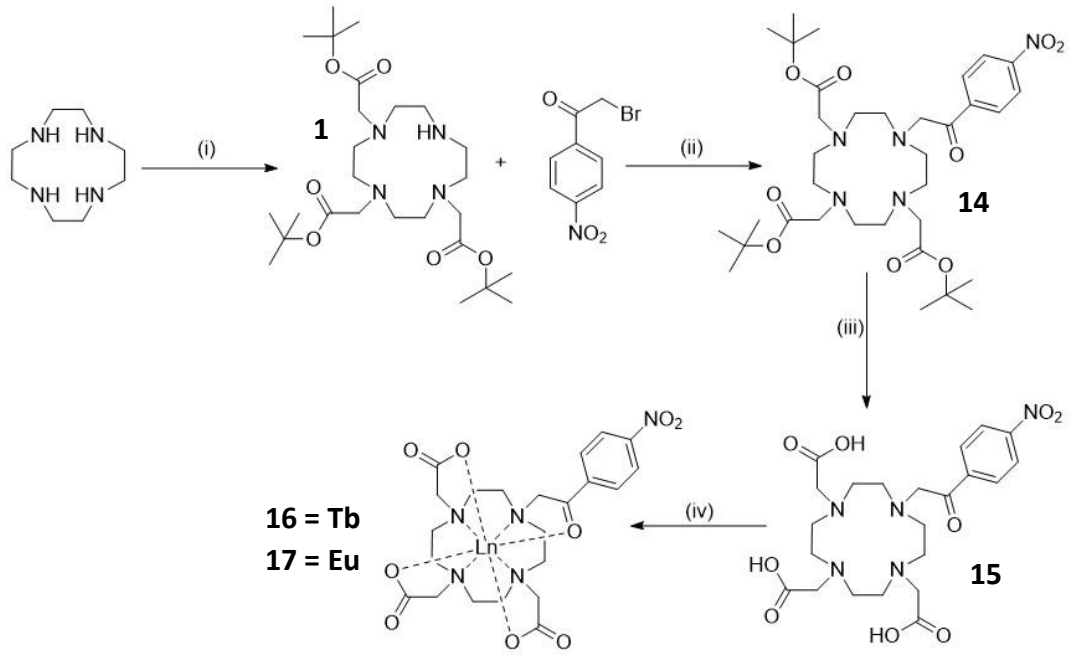


Figure 5 - 2 The general form of the complex of interest in this chapter

5.2 Synthesis and Characterisation

Synthesis was undertaken using the same schematic as the azide and monometallic anthryl lanthanide complexes, starting with synthesis of **1** and reacting **1** with 2-bromo-4'-nitroacetophenone to generate the core ligand structure **14**. This was generated in accordance with previously reported literature of the tert-butyl-arm-containing DO3A ligand.[148] This structure is reported, however in literature it is used in generation of a different final complex, and so novel synthesis was undertaken from this point on. The overall synthetic scheme can be found in **Scheme 5 - 1**.

Purification of **14** proved challenging, however, as impurities within the crude product possessed similar polarity to the targeted product and would elute from initial column chromatography attempts in tandem. Through trial and error, this was eventually circumvented through repeat purification of the product via column chromatography in a slow gradient eluent composed of DCM and MeOH to eventually yield a successfully separated structure that corresponded to previously reported literature.[148]



Scheme 5 - 1 Synthetic route for synthesis of nitrobenzene-functionalised probes. Reaction conditions: (i) $C_6H_{11}BrO_2$, $NaHCO_3$, CH_3CN, N_2, r.t.; (ii) $NaHCO_3$, CH_3CN, 80 °C; (iii) TFA, DCM, r.t.; (vi) $Ln(CF_3SO_3)_3$, MeOH, 60 °C

As synthesis after this step was novel in nature, steps from the previous projects were used to attempt successful synthesis of the complex. Deprotection on **14** was run using a 1:1 mixture of DCM:TFA over 48 hr to remove the tert-butyl arms, and washed thoroughly with DCM and MeOH to remove excess TFA and give the carboxyl structure of **15**, ^{1}H NMR of which can be seen in **Figure 5 - 3**. This was further purified through trituration with MeOH and Et_2O. Synthesis was confirmed through additional analysis via mass spectrometry, IR, and UV-Vis analysis.

15 was complexed with lanthanide sulfates in MeOH for 48 hr, before removing excess lanthanide salts as an insoluble hydroxide precipitate through adjustment of pH. Purification was undertaken through trituration with MeOH and Et_2O, and dialysis in MilliQ H_2O over 48 hr to remove excess lanthanide salts and other salts present to derive pure complexes of **16** and **17**.

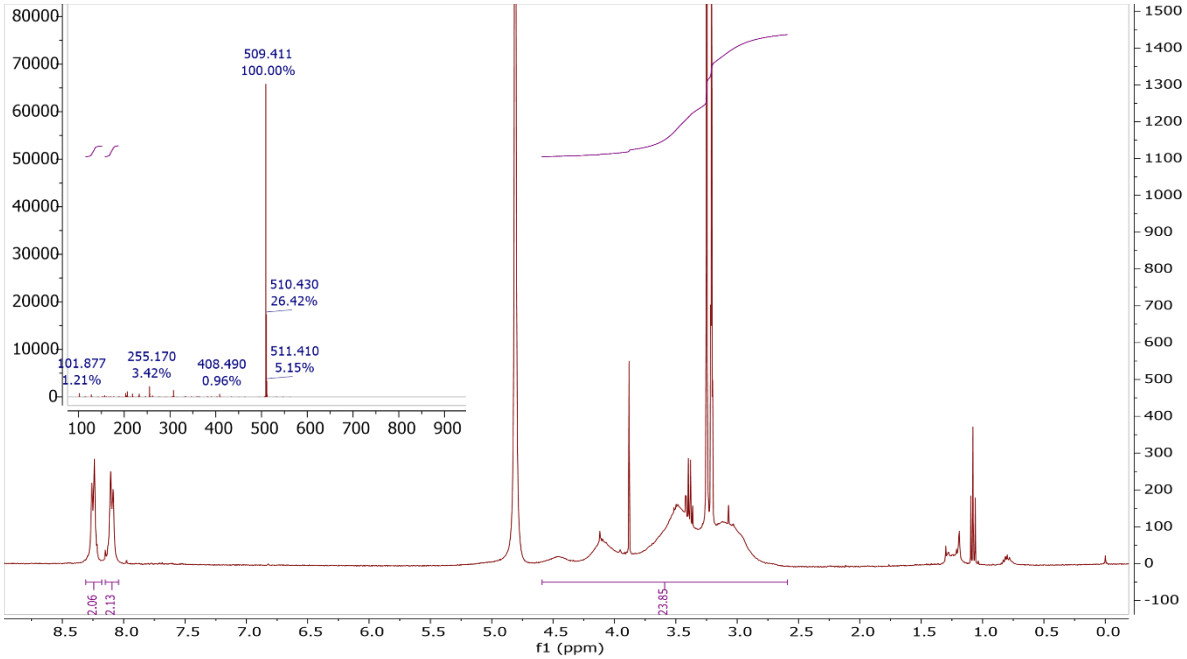


Figure 5 - 3 ^{1}H NMR Spectrum and MS Spectrum of 15

Complexes were characterised by NMR, mass spectrometry, UV-Vis, and IR spectroscopy. ^{1}H NMR of **16** suggests a successful incorporation of the lanthanide ion into the ligand structure, which correlates with the mass spectrometry data obtained as seen in **Figure 5 - 4**. This suggests that the structure is primarily SAP in nature with peaks between 200-300 ppm, with

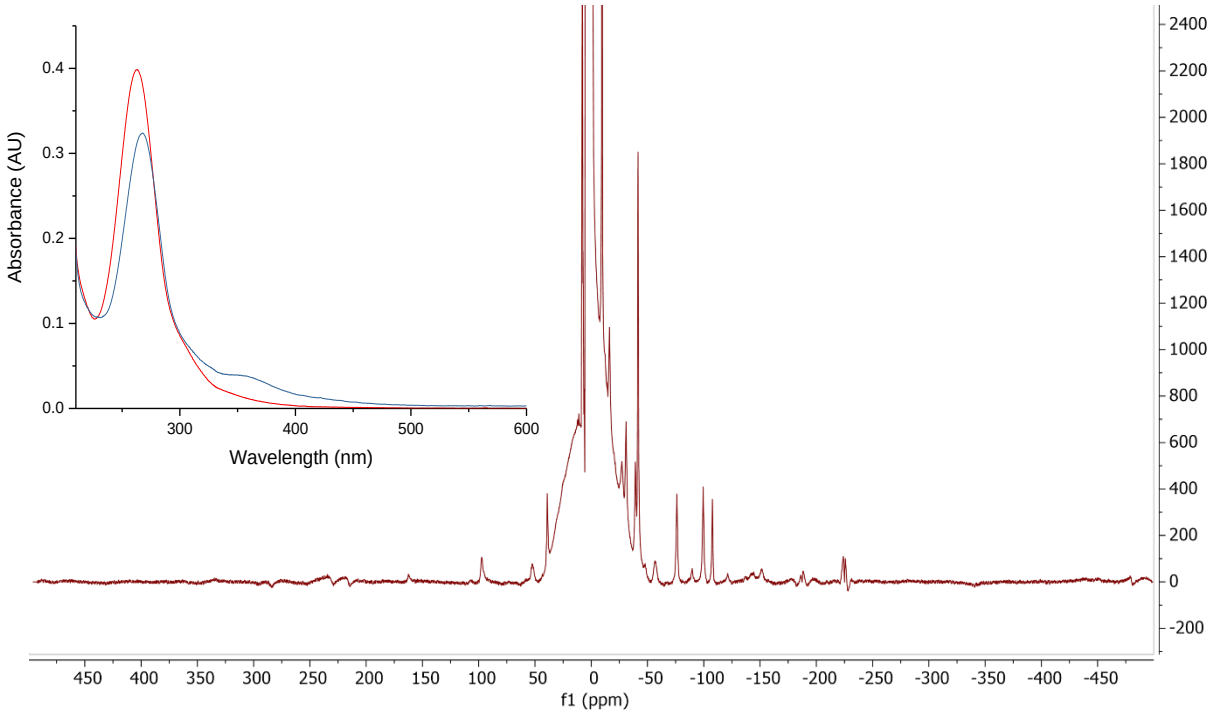


Figure 5 - 4 ^{1}H NMR spectrum of 16 with UV-Vis Spectra of 15 (red) and 16 (blue)

some possible minor TSAP isomerism occurring. The peaks between -50 and -250 ppm could be attributed to the ligand structure itself, as the pseudocontact shift mechanism caused by terbium induces a shift of peaks to the higher field.

The wide sweep width required for ^{1}H NMR of terbium complexes is close to the available radiofrequency window of most commercial spectrometers: this combines with the dramatic linewidth broadening observed with ^{1}H NMR of terbium, and resolution is hence lost in the detail of this region, but evidence still points to successful insertion of terbium into the ligand. This is supported by UV-Vis analysis, which shows addition of a round peak at 350 ppm that is not present in **15**, whilst both structures contain a nitrobenzene chromophore peak at around 262 ppm. It is thus inferred that the peak at λ = 350 ppm is caused by the successful incorporation of the lanthanide ion into the ligand structure. Similar results are observed in **17**.

5.3 Zinc Reduction of Nitrobenzene

This thesis has previously shown that azides can be selectively reduced to their amine counterpart through reduction with zinc (Zn) and ammonium chloride (NH_4Cl) as seen in Chapter 4.4. As NO_2^- can also be selectively reduced to an amine through use of Zn it was decided to run the same experimental method as was used in the initial azide zinc reduction. To determine the cause of any reduction that might occur, three samples were prepared of each complex: one to act as a control, one to react with NH_4Cl only, and one to be combined with both Zn and NH_4Cl. Complexes were dissolved to a concentration of 5 mg with D_2O as the chosen solvent and three aliquots of 400 µL taken and transferred to separate mass spectrometry vials. 10% NH_4Cl was added to all samples but the control, and zinc powder was added to the last vial.

The vials were then stirred at 37 °C for 24 hr with analysis performed at T = 0 and T = 24 hr via NMR, mass spectrometry, and photophysical analysis. To ensure removal of any excess unreacted zinc from solution, samples were run through a syringe filter to catch particulates. In the interest of preserving adequate sample for analysis, time points were reduced to these two points to maximise reduction of the complex and potential for analysis post-reduction and reduce deterioration of the deuterated solvent used.

^{1}H NMR spectra of **17** shown in **Figure 5 - 5** shows clear differences between reactivity with Zn and without Zn, with disappearance of the peaks between 7-27 ppm upon reaction with Zn, and generation of a small set of peaks around 30 ppm. In addition, the peak arrangement

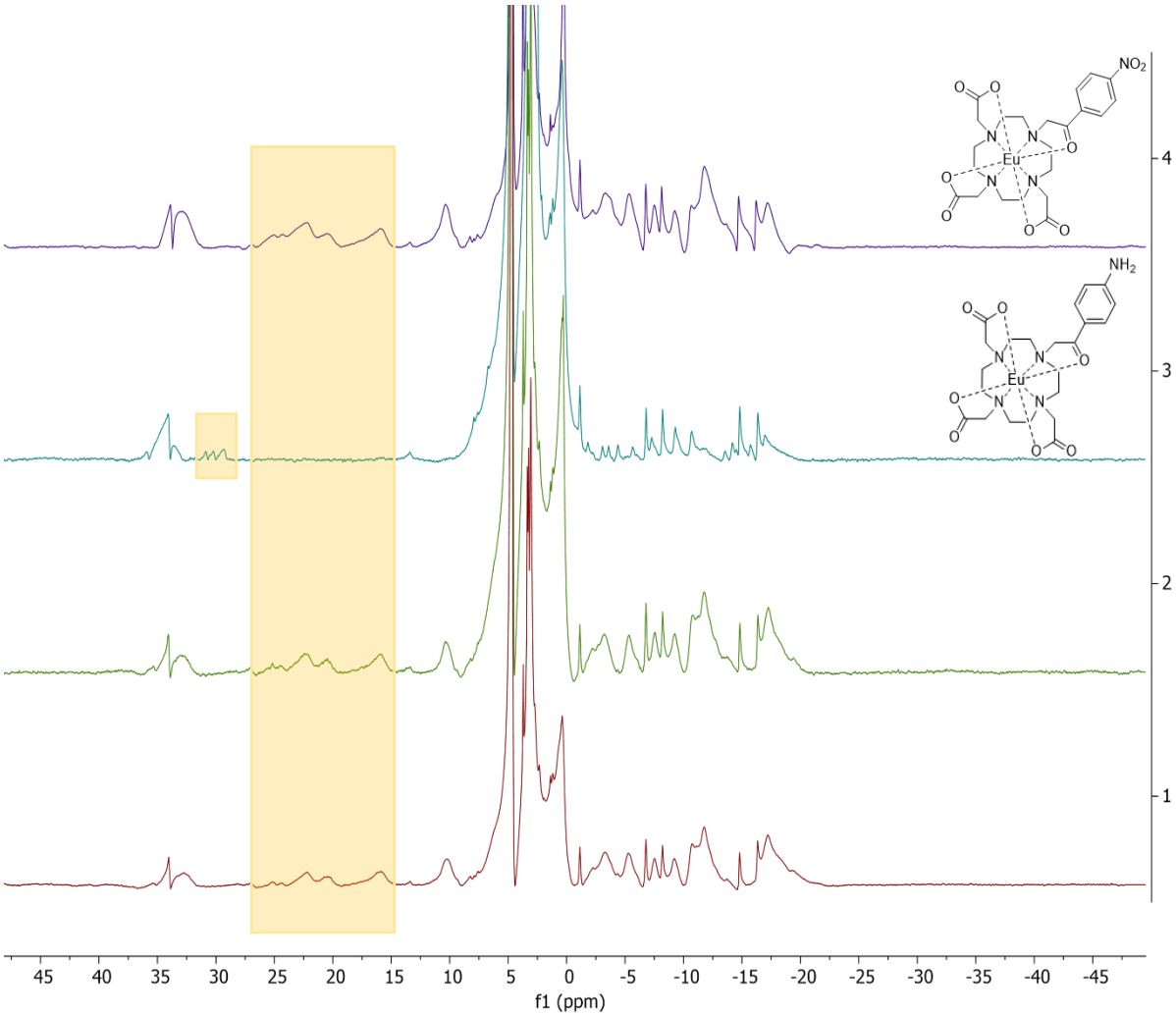


Figure 5 - 5 ^{1}H NMR Spectra of 17. Purple = Control at T = 0 hr; Blue = Zn+NH_4Cl at T = 24 hr; Green = NH_4Cl at T = 24 hr; Red = Control at T = 24 hr

between 0 and -20 ppm undergoes some clear changes, which can be attributed to the structural change as the reduction mechanism takes place. As structural changes are not evident upon exposure of the complex to heat or NH_4Cl alone, it becomes clear that zinc is the sole reductant. The structure observed here seems to be primarily TSAP in nature for all but the reduced sample, which shows a solely SAP arrangement. This change is further evidence that a structural change has occurred within the complex after reaction with zinc, suggesting that conversion to the amine has been successful. This correlates with the mass spectrometry obtained in tandem, and similar results are observed in **16**. It is also worth noting in this reduction that unlike the Béchamp reduction, excessive generation of side products does not appear to have occurred, suggesting this metal/acid combination is a better alternative for reduction of this particular nitrophenacyl-functionalised complex.

Analysis of the luminescence of **17** in **Figure 5 - 6** shows an exceptionally large rise in intensity upon reaction with Zn, showing a 2000% increase in fluorescence intensity at the peak maxima at λ = 616 nm and a 1900 % increase in phosphorescence intensity after 24 hr of reaction time. NH_4Cl showed in fact a slight decrease in both fluorescence and luminescence, with a 33% decrease in fluorescence and a near 38% decrease in phosphorescence. With no change observed in the control sample after 24 hr, it can therefore be said that zinc is the sole reductant responsible for generation of the amine product, as NH_4Cl on its own reduces luminescence, and heat offers no impact on the luminescence of the complex.

Similar results are observed in the spectra of **16** seen in **Figure 5 - 6** with a 61% increase in fluorescence around λ = 475 nm and a 36% increase at λ = 545 nm, however phosphorescence appears quenched after reaction with zinc. This confirms the results observed upon reduction of the azide analogue that the amine counterpart of these complexes has a distinctly reduced

luminescence potential in comparison to its precursors. It is hypothesised that this is due to the ligand triplet state too closely mirroring the lanthanide triplet state, resulting in quenching of luminescence after generation of the amine product. It is clear that lanthanide emission is relatively weak when compared to the fluorescence of the ligand. This reflects the possibility that the aminophenacyl triplet state is inducing quenching of the lanthanide excited state.

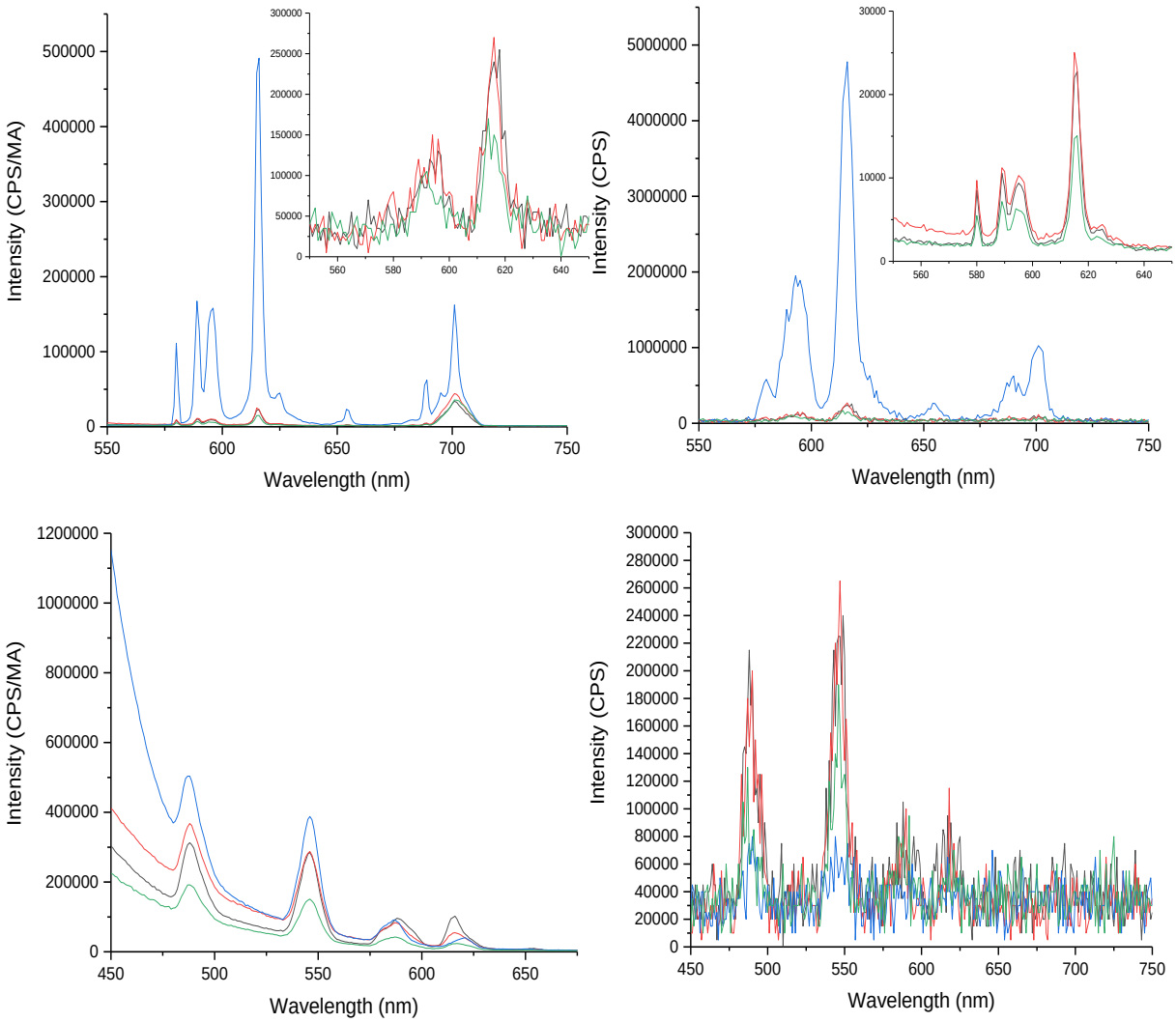


Figure 5 - 6 Top: Fluorescence (left) and phosphorescence (right) emission spectra of 17 with zoomed perspective of λ = 480-650 nm. Bottom: fluorescence (left) and phosphorescence (right) emission spectra of 16. Black = control at T = 0 hr, Red = Control at T = 24 hr, Blue = Zinc+NH_4Cl at T = 24 hr, Green = NH_4Cl only at T = 24 hr

5.4 CONCLUSION

This chapter investigates the reduction potential of semi-novel lanthanide complexes based off an intermediate previously reported in synthetic ventures of a different end complex.[148] Insertion of the lanthanide in this synthesis proves to be the more novel aspect of the report. Whilst these complexes do pose some issues synthetically regarding purity and yield, these are solvable problems and overall synthesis of the complex can be achieved. Both europium and terbium complexes prove readily reduced through use of the active metal zinc, and exhibit luminescence potential in both their original nitro-functionalised nature and their amine reduced form. Whilst they readily fluoresce, phosphorescence appears quenched after reaction with zinc, which reduces the overall luminescence potential affected due to the ligand triplet state too closely matching the triplet state of the lanthanide, causing luminescence quenching as the amine is formed. It remains to demonstrate the potential for biological reduction, however the initial promise of this is clear.

5.5 REFERENCES

1. Spain, J. C., BIODEGRADATION OF NITROAROMATIC COMPOUNDS. **1995,** *49* (1), 523-555.
2. Rickert, D. E., Metabolism of Nitroaromatic Compounds. *Drug Metabolism Reviews* **1987,** *18* (1), 23-53.
3. Bellamy, F. D.; Ou, K., Selective reduction of aromatic nitro compounds with stannous chloride in non acidic and non aqueous medium. *Tetrahedron Letters* **1984,** *25* (8), 839-842.
4. Kumar, P. S.; Lokanatha Rai, K. M., Reduction of aromatic nitro compounds to amines using zinc and aqueous chelating ethers: Mild and efficient method for zinc activation. *Chemical Papers* **2012,** *66* (8), 772-778.
5. Cohen, J. B.; McCandlish, D., CXXVII.—The mechanism of the hydrogen sulfide reduction of nitro-compounds. *Journal of the Chemical Society, Transactions* **1905,** *87* (0), 1257-1272.
6. Ono, N., The Nitro Group in Organic Synthesis. 2002; pp i-xvi.
7. Xu, C.; Yuan, Y.; Yuan, R.; Fu, X., Enhanced photocatalytic performances of TiO_2-graphene hybrids on nitro-aromatics reduction to amino-aromatics. *RSC Advances* **2013,** *3* (39), 18002-18008.
8. Qin, L.; Zeng, G.; Lai, C.; Huang, D.; Zhang, C.; Cheng, M.; Yi, H.; Liu, X.; Zhou, C.; Xiong, W.; Huang, F.; Cao, W., Synthetic strategies and application of gold-based nanocatalysts for nitroaromatics reduction. *Science of The Total Environment* **2019,** *652*, 93-116.
9. Ding, L.; Zhang, M.; Ren, Y.; Xu, J.; Zheng, J.; Alsulami, H.; Kutbi, M. A.; Zhang, F.-Y., Carbon-Supported Nickel Nanoparticles on SiO_2 Cores for Protein Adsorption and Nitroaromatics Reduction. *ACS Applied Nano Materials* **2020,** *3* (5), 4623-4634.
10. Mizukami, S.; Tonai, K.; Kaneko, M.; Kikuchi, K., Lanthanide-Based Protease Activity Sensors for Time-Resolved Fluorescence Measurements. *Journal of the American Chemical Society* **2008,** *130* (44), 14376-14377.

6 Conclusions

6.1 Conclusions and Future Work

This thesis has explored the use of DO3A-based derivatives with different aromatic chromophores in known and novel synthesis, as well as their potential in luminescence probes and imaging agents. Analysis has focused on their *in vitro* potential within the laboratory parameters only due to time constraints imposed by the COVID-19 pandemic.

Complexes functionalised with anthracene have been exhibited to be successfully synthesised with relative ease and exhibit adequate levels of redox potential for use within hypoxic and aerobic environmental conditions. Due to the encapsulated nature of the lanthanide ion, standard protonated solvent systems have proven more efficient than their deuterated counterparts for analysis. This is due to the lanthanide remaining strongly metalated and heavily protected in its macrocyclic pocket. Further investigations into these and similar systems would be advantageous to understand their crystal fields and magnetic anisotropies in greater depth.

Whilst the complex is light sensitive, data suggests that exposure to oxygen alone only induces a small level of photo-reactivity as whilst the redox mechanism is the preferential mode of energy transfer, this requires irradiation under an appropriate UV light to induce an adequate level of photo-reactivity. This is summarised in **Figure 6 - 1**. As such, whilst synthesis should be kept predominantly dark, it needn't be so extreme as to cause practical issues. It is possible therefore to exploit the reactivity of anthracene where emission is sensitised, and this could prove advantageous in potential future medical applications. Research into their biological

viability and usefulness would prove worthwhile as well, as their ability to react with oxygen would prove useful in differentiation of hypoxic and aerobic regions of biological tissue.

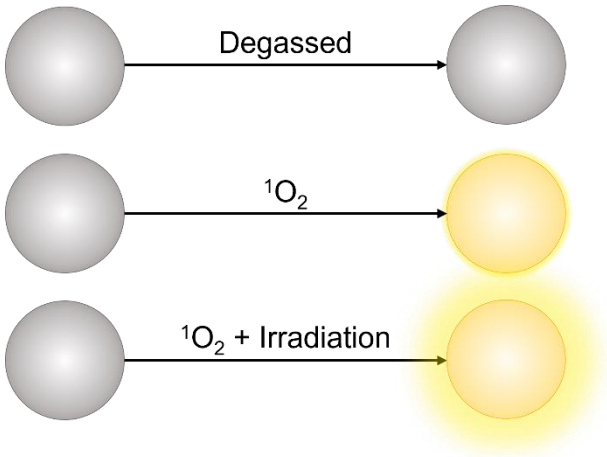


Figure 6 - 1 Summation of the levels of activation

Whilst the bimetallic synthesis had several synthetic issues that made success challenging to the point of surrender, the strategy itself does show potential to be successful. As previous literature has demonstrated, both bimetallic[131, 132, 136, 149] and tri-metallic[16] complexes are possible, however in the case of this attempted complex, methods for generation of the bridging ligand must first be heavily refined to yield products both high in purity and quantity. Any future studies on this complex must first focus on practical optimisation of the synthetic route, before exploring the redox potential of the structure both *in vitro* through similar mechanisms to its mononuclear analogue discussed above and *in vivo*.

The azide chromophore has been shown to be efficient in reduction at activating the sensing group and improving the efficiency of energy transfer between it and the lanthanide and has shown it is capable of this with multiple reductants including NaHS and zinc. High selectivity for NaHS has been previously reported in brief,[89] however the in-depth analysis seen in this thesis shows that oversaturation of this can negatively interfere with reduction of the complex and subsequent photophysical properties. Zinc has also been proven in this chapter to be an effective reductant for azide-functionalised macrocyclic lanthanide complexes, and

to a greater extent than NaHS. This is likely due to its status as an active metal lending greater reactivity when in an appropriate solvate environment. The difference between these reductants can be seen visualised in **Figure 6 - 2**.

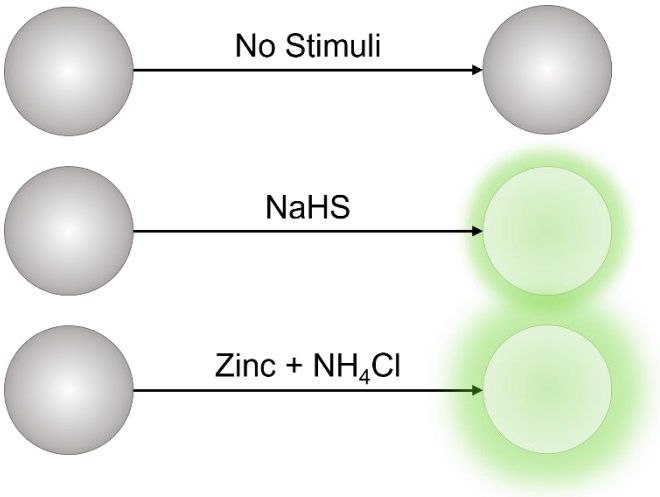


Figure 6 - 2 Summation of the reduction potentials of NaHS and zinc

These reductive studies showed that conversion to the amine analogue was not only possible but highly favoured, and this product produces a much greater fluorescence potential in all aspects of reduction. In these studies, europium proves the more efficient lanthanide of choice, with terbium showing limited phosphorescence luminescence. As oxygen was shown to inhibit the luminescence of the lanthanide metal through an oxidative quenching process, it is concluded as a result that the terbium amine structure possesses a reduced luminescence potential in comparison to the azide. The larger change overall observed within the terbium complex, however, suggests an additional issue with the reductant of choice. Other possibilities for selectivity may be possible and would be recommended to be explored in future studies before investigations into the biological potential these probes possess in enzyme studies and further biological testing.

Nitroaromatic compounds such as the nitrophenacyl-functionalised complexes studied in this thesis were seen to exhibit a similar reductivity to that seen in the azidophenacyl-

functionalised complexes when reacted with zinc, however their level of reactivity appears greater, likely due to the increased stability of the NO_2^- functional group compared to the amine. The europium amine complex in this situation exhibits exceptional luminescence potential in comparison to its precursor, whilst the terbium analogue demonstrates limited phosphorescence potential. This is likely due to the similar energy requirements between the ligand and lanthanide excited triplet (T_1) states. It is theorised this could also be the result of reduction influencing the lifetime of the terbium lanthanide, subsequently altering the luminescence properties observed. Future work on these complexes would be wise to investigate its biological potential for reduction with other key biomarkers (for example free radicals and other biologically relevant active metals) and biological pathways such as those examined in enzyme studies.

It can be concluded from this work on the azide and nitrobenzene structures that azide and nitro-functionalised systems form the same amine structure when reduced. To investigate and establish if there are any differences in the rate and reaction of this reductive chemical pathway, further work is necessary.

The overarching conclusion from this work that can be drawn is that DO3A-based ligand frameworks provide an excellent pocket for lanthanide binding and an effective pathway for lanthanide energy transfer to the lanthanide. It is also noted that the photophysical properties of these mononuclear lanthanide complexes are heavily influenced by the functionalising chromophore appended to the ligand, with small changes in this structure inducing changes in the possible mechanistic pathways of chemical change and subsequent photophysical properties.

6.2 REFERENCES

1. Beletskaya, I. P.; Voskoboynikov, A. Z.; Chuklanova, E. B.; Kirillova, N. I.; Shestakova, A. K.; Parshina, I. N.; Gusev, A. I.; Magomedov, G. K. I., Bimetallic lanthanide complexes with lanthanide-transition metal bonds. Molecular structure of $(C_4H_8O)(C_5H_5)2LuRu(CO)_2(C_5H_5)$. The use of 139La NMR spectroscopy. *Journal of the American Chemical Society* **1993,** *115* (8), 3156-3166.
2. Deiters, E.; Song, B.; Chauvin, A.-S.; Vandevyver, C. D. B.; Gumy, F.; Bünzli, J.-C. G., Luminescent Bimetallic Lanthanide Bioprobes for Cellular Imaging with Excitation in the Visible-Light Range. *Chemistry - A European Journal* **2009,** *15* (4), 885-900.
3. Su, Y.; Yu, J.; Li, Y.; Phua, S. F. Z.; Liu, G.; Lim, W. Q.; Yang, X.; Ganguly, R.; Dang, C.; Yang, C.; Zhao, Y., Versatile bimetallic lanthanide metal-organic frameworks for tunable emission and efficient fluorescence sensing. *Communications Chemistry* **2018,** *1* (1), 12.
4. Wang, Y.; Wu, Y.; Zhou, C.; Cao, L.; Yang, H., A new bimetallic lanthanide metal-organic framework as a self-calibrating sensor for formaldehyde. *Inorganic Chemistry Communications* **2018,** *89*, 5-9.
5. Faulkner, S.; Pope, S. J. A., Lanthanide-Sensitized Lanthanide Luminescence: Terbium-Sensitized Ytterbium Luminescence in a Trinuclear Complex. *Journal of the American Chemical Society* **2003,** *125* (35), 10526-10527.
6. Tropiano, M.; Faulkner, S., A lanthanide based sensor for the time-gated detection of hydrogen sulfide. *Chemical Communications* **2014,** *50* (36), 4696-4698.

7 Experimental

7.1 General

Cyclen was used as supplied by Chematech. Procedures were followed according to previously recorded literature procedures. Analytics corresponded with those previously recorded. Chosen lanthanides of interest were terbium and europium, which are previously proven efficient quenchers. Reagents were laboratory grade and obtained from standard commercial sources including Sigma-Aldrich, Fisher Scientific, Alfa Aesar, Fluorochem, CheMatech, ChemicalPoint, and Insight Biotechnology. Water was deionised and microfiltered with a Milli-Q Millipore machine.

NMR spectra were recorded with a Bruker Avance III HD 400 NanoBay (9.4T) and Bruker Avance III 500 (11.75T).

NMR data was processed using MestreLab MestreNova.

LCMS (ESI) results were recorded on a Waters LCT Premier bench-top orthogonal acceleration time-of-flight LC-MS system, connected to a CTC Analytics HTS PAL Sample Manager, Acquity PDA Detector, Acquity Column Heater/Cooler, Acquity Binary Solvent Manager. Samples (5 µL; 10 µL sample loop) were injected onto an ACE equivalence C18 (50 ´ 2.1 mm) column according to the following gradient profile:

Table 1. Open Access C gradient profile details

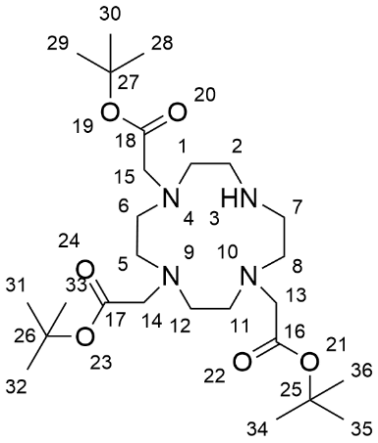
Time (min)	Flow rate (mL/min)	A MilliQ Water + 0.1% Formic Acid (%)	B Acetonitrile + 0.1 % Formic Acid (%)
0	0.3	95	5
1	0.3	95	5
8.5	0.3	5	95
9	0.3	5	95
9.1	0.3	95	5
10	0.3	95	5

Solid-state IR spectra were recorded using a Bruker Tensor 27 FT-IR spectrometer with an IR Diamond Attenuated Total Reflectance module, and the data processed using Bruker OPUS software.

Luminescence data was measured using a Horiba FluoroLog-3, Varian Cary Eclipse, or Perkin Elmer LS55 and processed using FluorEssence™, and OriginLab Origin®.

7.2 Experimental – Redox Active Luminescent Lanthanide Complexes

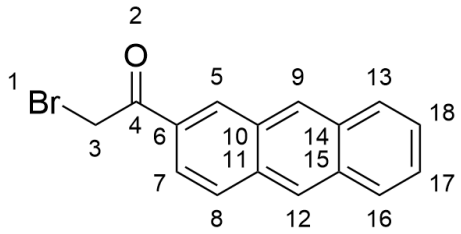
Tri-tert-butyl 2,2',2''-(1,4,7,10-tetraazacyclododecane-1,4,7-triyl) triacetate (1)



Following the procedure described by Dadabhoy *et al.*[123]

Yield 5.590 g, 76% **^{1}H NMR** (400 MHz, $CDCl_3$) δ (ppm) 9.97 (s, 2H, NH, HBr), 3.31 (s, 4H, NC*H*$_2$CO), 3.23 (s, 2H, NC*H*$_2$CO), 3.03 (d, *J* = 5.0 Hz, 4H, NC*H*$_2$), 2.86 (d, *J* = 5.3 Hz, 8H, NC*H*$_2$), 2.81 (d, *J* = 5.7 Hz, 4H, NC*H*$_2$), 1.40 (s, 18H, CC*H*$_3$), 1.39 (s, 9H, CC*H*$_3$) **^{13}C NMR** (101 MHz, $CDCl_3$) δ (ppm) 170.51, 169.62, 81.82, 81.65, 58.18, 51.33, 49.18, 48.78, 47.51, 28.22, 28.18, 27.88 **ES$^+$ MS** *m/z* 515.4 $[M+H]^+$

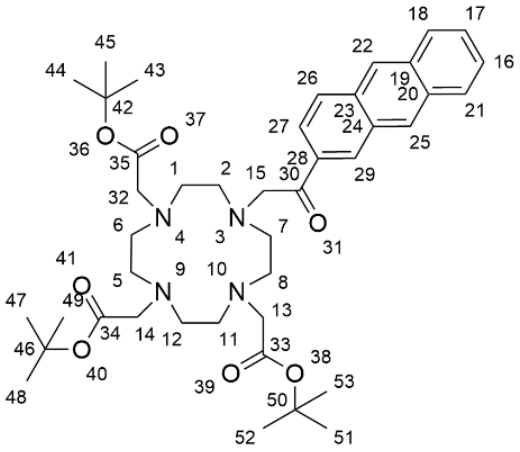
2-bromoacetylanthracene (2)



Following the procedure described by Ung *et al.*[122]

Yield 0.283 g, 96% **^{1}H NMR** (400 MHz, $CDCl_3$) δ (ppm) 8.58 (s, 1H), 8.46 (d, *J* = 3.9 Hz, 1H, C*H*), 8.32 (s, 1H, C*H*), 7.96 – 7.89 (m, 4H, C*H*), 7.47 – 7.41 (m, 2H, C*H*), 4.50 (s, 2H, BrCH_2). **^{13}C NMR** (101 MHz, $CDCl_3$) δ (ppm) 207.19, 198.11, 191.26, 134.10, 133.64, 133.35, 132.75, 132.64, 132.25, 132.15, 131.77, 130.46, 130.16, 129.46, 129.26, 129.07, 128.82, 128.60, 128.52, 128.32, 127.13, 126.80, 126.48, 126.34, 126.28, 126.07, 122.84, 122.79, 60.52, 31.02, 30.92, 26.63, 21.16, 14.30. **ES$^+$ MS** (*m/z*) 322.8 $[M+Na]^+$ **UV-Vis** (MeOH) λ_{max}/nm = 241, 260, 268, 325, 341, 359, 400 **IR** 3000 (CH=CH), 1750 (C=O)

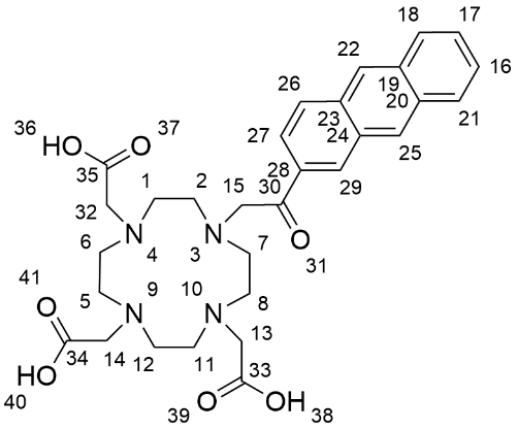
Tri-tert-butyl 2,2',2''-(10-(2-(anthracen-2-yl)-2-oxoethyl)-1,4,7,10-tetraazacyclododecane-1,4,7-triyl) triacetate (3)



2 (0.250 g, 0.82 mmol), **1** (0.380 g, 0.75 mmol) and K_2CO_3 (0.210 g, 1.50 mmol) were combined in a flask with MeCN (40 mL), stirred under nitrogen and heated to reflux for 18 hr at 80 °C. Solution was filtered, and solvent removed *in vacuo*. Resulting solid was purified using silica gel column chromatography with MeOH:DCM (5:95) to give a brown solid.

Yield 0.340 g, 54% **^{1}H NMR** (400 MHz, $CDCl_3$) δ (ppm) 8.36 (d, *J* = 6.2 Hz, 1H, C*H*), 7.99 – 7.89 (m, 6H, C*H*), 7.45 – 7.35 (m, 2H, C*H*), 3.82 – 2.54 (m, 24H, NCH_2, NCH_2CO_2), 1.44 – 1.34 (m, 27H CCH_3). **^{13}C NMR** (101 MHz, $CDCl_3$) δ (ppm) 197.97, 134.06, 133.28, 132.69, 132.09, 131.68, 130.41, 128.99, 128.75, 128.44, 128.24, 126.72, 126.27, 125.99, 122.74, 26.57. **ES$^+$ MS** (*m/z*) 755.4 $[M+Na]^+$ **UV-Vis** (MeOH) λ_{max} /nm = 241, 260, 269, 325, 341, 359, 400 **IR** 3000 (C=C), 1705 (C=O)

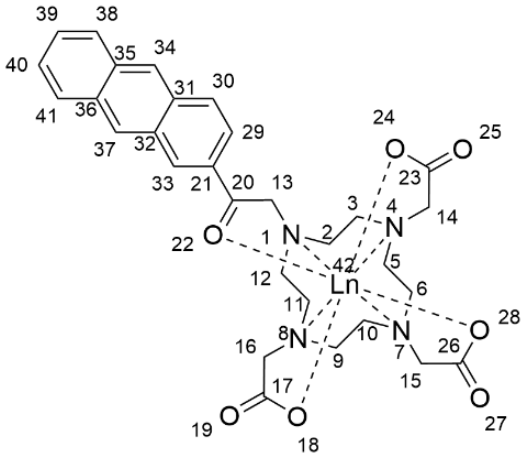
2,2’,2’’-(10-(2-(anthracen-2-yl)-2-oxoethyl)-1,4,7,10-tetraazacyclododecane-1,4,7-triyl) triacetic acid (4)



3 (0.170 g, 0.24 mmol) was dissolved in DCM (2 mL) in an ice bath and an equal amount of TFA (2 mL) added dropwise. Reaction was stirred at room temperature for 24 hr before removing solvents *in vacuo.* Product was washed using DCM (2 x 10 mL) and MeOH (3 x 10 mL) to remove remaining TFA, dissolved in minimal MeOH, and triturated with Et_2O remove sticky non-polar impurities. Remaining solvent was removed *in vacuo*.

Yield 0.168 g, 67% **^{1}H NMR** (400 MHz, $CDCl_3$) δ (ppm) 8.61 – 7.38 (m, 9H C*H*), 3.42 (s, 24H, NCH_2CO, NCH_2) **ES$^+$ MS** (*m/z*) 565.4 $[M+H]^+$ **UV-Vis** (MeOH) λ_{max} /nm = 256, 323, 339, 359, 378 **IR** 3020 (OH), 1723 (C=O), 1664 (C=C), 1411-1362, 1196 (C-N)

General Procedure for the Insertion of Lanthanides into 4



4 (1 eq.) and $Ln(CF_3SO_3)_3$ (1.05 eq.) were dissolved in minimal MeOH and stirred at 60 °C for 30 min. pH was adjusted to 4 before stirring at 60 °C for 48 hr and removing solvent *in vacuo*. Solid was dissolved in minimal H_2O, and pH adjusted to 10 through addition of aqueous NaOH to remove excess lanthanide as an insoluble hydroxide. Product was dissolved in minimal MeOH and triturated with Et_2O before removing excess solvent *in vacuo.*

Tb(2,2',2''-(10-(2-(anthracen-2-yl)-2-oxoethyl)-1,4,7,10-tetraazacyclododecane-1,4,7-triyl) triacetic acid) (5)

The above general procedure was followed using **4** (0.060 g, 0.11 mmol) and $Tb(CF_3SO_3)_3$ (0.069 g, 0.11 mmol) to give product as a yellow solid.

Yield 0.049 g, 31% **ES$^+$ MS** (*m/z*) 759.2 $[M+K]^+$ **UV-Vis** (MeOH) λ_{max}/nm = 256, 300, 323, 335, 339, 359, 378

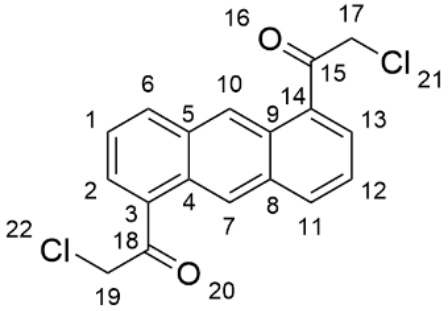
Eu(2,2',2''-(10-(2-(anthracen-2-yl)-2-oxoethyl)-1,4,7,10-tetraazacyclododecane-1,4,7-triyl) triacetic acid) (6)

The above general procedure was followed using **4** (0.101 g, 0.18 mmol) and $Eu(CF_3SO_3)_3$ (0.122 g, 0.19 mmol) to give product as an opaque white solid.

Yield 0.1271 g, 80% **ES+ MS** (*m/z*) 737.14, found 737.4 $[M+Na^+]$ **UV-Vis** (MeOH) λ_{max}/nm = 256, 339, 359, 378

7.3 Experimental – Attempts on a Hetero-Metallic Luminescent Lanthanide Complex

1,5-bis(chloroacetyl)anthracene (7)

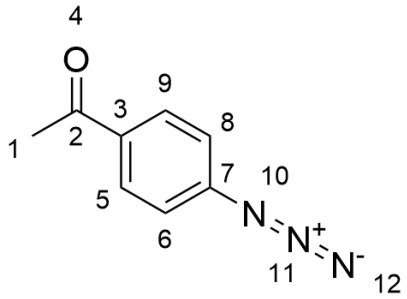


Prepared in accordance with the procedure described by Morita *et al.*[150]

Yield 0.008 g, 3% **^{1}H NMR** (400 MHz, $CDCl_3$) δ (ppm) 8.49 (s, 2H, C*H*), 8.03 – 7.96 (m, 2H, C*H*), 7.70 (d, *J* = 8.8 Hz, 2H, C*H*), 7.52 – 7.43 (m, 3H, C*H*), 4.68 (s, 4H, CO_2CH_2Cl). **ES$^+$ MS** (*m/z*) 685.4 [2M+Na^+] **UV-Vis** (MeOH) λ_{max}/nm = 258, 272, 366, 390, 400 **IR:** 2922, 1683-1359 (C-H)

7.4 EXPERIMENTAL – REDUCIBLE LUMINESCENT LANTHANIDE COMPLEXES

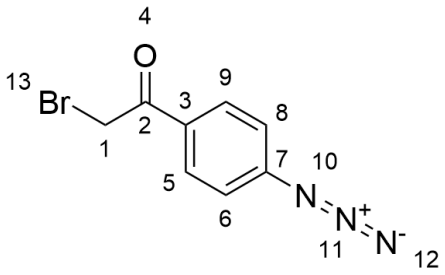
Synthesis of 4-azidoacetophenone (8)



4'-aminoacetophenone (1.000 g, 7.4 mmol) was dissolved in HCl (4.81 mL, 6 M) and cooled to -15 °C. A solution of $NaNO_2$ (0.516 g, 7.48 mmol) in water (2.59 mL) was added dropwise slowly using a syringe and stirred for 15 min at -10 °C, making sure to keep the temperature below 5 °C. At -5 °C, a solution of NaN_3 (0.486 g, 7.48 mmol) in water (2.59 mL) was added dropwise with a syringe before allowing the reaction to warm up to room temperature. The crude mixture was extracted twice with Et_2O, the organic layer washed once with water before drying with $MgSO_4$, filtering and removing solvent under reduced pressure. Product was observed as an orange oil which crystallised after approximately one-hour.

Yield 0.592 g, 50% **^{1}H NMR** (400 MHz, $CDCl_3$) δ (ppm) 7.93 – 7.84 (m, 2H, C*H*), 7.04 – 6.96 (m, 2H, NCC*H*), 2.50 (s, 3H, CH_3) **^{13}C NMR** (101 MHz, $CDCl_3$) δ (ppm) 196.53, 144.91, 133.85, 130.27, 118.97, 26.47. **ES$^+$ MS** (*m/z*) 239 [M+H$^+$] **UV-Vis** (MeOH) λ_{max}/nm = 216, 281 nm **IR** 3067, 2884, 2127-2092 (N=N=N), 1672 (C=O)

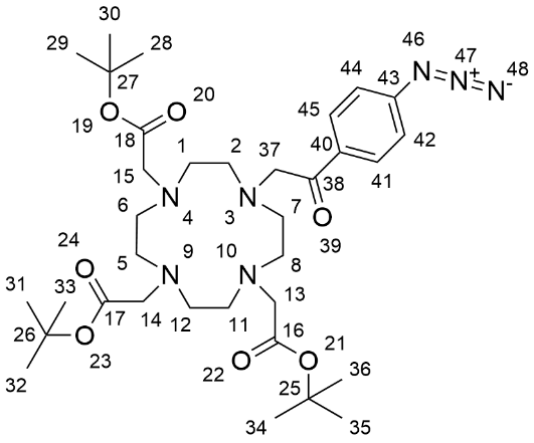
Synthesis of 4-azidophenacyl bromide (9)



8 (1 eq.) was dissolved in Et_2O (17.5 mL) and dioxane (9.4 mL) and cooled with an ice bath. Br_2 (1.72 mL) was added dropwise with a syringe and stirred in the ice bath for 3 hr. To stop the reaction, water was added and extraction with Et_2O was performed. The combined organic phase was dried over $MgSO_4$, filtered and concentrated under reduced pressure, before dissolving in minimal DCM and purifying using gradient column chromatography, starting with Pet Ether:DCM (95:5).

Yield 1.010 g, 99% **^{1}H NMR** (400 MHz, $CDCl_3$) δ (ppm) 8.06 – 8.01 (m, 2H, C*H*), 7.11 – 7.02 (m, 2H, C*H*), 4.41 (s, 2H, BrC*H*$_2$) **^{13}C NMR** (101 MHz, C_3D_6O) δ (ppm) 189.82, 145.53, 131.58, 130.93, 130.91, 119.51, 119.26, 41.35 **ES$^+$ MS** (*m/z*) 238.78 $[M]^+$ **UV-Vis** (MeOH) λ_{max}/nm = 295 **IR** 3032, 2126 (N=N=N), 1680 (C=O)

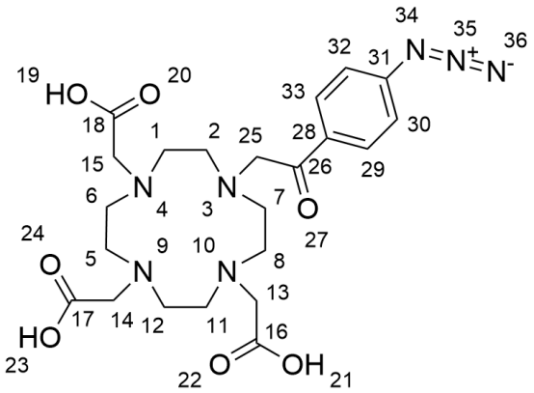
Synthesis of tri-tert-butyl 2,2',2''-(10-(2-(4-azidophenyl)-2-oxoethyl)-1,4,7,10-tetraazacyclododecane-1,4,7-triyl)triacetate (10)



1 (0.500 g, 0.97 mmol) and **9** (0.245 g, 1.02 mmol) were combined with K_2CO_3 (0.268 g, 1.94 mmol) in MeCN (30 mL) and heated to reflux at 80 °C for 4 hr before filtering and removing solvent. Product was purified using gradient elution column chromatography, initially with DCM:MeOH (100:0) and transitioning to DCM:MeOH (95:5).

Yield 0.254 g, 38% **^{1}H NMR** (400 MHz, $CDCl_3$) δ (ppm) 8.02 – 7.95 (m, 2H, C*H*), 6.97 – 6.89 (m, 2H, C*H*), 3.47 – 2.71 (m, 24H, NCH_2, NCH_2CO_2), 1.13 (t, *J* = 7.3 Hz, 27H, CCH_3).**^{13}C NMR** (101 MHz, $CDCl_3$) δ (ppm) 172.80, 129.68, 119.07, 81.97, 81.94, 28.20, 27.91 **UV-Vis** (MeOH) λ_{max}/nm = 202 nm **IR** 3357 (NH), 2970 (OH), 2114 (N=N=N), 1726 (C=O)

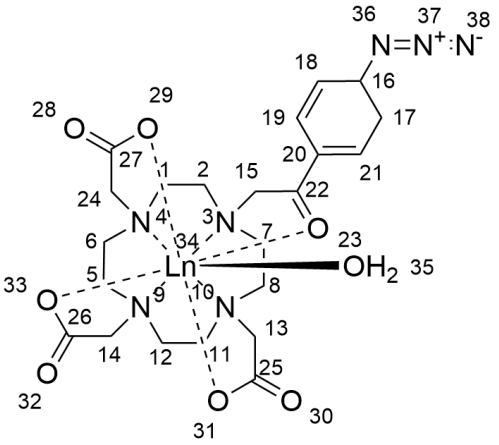
Synthesis of 2,2',2''-(10-(2-(4-azidophenyl)-2-oxoethyl)-1,4,7,10-tetraazacyclododecane-1,4,7-triyl)triacetic acid (11)



10 (0.17 g, 0.24 mmol) was dissolved in DCM (2 mL) in an ice bath and an equal amount of TFA (2 mL) was added dropwise. Reaction was stirred at room temperature for 24 hr before removing solvents *in vacuo.* Product was washed using DCM (2x10 mL) and MeOH (3x10 mL) to remove remaining TFA, dissolved in minimal MeOH and triturated with Et_2O to remove sticky non-polar impurities. Remaining solvent was removed *in vacuo*.

Yield 0.292 g, 86% **^{1}H NMR** (400 MHz, $CDCl_3$) δ (ppm) 8.05 – 7.98 (m, 2H, C*H*), 7.04 – 7.00 (m, 2H, C*H*), 3.13 – 2.84 (m, 24H, NCH_2, NCH_2CO_2) **^{13}C NMR** (151 MHz, MeOD) δ (ppm) 161.53 (d, *J* = 34.4 Hz), 130.07, 119.75, 118.77, 117.80, 115.86, 113.92, 47.60 (dp, *J* = 42.9, 21.4 Hz). **ES$^+$ MS** (*m/z*) 506.23 [M+H$^+$] **UV-Vis** (MeOH) λ_{max}/nm = 291 nm

General Procedure for the Insertion of Lanthanides into 11



11 (1 eq.) and $Ln(CF_3SO_3)_3$ (1.05 eq.) were dissolved in MeOH, and stirred at 60 °C for 30 min. Using aqueous NaOH added dropwise, the pH was adjusted to 4, and stirred at 60 °C for 48 hr before removing solvent *in vacuo*. The resulting compound was dissolved in minimal water, and pH adjusted to 10 through addition of aqueous NaOH to remove excess lanthanide as an insoluble hydroxide. Product was dissolved in minimal MeOH and triturated with Et_2O before removing excess solvent *in vacuo.*

Synthesis of Tb(2,2',2''-(10-(2-(4-azidophenyl)-2-oxoethyl)-1,4,7,10-tetraazacyclododecane-1,4,7-triyl)triacetic acid) (12)

The above general procedure was followed using **11** (0.060 g, 0.11 mmol) and $Tb(CF_3SO_3)_3$ (0.0692 g, 0.114 mmol) to give product as a yellow solid.

Yield 0.021 g, 45% **ES$^+$ MS** (*m/z*) 661.13, found 661.02 $[M]^+$ **IR** 3422 (N-H), 2923 (OH), 2127 (N=N=N), 1596 (C=C) **UV-Vis** (MeOH) λ_{max}/nm = 210, 318, 360

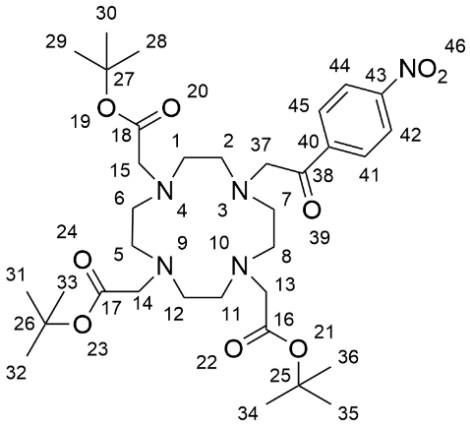
Synthesis of Eu(2,2',2''-(10-(2-(4-azidophenyl)-2-oxoethyl)-1,4,7,10-tetraazacyclododecane-1,4,7-triyl)triacetic acid (13)

The above general procedure was followed using **11** 0.101 g (0.178 mmol) and $Eu(CF_3SO_3)_3$ (0.122 g) to give product as an opaque white solid.

Yield 0.037 g, 87% **ES$^+$ MS** (*m/z*) 657.14, found 690.1 $[M+CH_3OH+H]^+$ **UV-Vis** (MeOH) λ_{max}/nm = 265, 313 **IR** 3424 (N-H), 2128 (N=N=N), 1634 (C=O), 1258 (C-O)

7.5 Experimental – Alternative Reducible Luminescent Lanthanide Complexes

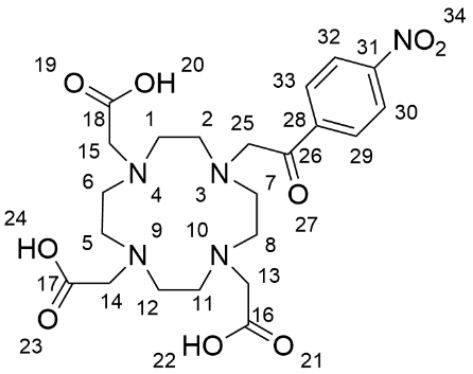
Synthesis of tri-tertbutyl 2,2',2''-(10-(2-(4-nitrophenyl)-2-oxyethyl)-1,4,7,10-tetraazacyclododecane-1,4,7-triyl)triacetate (14)



1 (0.500 g, 0.92 mmol) and 2-bromo-4-nitrobenzene (0.237 g, 0.92 mmol) were combined with K_2CO_3 (0.268 g, 1.94 mmol) in MeCN (30 mL) and heated to reflux at 80 °C for 4 hr before filtering and removing solvent. Product was purified using gradient elution column chromatography, initially with $CHCl_3$:EtOH (100:0) and transitioning to $CHCl_3$:EtOH (95:5).

Yield 0.476 g, 55% **^{1}H NMR** (400 MHz, $CDCl_3$) δ (ppm) 8.29 – 8.22 (m, 2H, C*H*), 8.16 – 8.09 (m, 2H, C*H*), 3.79 – 2.40 (m, 24H, NCH_2, NCH_2CO_2), 1.43 – 1.31 (m, 27H, CCH_3). **ES$^+$ MS** (*m/z*) 677.4, found 677.31 $[M]^+$ **IR** 3367 (N-H), 2945 (C-H), 1732 (C=O), 1524 (N-O) **UV-Vis** (MeOH) λ_{max}/nm = 267.5

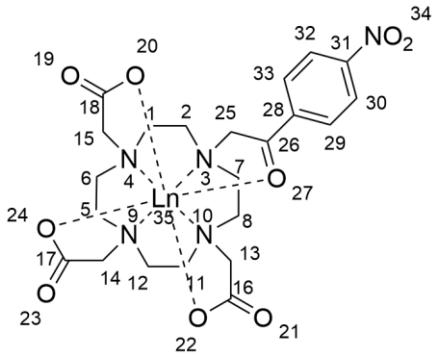
Synthesis of 2,2',2''-(10-(2-(4-nitrophenyl)-2-oxoethyl)-1,4,7,10-tetraazacyclododecane-1,4,7-triyl)triacetic acid (15)



14 (0.250 g, 0.37 mmol) was dissolved in DCM (2 mL) in an ice bath, and TFA (2 mL) added dropwise. Solution was stirred 24 hr at room temperature before removing solvent *in vacuo*. Solid was washed using DCM (2 x 10 mL) and MeOH (2 x 10 mL) to remove remaining TFA before dissolving in minimal MeOH and triturating with Et_2O to remove sticky non-polar impurities. Remaining solvent was removed *in vacuo*.

Yield 0.331 g, 93 % **^{1}H NMR** (400 MHz, MeOD) δ (ppm) 8.25 (d, *J* = 8.4 Hz, 2H), 8.10 (d, *J* = 8.5 Hz, 2H), 4.59 – 2.59 (m, 24H). **^{13}C NMR** (151 MHz, MeOD) δ (ppm) 160.84, 157.70, 150.83, 129.22, 123.32, 119.54, 117.60, 115.59, 113.72 (d, *J* = 3.8 Hz), 65.49, 54.45 – 50.72 (m), 42.03, 26.92 (d, *J* = 7.3 Hz), 14.03. **ES$^+$ MS** (*m/z*) 509.21, found 509.41 $[M]^+$ **IR** 3096 (O-H), 1680 (C=O), 1529 (N-O), 1427 (O-H) **UV-Vis** (MeOH) λ_{max}/nm = 263

General Procedure for the Insertion of Lanthanides into 15



15 (1 eq.) and $Ln(CF_3SO_3)_3$ (1.05 eq.) were dissolved in MeOH, and stirred at 60 °C for 30 min. Using aqueous NaOH added dropwise, pH was adjusted to 4, and the reaction stirred at 60 °C for 48 hr before removing solvent *in vacuo*. The resulting compound was dissolved in minimal water, and pH adjusted to 10 through addition of aqueous NaOH to remove excess lanthanide as an insoluble hydroxide. Product was dissolved in minimal MeOH and triturated with Et_2O before removing excess solvent *in vacuo.*

Synthesis of Tb(2,2',2''-(10-(2-(4-nitrophenyl)-2-oxoethyl)-1,4,7,10-tetraazacyclododecane-1,4,7-triyl)triacetic acid) (16)

The above general procedure was followed using **15** (0.060 g, 0.11 mmol) and $Tb(CF_3SO_3)_3$ (0.069 g, 0.11 mmol) to give product as a yellow solid.

Yield 0.192 g, 91% **ES$^+$ MS** (*m/z*) 665.110, found 666.039 $[M+H]^+$ **UV-Vis** (MeOH) λ_{max}/nm = 267.8 **IR** 3492 (OH), 1635 (NO), 1259 (C-N)

Synthesis of Eu(2,2',2''-(10-(2-(4-nitrophenyl)-2-oxoethyl)-1,4,7,10-tetraazacyclododecane-1,4,7-triyl)triacetic acid) (17)

The above general procedure was followed using **15** 0.313 g, 0.61 mmol) and $Eu(CF_3SO_3)_3$ (0.423 g, 0.65 mmol) to give product as a white solid.

Yield 0.274 g, 59 % **ES$^+$ MS** (*m/z*) 701.14, found 702.18 $[M+ACN+H]^+$ **IR** 3432, 2914, 1771, 1540 (N-O stretching, nitro) **UV-Vis** (MeOH) λ_{max} / nm = 266

7.6 REFERENCES

1. Dadabhoy, A.; Faulkner, S.; Sammes, P. G., Long wavelength sensitizers for europium(iii) luminescence based on acridone derivatives. *Journal of the Chemical Society, Perkin Transactions 2* **2002,** (2), 348-357.

2. Ung, P.; Clerc, M.; Huang, H.; Qiu, K.; Chao, H.; Seitz, M.; Boyd, B.; Graham, B.; Gasser, G., Extending the Excitation Wavelength of Potential Photosensitizers via Appendage of a Kinetically Stable Terbium(III) Macrocyclic Complex for Applications in Photodynamic Therapy. *Inorganic Chemistry* **2017,** *56* (14), 7960-7974.

3. Routledge, J. D.; Jones, M. W.; Faulkner, S.; Tropiano, M., Kinetically Stable Lanthanide Complexes Displaying Exceptionally High Quantum Yields upon Long-Wavelength Excitation: Synthesis, Photophysical Properties, and Solution Speciation. *Inorganic Chemistry* **2015,** *54* (7), 3337-3345.

4. Beeby, A.; Bushby, L. M.; Maffeo, D.; Gareth Williams, J. A., Intramolecular sensitisation of lanthanide(iii) luminescence by acetophenone-containing ligands: the critical effect of para-substituents and solvent. *Journal of the Chemical Society, Dalton Transactions* **2002,** (1), 48-54.

5. Morita, K.; Aida, T.; Morinaga, K.; Tsunetsugu, J., A five fused ring non-benzenoid quinone containing a seven-membered ring: synthesis and properties of cyclohept[f,g]aceanthrylene-5,8-dione and 1,2-dihydrocyclohept[f,g]aceanthrylene-5,8-dione. *Journal of the Chemical Society, Perkin Transactions 1* **1994,** (9), 1215-1220.